8-7-2015 12:00 AM

Epithelial to mesenchymal transition in the metastatic progression of gastroenteropancreatic neuroendocrine tumours

Stephanie Mok, *The University of Western Ontario*

Supervisor: Dr. Christopher J. Howlett, *The University of Western Ontario*
Joint Supervisor: Dr. Douglas Quan, *The University of Western Ontario*
A thesis submitted in partial fulfillment of the requirements for the Master of Science degree in Pathology

EPITHELIAL TO MESENCHYMAL TRANSITION IN THE METASTATIC PROGRESSION OF GASTROENTEROPANCREATIC NEUROENDOCRINE TUMOURS

(Thesis format: Monograph)

by

Stephanie Yee-Ching Mok

Graduate Program in Pathology and Laboratory Medicine

A thesis submitted in partial fulfillment
of the requirements for the degree of
Master of Science

The School of Graduate and Postdoctoral Studies
The University of Western Ontario
London, Ontario, Canada

Abstract

Gastroenteropancreatic neuroendocrine tumors (GEP-NETs) are a rare type of malignant epithelial cancer arising from the diffuse neuroendocrine system. In this study, we have performed gene expression profiling along with immunohistochemistry (IHC) to highlight key molecular pathways underlying the pathogenesis of GEP-NETs. We used formalin-fixed paraffin-embedded archived tissue samples of NETs arising from small intestine (SI-NETs), pancreas (P-NETs), and distal colon/rectal region (R-NETs) to extract RNA for real-time PCR-based gene profiling, and to construct tissue microarrays (TMAs) for high-throughput immunohistochemistry. Our results show evidence of epithelial to mesenchymal transition (EMT) at the mRNA and protein levels. From the genes highlighted by our gene expression studies, TGF-β/BMP signalling could be a key mediator towards this EMT event. Therefore, we investigated whether TGF-β signalling is active in GEP-NETs and determined whether its activation is linked to an EMT phenotype.

Keywords

Gastroenteropancreatic neuroendocrine tumours, epithelial to mesenchymal transition, gene expression, tissue microarray, immunohistochemistry, transforming growth factor beta

Acknowledgments

I would like to acknowledge my supervisors, Drs. Chris Howlett and Douglas Quan, for providing me the opportunity to pursue these studies, as well as the guidance and support to see them through to the end. To Dr. Zia Khan, thank you for welcoming me into your lab family as an “adoptive” graduate student all these years. I could not have accomplished this work without your help either.

Table of Contents

List of Tables

List of Figures

Chapter 1

1 Introduction

1.1 Diffuse Neuroendocrine System

The diffuse neuroendocrine system (DNS) refers to a group of cells characterized by the expression of neuropeptides, chromogranins, and neuropeptide processing enzymes. These cells are widely distributed throughout the body, dispersed throughout different tissues in a seeded manner giving it the 'diffuse' aspect. Under electron microscopic examination, dense core secretory granules can be seen in the cytoplasm of neuroendocrine cells. A "salt and pepper" appearance under light microscopy is also commonly used to describe their nuclei which contain granular chromatin. However, the key aspects of a neuroendocrine cell can be further defined by several traits. They have the capacity to produce neurotransmitter, neuromodulator, or neuropeptide hormones, and their product is contained within vesicles which are released, upon neural stimulation, via exocytosis. Their mode of transmission is thus endocrine. Although they stain for some neuromarkers such as synaptophysin, they differ from neurons by their lack of axons and nerve terminals.

The DNS provides coordinated actions for the nervous system to influence the functions of internal organs, especially along the gastrointestinal tract where a number of different neuroendocrine cells and their specific hormone products act in concert to facilitate digestion (**Table 1.1**). The embryonic origins of the diffuse neuroendocrine cells are controversial. Early postulates believed that neuroendocrine cells, despite their distribution throughout the body, arose from a common embryological origin in the neuroectoderm or neural crest given their coordinated actions with the nervous system.[1, 2] However, a number of cells having neuroendocrine features have been shown to originate from other regions.[3] Neuroendocrine cells in the gastrointestinal system are now thought to have the same endodermal origins as their other epithelial counterparts.[4, 5]

Table 1.1: Neuroendocrine cells found along the gastrointestinal system

Neuroendocrine cell	Hormone Product	Effect
Enterochromaffin	Serotonin	Regulates intestinal movement
Delta	Somatostatin	Reduces acid production of parietal cells
Epsilon (Gr)	Ghrelin	Inducing appetite
L	Glucagon-like peptide	Stimulates insulin release; decrease glucagon release
N	Neurotensin	Smooth muscle contraction
VIP	Vasoactive intestinal peptide	Regulates secretion and absorption to increase motility
Alpha (A)	Glucagon	Elevates blood glucose level
Beta	Insulin	Lowers blood glucose level
I	Cholecystokinin (CCK)	Bile secretion
Gamma (PP)	Pancreatic polypeptide	Inhibits secretions by CCK
G	Gastrin	Stimulates gastric acid secretion
S	Secretin	Regulates exocrine pancreatic secretions
K	Gastric inhibitory peptide	Incretin; promotes triglyceride storage

1.2 Gastroenteropancreatic Neuroendocrine Tumours

Tumours can arise from cells of the diffuse neuroendocrine system and may appear anywhere in the body. The last few decades has seen an increase in incidence of neuroendocrine tumours (NETs) from 1.09 per 100,000 in 1973 to 5.25 per 100,000 in 2004,[6] with the majority of these tumours appearing along the gastrointestinal tract (60.52%) and the bronchopulmonary system (27.4%).[7]

Scattered in the mucosa of the entire digestive tract and pancreatic ducts, gastrointestinal neuroendocrine cells are responsible for producing and secreting over 20 different peptide hormones including gastrin, cholecystokinin (CCK), serotonin and somatostatin. Lesions that appear along the gastrointestinal tract, including the pancreas, are collectively referred to as gastroenteropancreatic neuroendocrine tumours (GEP-NETs). Within this classification, the most common sites for GEP-NETs are the small intestine (also colloquially referred to as carcinoid tumours), rectum, colon, followed by the pancreas.[7]

1.2.1 Signs and Symptoms

GEP-NETs are typically small (less than 1 cm), slow-growing tumours that tend to remain clinically silent for many years. Discovery of these lesions are often incidental, and sometimes a distant metastasis is discovered before the primary lesion is located. The symptoms caused by GEP-NETs tend to be non-specific and are often overlooked or misdiagnosed. Common signs and symptoms pertaining to GEP-NETs include diarrhoea, flushing, abdominal pain, gastrointestinal bleeding, bronchoconstriction, and cardiac palpitations.[8] The combination of these symptoms due to a GEP-NET is known as carcinoid syndrome. This syndrome does not manifest in every case of GEP-NET, but it often represents a later stage in the disease when it appears. For this constellation of symptoms to appear, a number of events typically occur beforehand. First, the GEP-NET must be a functional tumour capable of producing an active and secreted hormone product. Second, the hormone product has to be able to pass through the liver without being metabolized to access the systemic circulation and exert its effect. The second

condition is typically met after a metastatic event has occurred to the liver such that the hormone product bypasses hepatic circulation. This is why the appearance of the carcinoid syndrome is a late event in the disease progression.

1.2.2 Classification, Grading, and Staging

GEP-NETs are commonly classified as a group of heterogeneous tumours. Part of this heterogeneity comes from the difficulty in predicting its clinical behaviour when identified. The current grading systems rely heavily on Ki-67 proliferation index to make these predictions (**Table 1.2**). Variations in Ki-67 grade cut-offs and interpersonal variation in interpreting Ki-67 results may account for some problems in accurately grading the disease, however it reflects a greater need for a more precise grading scheme.[9, 10] The classification of GEP-NETs relies on three main parameters: degree of differentiation, whether the tumour is functional (hormone-secreting) or non-functional, and its proliferation index measured by Ki-67 or mitotic figure counts.[11] There are several parallel grading and staging systems that use these parameters as a foundation for classifying GEP-NETs: the 2010 World Health Organization (WHO) classification system, the European Neuroendocrine Tumour Society guidelines, and the American Joint Committee on Cancer/Union for international Cancer Control guidelines. Unfortunately, these systems are largely viewed as an imprecise way of assigning grade and stage to the NETs because the biological behaviour of the tumours are quite variable within a given grade and do little to predict malignant behaviour. Furthermore, the differences between the staging systems can create confusion.[12] Thus, there is need for a better understanding of the molecular mechanisms involved in the pathogenesis of the disease and a more unified classification system.[13, 14] This limitation may explain why the overall 5-year survival rate of NETs has remained unchanged at 60% over the last few decades.[15]

Table 1.2: 2010 WHO Grading for GEP-NETs

Differentiation	Grade	GEP-NETs
Well Differentiated	Low (G1)	<2 mitoses / 10 hpf AND <3% Ki67 index
	Intermediate (G2)	2-20 mitoses / 10 hpf OR 3%-20% Ki67 index
Poorly Differentiated	High (G3)	>20 mitoses / 10 hpf OR >20% Ki67 index

1.2.3 Histology of GEP-NETs – Characteristics and stains

GEP-NETs can extend from the mucosa through the serosa depending on its size. Confirmation of a GEP-NET is done by immunohistochemical reactivity to common neuroendocrine markers including chromogranin, synaptophysin, CD56, and neuron specific enolase (NSE). Morphologically, the growth pattern of GEP-NETs can be described as gyriform, nesting, solid/insular, trabecular and/or acinar, but they have no influence on its classification (**Figure 1.1**). Cytologically, they have round nuclei with speckled chromatin giving it a "salt and pepper" appearance along with small nucleoli that may or may not be prominent depending on the site of origin (**Figure 1.2**). At low power magnification, the cells look small with abundant cytoplasm that, at higher magnification, shows granularity. The cells of a well-differentiated GEP-NET look similar between tumours from different anatomical sites. Sometimes the cells of GEP-NETs are described as monotonous given how similar they look to one another. Furthermore, the well-differentiated appearance of most of these tumours belies its metastatic potential. Despite these similarities, GEP-NETs from different anatomical sites demonstrate some histological differences, and certain neuroendocrine markers are more effective at detecting neuroendocrine phenotypes in different locations.[16] For example, rectal NETs can stain for more specific polypeptides such as somatostatin, glucagon, substance P, and peptide YY as well.

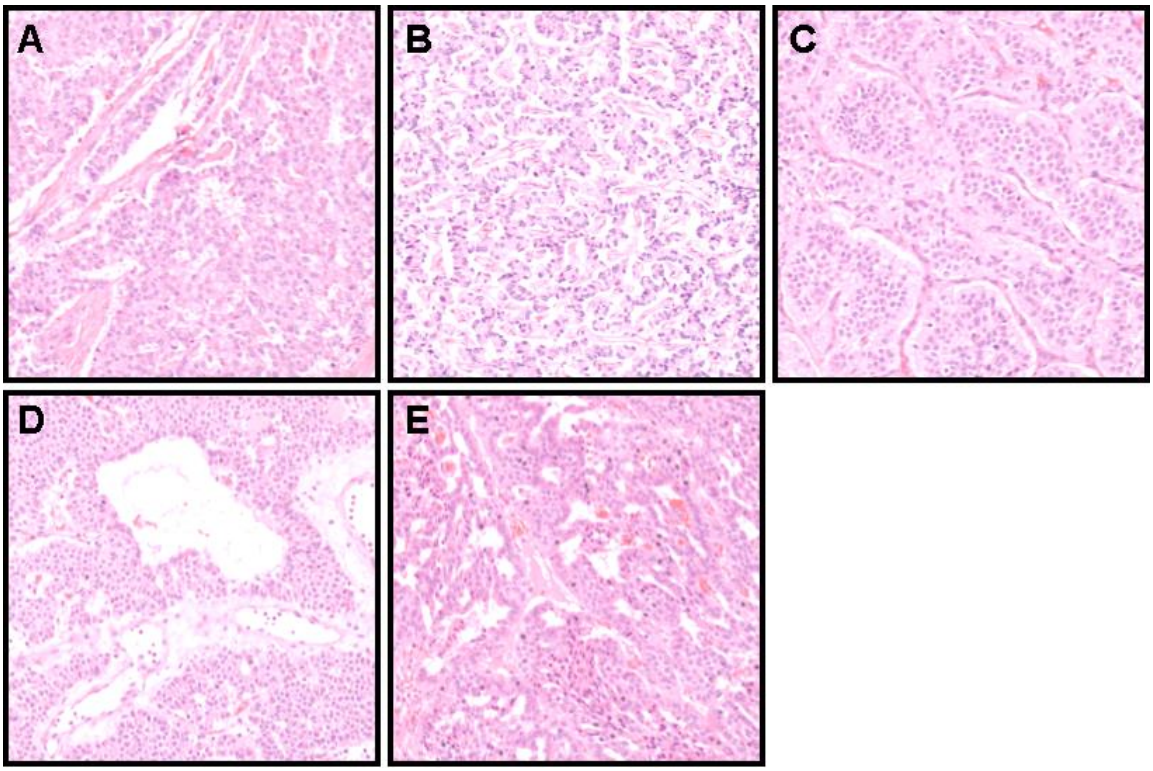

Figure 1.1. Representative images of GEP-NET morphologic growth patterns. Tumours pictured here show (A) acinar, (B) gyriform, (C) nested, (D) solid, and (E) trabecular growth patterns.

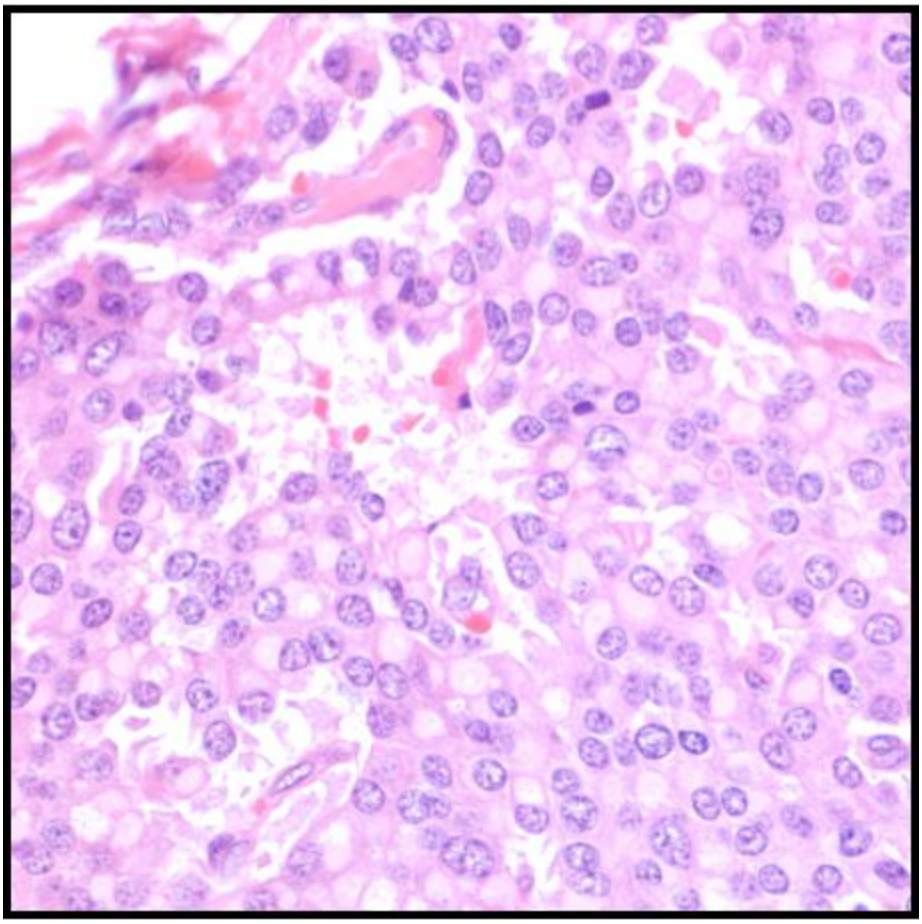

Figure 1.2. High powered image showing "salt and pepper" chromatin pattern, characteristic of neuroendocrine tumours.

1.2.4 Treatments

Treatment for these tumours is often done in consultation with a multidisciplinary team of physicians from different specialities. Complete surgical excision is often the best and the only curative option for individuals diagnosed with GEP-NETs. However, this may not always be feasible given the patient profile, location of the lesion or tumour burden. In this case, symptomatic management and control of tumour growth become the primary treatment goals. Debulking surgery may be part of this treatment regime to reduce a patient's tumour burden and its mass effect. Many patients diagnosed with a GEP-NET will begin with Octreotide therapy, a somatostatin analogue that can inhibit or reduce the effects of hormones that may be excessively produced by the tumour. Cytoreductive therapy including the use of certain chemotherapeutic agents may also be part of treating the GEP-NET, although with varying efficacy possibly due to the low proliferation rate of these tumours. Novel and investigational therapeutic agents aim to control tumour growth such as the mammalian target of rapamycin (mTOR) inhibitor, Everolimus, and the anti-angiogenic agent Sunitinib.[17, 18]

Unfortunately, with time, many of these tumours will eventually metastasize despite their benign appearance. In fact, lesions of any size have the potential to metastasize and patients not uncommonly present with a metastasis at initial diagnosis.[19]

1.3 The PI3K-AKT/mTOR signalling pathway and GEP-NETs

Numerous studies on GEP-NETs have recently demonstrated a key role for the PI3K-AKT/mTOR pathway in tumourigenesis, particularly in pancreatic neuroendocrine tumours (P-NETs). mTOR signalling is key in regulating protein translation and dysregulation along this pathway is thought to allow for uncontrolled, elevated protein synthesis driving tumour growth. In this pathway, the mammalian target of rapamycin (mTOR) protein, as either mechanistic target of rapamycin complex 1 or 2 (mTORC1 or mTORC2) has serine/threonine kinase activity (**Figure 1.3**). It acts to phosphorylate transcription factors ribosomal protein S6 kinase beta-1 (S6K1) and eukaryotic translation initiation factor 4E-binding protein 1 (4EBP1). Phosphorylated S6K1 (p-S6K1) goes on to enhance the translation of proteins whereas phosphorylated 4EBP1 (p-4EBP1) relieves inhibition of the eukaryotic transcription factor its non-phosphorylated form exerts. Regulating the mTOR protein are several upstream checkpoints. Phosphoinositide 3-kinase (PI3K), which normally resides at the cell membrane, is responsible for converting phosphatidylinositol 4,5-bisphosphate (PIP2) to phosphatidylinositol 3,4,5-trisphosphate (PIP3). PIP3 is then able to promote the phosphorylation of protein kinase B (AKT) which goes on to phosphorylate tuberous sclerosis complex (TSC) proteins that constitutively repress mTOR. Phosphatase and tensin homolog (PTEN) converts PIP3 back to PIP2 to reduce mTOR activation. PI3K activation is dependent on receptor tyrosine kinases like the vascular endothelial growth factor receptor (VEGFR).

Exomic sequencing of pancreatic neuroendocrine tumours (P-NETs) revealed that 14% of tumours had mutations in genes along this pathway.[20] Similar proportions of GEP-NET patients were found to have alterations in the PI3k-AKT/mTOR pathway in an exome sequencing study for neuroendocrine tumours of the small intestine (SI-NETs), which also revealed amplification of AKT genes were the most common event.[21] Based upon finding phosphorylated (activated) mTOR pathway related proteins such as phosphorylated mTOR (p-mTOR) in poorly differentiated GEP-NETs, other studies have suggested that mTOR inhibitors would be effective in treating advanced disease.[22]

mTOR expression was similarly found in cases with higher proliferative capacity and expression with its downstream effector, phosphorylated S6K1 (p-S6K1), was associated with poorer prognosis.[23] Upstream inhibitors of mTOR, namely TSC2 and PTEN, were found to be down-regulated in a significant number of tumours.[24]

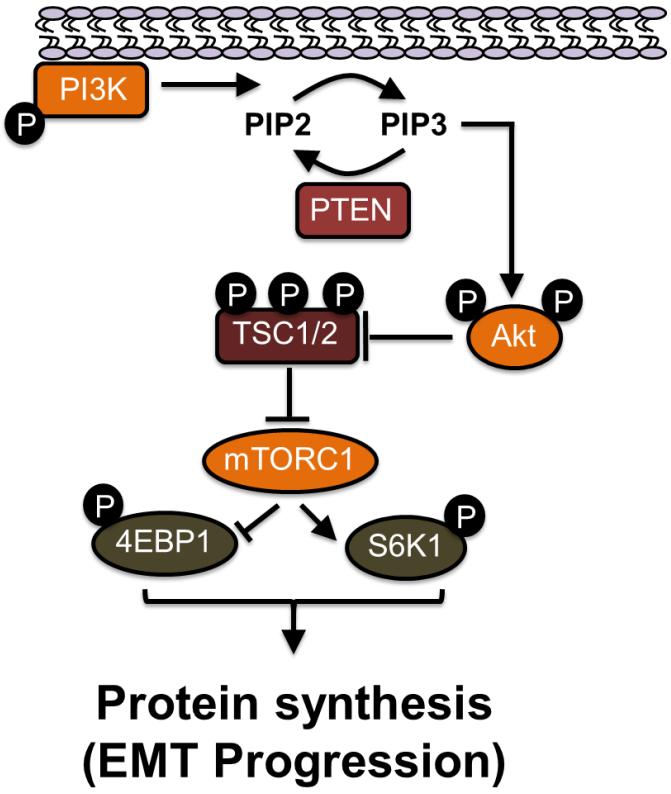

Figure 1.3. Schematic illustrating PI3K-AKT/mTOR signalling.

1.4 Transforming growth factor beta superfamily

Transforming growth factor beta (TGFβ) superfamily and its downstream signalling pathways have a broad spectrum of effects depending on cell type, environment, and magnitude of signalling. Members of this superfamily including TGFβ, BMP, and activins, have been implicated as effectors of epithelial to mesenchymal transition (EMT) via suppression of epithelial traits and promotion of mesenchymal ones.[25, 26] For example, transforming growth factor beta 3 ligand (TGF-β3) is essential for proper cleft palate fusion, as knockout TGF-β3 mice are born with a cleft palate.[27] Furthermore, it has a role in extracellular matrix (ECM) production and growth factors that encourage cell migration and invasiveness.

TGFβ ligands exist in three isoforms (-β1, -β2, -β3). Although they share >76% of their sequence homology[28], they seem to play non-redundant roles in embryonic development and wound healing, as reviewed by Finnison et al. (2013).[29] TGF-β1 is the predominant isoform in adults. This molecule is synthesized as a pro-protein and exists as a homodimer. When secreted, TGF-β1 still contains the latency-associated peptide (LAP), which couples with the latent TGFβ binding protein (LTBP) ultimately forming the larger latent complex (LLC). The LLC attaches to ECM proteins where it remains until the active form is released by matrix metalloproteinases (MMPs), plasmin or any number of conditions involving pH, temperature, and shear stress.[30-33]

The TGFβ receptors are transmembrane serine/threonine receptor kinases. There are three types of TGFβ receptors which are often present at the membrane in pairs. The complete TGFβ receptor signalling complex exists as a tetramer. Binding of a TGFβ ligand brings the two pairs of receptors together to form the complete signalling complex. In the canonical TGFβ/SMAD signalling axis, the association of the two receptor pairs allows the receptor to phosphorylate particular SMAD proteins which can then form a protein trimer complex with SMAD4 to translocate into the nucleus and regulate transcription.[34] Specific TGFβ superfamily ligands bind to certain receptors to activate a specific set of SMAD proteins. TGFβ ligand binding and receptor activation results in the phosphorylation of SMAD2 and SMAD3 whereas BMP binding to its respective

receptor results in the phosphorylation of SMAD1, SMAD5 and SMAD8 (**Figure 1.4**). Within the nucleus, these SMAD complexes have been shown to upregulate the transcription of EMT transcription factors such as ZEB1, ZEB2, SNAIL, and TWIST which act to suppress E-cadherin expression.[35]

In wound healing, elevated TGFβ signalling has been shown to promote fibrosis to levels that compromise normal tissue function.[36] Interestingly, GEP-NETs tend to be surrounded by fibrotic tissue. In fact, certain symptoms, such as abdominal pains, are a result of the extensive fibrosis surrounding the primary lesion, rather than the tumour itself. Given that TGFβ signalling is related to fibrosis, it is possible that this pathway is active in GEP-NETs and could contribute to the malignant potential of these tumours.

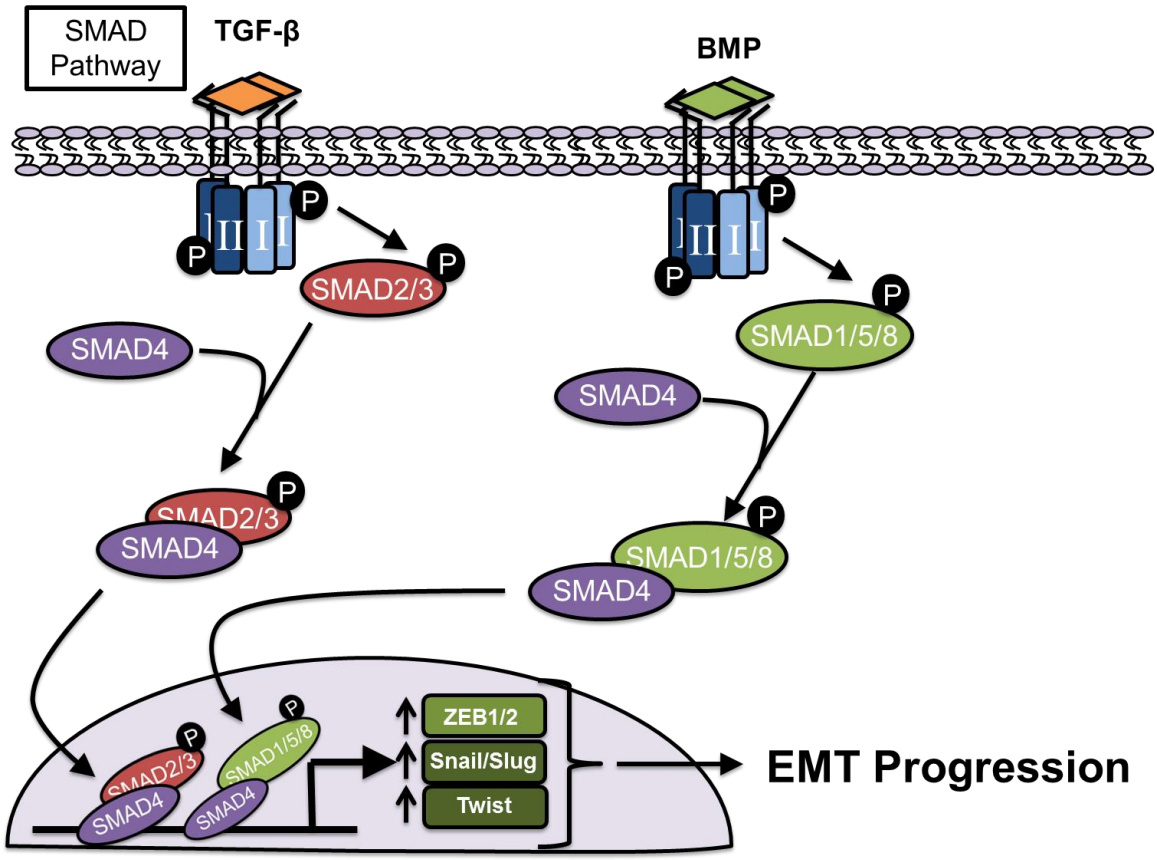

Figure 1.4. Schematic illustrating canonical TGF-β/BMP/SMAD signalling axis in initiating EMT.

1.5 Epithelial to Mesenchymal Transition

1.5.1 Epithelial phenotype vs mesenchymal phenotype

Epithelial cells have an organized cobble stone-like appearance where they maintain complete contact with one another through a combination of tight junctions, adherens junctions, desmosomes, and gap junctions. These cells form layers with apical-basolateral polarization evident through their organization of actin cytoskeleton, presence of a basal lamina at the basal side, and cell-cell junctions keeping the cells bound laterally. Epithelial cells are capable of moving within the epithelial layer, and do not move away from it under normal conditions.

In contrast, mesenchymal cells are not as closely attached to one another as epithelial cells are. They interact more closely with the extracellular matrix through focal adhesions, and their cytoskeletal structure differs in protein composition and organization as well. These cells are characterized as long, thin, and spindle-shaped in their morphology and are not associated with a basal lamina. Mesenchymal cells are known to be more mobile than epithelial cells.

Epithelial to mesenchymal transition (EMT) describes the process of epithelial cells losing their cell-cell interactions and adhesions to gain a more mobile, mesenchymal phenotype. This transition can be noted through changes in protein expression and/or subcellular localization, polarity, morphology, and migratory or invasive behaviour.[37] The process begins with an EMT effector that triggers a loss of tight junctions, adherens junctions and desmosomes that previously anchor the epithelial cells to each other. Following this, cytoskeletal changes occur, including the formation of actin stress fibres that help promote cell mobility. Genes involved in matrix remodelling are also transcribed and expressed during the transition, ultimately leading to increased motility, invasiveness, and migration through the basement membrane.

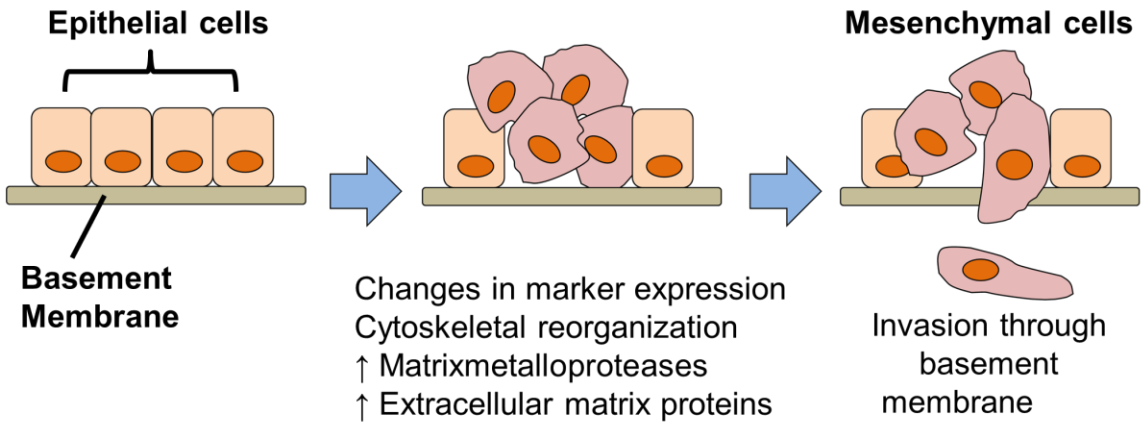

Figure 1.5. Schematic illustrating the changes involved in epithelial to mesenchymal transition.

EMT status can be implicated through fluctuations in epithelial and mesenchymal marker expression (**Table 1.3)**. For example, cells demonstrating a diminished expression of epithelial markers like E-cadherin and cytokeratin, with an increase in mesenchymal markers like vimentin and α-smooth muscle actin could be interpreted as undergoing EMT. E-cadherin is an especially important epithelial marker because it is involved in the formation of adherens junctions (with actin) and desmosomes (with intermediate filaments) which make up some of the cell-cell adhesions typically seen in an epithelial tissue.[38, 39] They associate with β-catenin along the membrane to interact with these cytoskeletal components in the cell. The loss of E-cadherin also results in the release of β-catenin into the cytoplasm where it can either be ubiquitinated and degraded, or be stabilized by active Wnt signalling to translocate into the nucleus and act as a transcription factor.[39, 40]

The induction of EMT can also be represented morphologically as changes in the apical-basal polarity and cytoskeletal rearrangements during the process produces spindle-shaped cells versus their previous cobble-stone appearance. This can be visualized through the shift from cytokeratin expression to α-smooth muscle actin expression. The elongated striations of the contractile α-smooth muscle actin facilitate mesenchymal cell-

like migration. Demonstrating the functional changes associated with EMT through migration assays of transformed epithelial cells is another way of demonstrating the process.

Although the phenotypic changes seem dramatic, the EMT process is entirely reversible through a complementary process known as mesenchymal to epithelial transition (MET). Furthermore, a cell may not need to shed all of its epithelial traits and shift entirely towards a mesenchymal phenotype. Intermediate or hybrid states with cells expressing a mixed lineage exist and these states may confer enough traits for the transition cell to achieve its goal. Studies have described a spectrum of EMT intermediates which have been characterized based on their invasiveness, adhesion, and motility.[41, 42] Thus there is an element of phenotypic fluidity in epithelial cells to shift towards a mesenchymal phenotype and back.

Table 1.3: Common epithelial and mesenchymal markers

Epithelial markers	Mesenchymal markers
E-cadherin	N-cadherin
Cytokeratin	Vimentin
Zona occludens protein 1	Alpha smooth muscle actin
Claudin	Fibronectin
Occludin	Fibroblast specific protein 1

1.5.2 Different types of EMT

Epithelial to mesenchymal transition has been characterized in three different biological contexts, described as the three types of EMT.[43] Type 1 occurs during development. EMT plays a role in implantation and embryogenesis including the formation of the mesendoderm that gives rise to the mesoderm and endoderm, neural crest formation, and heart valve formation.

Type 2 EMT is associated with wound healing and fibrosis. When injury occurs in epithelial tissue, cells from the remaining epithelial layer undergo an EMT to manoeuvre past the basement membrane into the interstitial space, become fibroblastic and contribute to tissue regeneration.

The third type of EMT occurs in the context of cancer referring to an early step in the metastatic process whereby cancer cells transiently gain a more mobile, mesenchymal-like phenotype giving it the ability to migrate past the basement membrane, leave their primary site, enter the blood stream and travel to a distant site to form a secondary tumour after transition back to an epithelial phenotype by MET. EMT has been demonstrated in many epithelial derived cancers including breast, lung, prostate, and ovarian.

1.5.3 Transcription factors in EMT

Several families of transcription factors are involved in inducing EMT, three of which are related to transforming growth factor beta (TGFβ)/bone morphogenetic protein (BMP) signalling and include the Snail, zinc finger E-box binding proteins (ZEB), and helix-loop-helix family factors. All these transcription factors share a common role in repressing E-cadherin while promoting certain mesenchymal characteristics, be it marker expression or invasive capabilities.[44]

The Snail family is comprised of SNAIL1, SNAIL2 (also known as SLUG), and SNAIL3. The Snail proteins differ in the combination of co-repressors they complex with, and affinities for different target genes.[45, 46] Their expression downstream of TGFβ results in cadherin switch (i.e. E-cadherin to N-cadherin) and allows for EMT. The Snail promoter has been shown to be directly activated by TGFβ signalling via SMAD2, 3 and 4.[47-49] BMP signalling has been shown to directly activate SLUG promoters as well.[50] The role of Snail proteins in the EMT process was hinted at by the failure of Snail-deficient mouse embryos to form a proper mesodermal layer with sustained E-cadherin expression.[51] Similar mesodermal defects as well as malformations of the neural crest were seen in SLUG deficient chick embryos.[52]

ZEB transcription factors exist as either ZEB1 or ZEB2, also known as SMAD-interacting protein 1 (SIP1), in humans. ZEB proteins have been shown to interact with SMAD3 to regulate TGFβ signalling though they have opposing effects in activation

(ZEB1) and repression (ZEB2) of target genes.[53] Functions include repression of tight junction proteins claudin-4, zona occludens protein 3, and desmosome protein plakophilin-2, and the activation of vimentin and matrix metalloproteinase 2 (MMP2) expression.[54] ZEB proteins are subject to microRNA regulation by the miR-200 family and miR-205 adding a layer of complexity to EMT regulation.[55]

The main EMT-related helix-loop-helix transcription factors are the twist-related proteins 1 and 2 (TWIST1 and TWIST2). Predominantly expressed in neural crest cells during embryogenesis, mutations in TWIST lead to defective neural tube closure at the head in mouse models, suggesting a role in EMT.[56] TWIST expression has been observed in several types of malignant human tumours including melanoma, invasive lobular breast carcinomas and diffuse-type gastric cancers.[57-59] As with the other transcription factors, TWIST acts to repress cell-cell adhesion genes E-cadherin, occludin, and claudin-7 while increasing expression of vimentin and enhancing migratory capabilities.[57] TGFβ has been shown to induce TWIST promoter activity involving SMAD4 activity and likely SMAD2 and 3.[60] A link between TWIST and BMP-related SMADs has yet to be specifically demonstrated in the literature.

Given that the survivability of NETs drastically decreases once a metastatic event has occurred, an understanding of the mechanisms involved in NET progression may uncover novel prognostic biomarkers and therapeutic targets that can extend the overall survival time of this disease. Other studies that have looked at the role of EMT markers in GEP-NETs have shown the potential relevance of this process in the differential diagnosis of small versus large cell G3 tumours but have yet to demonstrate evidence of EMT in these tumours.[61] Determining whether this early initiating step in metastasis exists in GEP-NETs will also contribute to the limited body of knowledge surrounding the biology of NETs.

1.6 Rationale

To gain a better understanding of the biology of gastroenteropancreatic neuroendocrine tumours which may lead to better diagnostic and therapeutic targets.

1.7 Hypothesis

Epithelial to mesenchymal transition is involved in the pathogenic progression of GEP-NETs.

1.8 Specific Aims

1. To profile and identify gene expression patterns of primary and secondary GEP-NETs indicative of an EMT event.
2. To confirm gene expression findings at the protein level and provide evidence of EMT occurring in GEP-NETs.
3. To study differences between GEP-NETs of different primary sites, clinical grades, and metastatic status with respect to EMT.

Chapter 2

2 Materials and Methods

2.1 Clinical Samples

Surgically resected samples of primary neuroendocrine tumours originating from the small intestine (SI-NET), pancreas (P-NET), and distal colon/rectal region (R-NET), as well as liver metastases derived these sites were retrieved from the pathology archives at the London Health Sciences Centre (London, ON Canada) with approval from UWO Health Sciences Research Ethics Board and LHSC Pathology Archives Committee. The case group was mostly limited to grade 1 (G1) and grade 2 (G2) well-differentiated GEP-NETs, as defined by the 2010 WHO guidelines. The majority of samples were obtained between 2003 and 2014. A total of 107 unique cases were studied with 42 cases having both primary and secondary tumours available for study. **Table 2.1** further describes the cases studied.

Table 2.1. Cases studied divided by (A) site of origin, (B) grade, and (C) metastasis status.

A. Site of Origin

Site	Primary	Secondary
Others	2	6
Pancreas	26	20
Colorectal	3	5
SB	45	42
Total	76	73

B. Grade

Grade	Primary	Secondary
G1	51	50
G2	21	18
G3	2	1
Unknown	2	4
Total	76	73

C. Metastasis Status

Metastasis	Primary
Liver (± Lymph node)	52
Lymph node only	15
No metastasis	9
Total	76

2.2 Tissue Microarray Construction

Tissue microarrays (TMA) were constructed using manual tissue arrayer (Beecher Instruments MTA-1 Model; Sun Prairie, WI, United States). Blank paraffin blocks were shaved down to a smooth, flat surface to serve as recipient blocks. Three 0.6 mm cores were sampled from each case where possible depending on tissue availability and placed into the recipient paraffin block to make a TMA block. A hematoxylin and eosin (H&E) stained slide from the donor block was used to verify and aid in targeting areas of tumour. The TMA was then placed upside down onto a glass slide and placed in an oven at 40°C for 40 minutes. After removing the TMA and glass slide from the oven, the slide was gently pressed down onto the TMA block to ensure cores were flush against the surface of the slide. The glass slide was then removed to complete the TMA block.

2.3 Immunohistochemistry

TMA blocks were sectioned at 4 µm and placed on a charged glass slide for immunohistochemistry (IHC) work up. The cut sections were then deparaffinized in xylene for several minutes and rehydrated through a graded ethanol series. Washes were done using Tris-buffered saline (TBS) +/- tween 20 measured at a pH of 7.6. Depending on the antibody used, a specific antigen retrieval method and dilution was used as outlined in **Table 2.2**. The immunohistochemical signal was amplified using the avidin-biotin complex and visualized with horseradish peroxidase. Validation and optimization of each antibody was done using a separate TMA comprised of several colorectal cancers. The staining in each core was semi-quantitatively evaluated based on an intensity score and, in certain stains, also had a percentage of cells stained score (**Table 2.3**) which could be multiplied together to give an individual immunoreactivity score (IRS). The staining pattern was also noted in the evaluation. Assessment of these parameters was done using the Olympus BX51 microscope (Centre Valley, PA).

Table 2.2: Antibodies used for immunohistochemistry

Target	Host species	Catalogue name	Antigen retrieval	Dilution
SNAIL+SLUG	Rabbit polyclonal	AB85936	Low	1:400
p-mTOR	Rabbit monoclonal	S448 (49F9)	High	1:50
p-4EBP1	Rabbit monoclonal	Thr37/46 (236B4)	High	1:100
PTEN	Rabbit monoclonal	(D4.3) XP	High	1:50
Vimentin	Mouse monoclonal	Clone V9 DAKO IR630	High	RTU
Beta-Catenin	Mouse monoclonal	Clone β-Catenin-1 DAKO IR702	High	RTU
E-Cadherin	Mouse monoclonal	Clone NCH-38 DAKO IR059	High	RTU
p-SMAD2/3	Rabbit polyclonal	SC-11769-R	Low	1:200
p-SMAD1/5/8	Rabbit polyclonal	SC-12353-R	Low	1:50
SMAD4	Mouse monoclonal	SC-7966	High	1:200
Ki-67	Mouse monoclonal	MIB-1 DAKO IR626	Low	RTU

Note: RTU stands for “ready to use”. Antigen retrieval solution pH as measured in lab: Low pH = 5.3 (citrate); High pH = 8.3 (Tris/EDTA).

Table 2.3: Immunohistochemistry scoring system

Staining intensity	Score	% of Cells stained	Score
Negative	0	1-10%	1
Weak	1	11-50%	2
Moderate	2	51-80%	3
Strong	3	>80%	4

2.4 RNA Extraction and Real Time RT-PCR

For RNA extraction, two 1 mm cores were sampled from the formalin fixed, paraffin embedded (FFPE) tissue blocks using a biopsy punch (Integra Miltex; York, PA, USA). Similar to the TMA construction, an H&E slide was referred to in order to ensure the sampled area was tumour tissue. RNA was extracted from the sampled cores using a High Pure FFPE RNA Micro kit (Roche; Laval, Quebec, Canada) and quantified with the Qubit Broad Range RNA assay and Qubit Fluorometer (Life Technologies; Burlington, Ontario, Canada). To facilitate the RNA extraction yield, disposable tissue grinder pestles (Axygen PES-15-B-SI; Capitol Scientific, Austin, TX, USA) were used during the digestion step. cDNA synthesis was done with an iScript cDNA Synthesis Kit (Bio-Rad Laboratories, Hercules, CA, USA).

For the pathway specific 96-well RT^2 Profiler PCR Arrays (Qiagen; Mississauga, Ontario, Canada) (**Table 2.4**), cDNA was mixed with RT^2 SYBR Green Mastermix (Qiagen). PCR reactions were performed for 50 cycles using 25 µL per well at a temperature profile of 95°C for 10 minutes at initial denaturation, then cycling through 95°C for 15 seconds and then 60°C for 1 minute as recommended by the manufacturer. The resulting data was normalized to five housekeeping genes (β-actin, β_2 microglobulin, glyceraldehyde-3-phosphate dehydrogenase, hypoxanthine phosphoribosyltransferase 1, and large ribosomal protein P0).

For PCR using individually purchased primers (**Table 2.5**), the cDNA was mixed with SsoFast EvaGreen Supermix (Bio-rad; Misssissauga, Ontario, Canada). These results were normalized to β-actin.[62] In these PCR reactions, the sample volume was 20 µL

performed for 45 cycles with a temperature profile of 95°C for 2 minutes initially, then cycling through 95°C for 2 seconds and then 55°C for 12 seconds as recommended by the manufacturer.

In both instances, gene expression levels of the primary and metastasis groups were normalized to their respective normal epithelial tissue based on site and fold change was determined using the $2^{-\Delta\Delta CT}$ method.[63] Melting curve analysis was used to assess PCR specificity from a temperature spectrum of 65°C – 95°C at 0.2°C increments for 5 seconds.

Table 2.4: RT^2 profiler PCR arrays used

Array	Catalogue number
Angiogenesis	PAHS-024Z
EMT	PAHS-090Z
mTOR signalling	PAHS-098Z
PI3K-AKT signalling	PAHS-058Z

Table 2.5: Individual primers used for PCR

Target gene	Catalogue number
SNAI1	QT00010010
TWIST1	QT00011956
ZEB1	QT00020972
ZEB2	QT00008554
TGFB1	QT00000728
TGFBR1	QT00083412
BMP1	QT00000819
BMP2	QT00012544
BMPR1B	QT00084469
BMPR2	QT00226065
BMPR1A	QT00085358
PTEN	QT00086933
HIF1A	QT00083664
MMP2	QT00088396
MMP9	QT00040040
E-CAD	QT00080143
VIM	QT00095795
ACTB	QT01680476

2.5 Statistical Analysis

All the statistical analyses were done using GraphPad Prism 5 (La Jolla, CA, USA). Statistical analysis for immunohistochemistry studies was done using an unpaired t-test or one-way ANOVA with Tukey's multiple comparison post hoc test. For gene expression studies, analysis was conducted using the Mann-Whitney test or Kruskal-Wallis test (with Dunn's multiple comparison post hoc test) where appropriate. Correlation analyses were done using Pearson's correlation, χ^2 tests, or Fisher's exact test. For all statistical tests done, a p-value of < 0.05 was considered significant.

Chapter 3

3 Results

3.1 An EMT phenotype in GEP-NETs defined by IHC

In pilot real time RT-PCR experiments, we focused on angiogenesis-related genes because GEP-NETs are well known to be highly vascular tumours. We limited our initial survey to primary tumours and liver metastases originating from SI-NETs, as these are the most common of the GEP-NETs. Overall, gene expression results showed elevated vascular endothelial growth factor (VEGF) receptor and ligand expression patterns, increased expression of TGFβ related genes and growth factors, and variations in expression patterns of ECM remodeling genes (**Figure 3.1**). This pattern pointed towards a gene expression profile that facilitates cell guidance and migration, possibly associated with EMT, which led us to confirm these findings using immunohistochemistry (IHC).

The expression of E-cadherin, β-catenin, and vimentin was studied using IHC to determine whether an EMT phenotype exists and how it would be defined in GEP-NETs from the small intestine, pancreas, and rectum. The majority of cases showed an expected epithelial staining pattern of membrane staining E-cadherin and β-catenin, with no vimentin expression (**Figure 3.2**). However, a subset of cases from each GEP-NET site of origin displayed a clear EMT phenotype, i.e. lack of E-cadherin and β-catenin membrane reactivity, with vimentin staining **(Figure 3.3**). There were also cases which show an "in transition" phenotype where E-cadherin and β-catenin membrane staining was intact, as expected in an epithelial derived tumour, but also had vimentin reactivity (**Figure 3.4**). Based on a survey of all the cases represented in the TMAs, we defined an EMT phenotype as loss of E-cadherin/β-catenin membrane reactivity and/or vimentin expression, similar to definitions used by other groups.[61] Using this definition, we saw that a large proportion of P-NET cases and all of the R-NETs included in the study demonstrated an EMT phenotype (**Figure 3.5**). We can further subdivide the EMT phenotype cases to those that have full EMT (loss of both E-cadherin/β-catenin membrane reactivity and vimentin expression), those that are "in transition" (E-

cadherin/β-catenin membrane staining is intact, with vimentin reactivity), or those with "integrity lost" (loss of E-cadherin/β-catenin integrity only with no vimentin reactivity). The remaining cases that have E-cadherin/β-catenin integrity with no vimentin reactivity were considered to have a non-EMT phenotype.

Of interest, there was a notable amount of variability in staining reactivity and percentage of cells staining among core samples from a given tumour (**Figure 3.6**), reinforcing the notion of heterogeneous EMT-associated protein expression within these tumours. This raises the possibility that location of sampling within a given tumour and/or timing of the EMT transition affects the likelihood of capturing the transition in our sampling.

These results show that an EMT phenotype exists among GEP-NETs, to varying degrees of transition, suggesting that EMT does occur in these tumours. Furthermore, there is a higher prevalence of EMT among GEP-NETs originating from the pancreas and distal colon/rectal region which may explain why these tumours tend to be clinical more aggressive. However, EMT could be occurring more frequently than observed due to intratumoural heterogeneity and the possibility of failing to sample an area of EMT in a tumour that has undergone it.

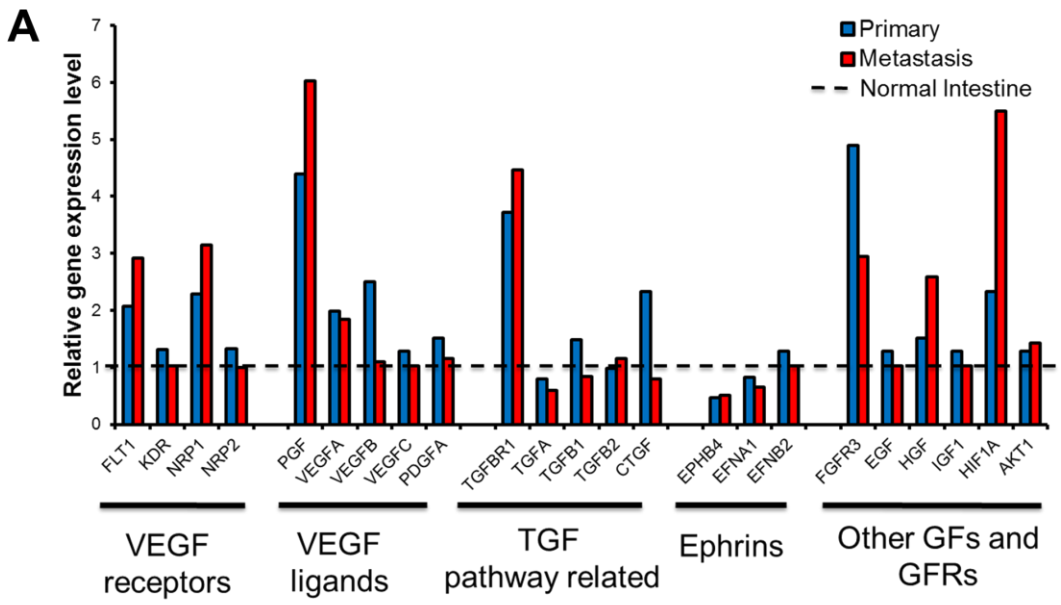
A
Relative gene expression level
Primary
Metastasis
Normal Intestine
FLT1
KDR
NRP1
NRP2
PGF
VEGFA
VEGFB
VEGFC
PDGFA
TGFBR1
TGFA
TGFB1
TGFB2
CTGF
EPHB4
EFNA1
EFNB2
FGFR3
EGF
HGF
IGF1
HIF1A
AKT1
VEGF receptors
VEGF ligands
TGF pathway related
Ephrins
Other GFs and GFRs

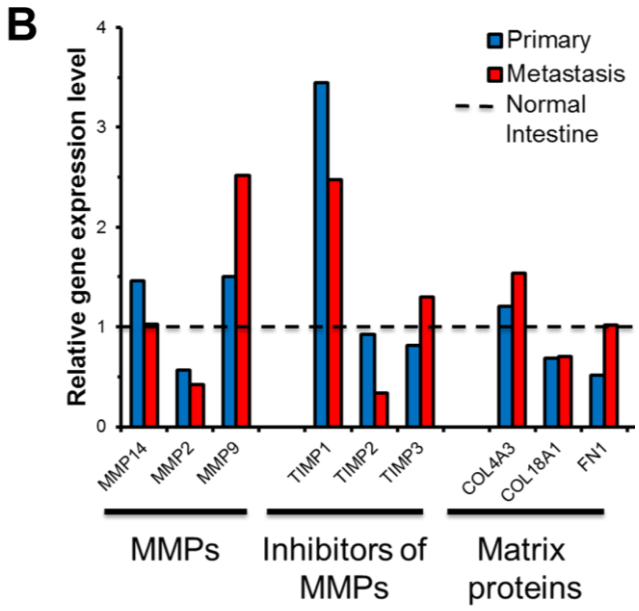
B
Relative gene expression level
Primary
Metastasis
Normal Intestine
MMP14
MMP2
MMP9
TIMP1
TIMP2
TIMP3
COL4A3
COL18A1
FN1
MMPs
Inhibitors of MMPs
Matrix proteins

Figure 3.1. Relative gene expression levels of selected genes of interest from FFPE primary and liver metastasis samples of SI-NETs compared to normal small intestinal epithelium.

(A) Expression levels of vascular endothelial growth factor receptors and ligands, transforming growth factor related genes, ephrins and other growth factors and receptors. (B) Expression levels of matrix and matrix remodelling proteins. [Primary tumours n = 9; Metastasis n = 4; Normal intestine n = 3].

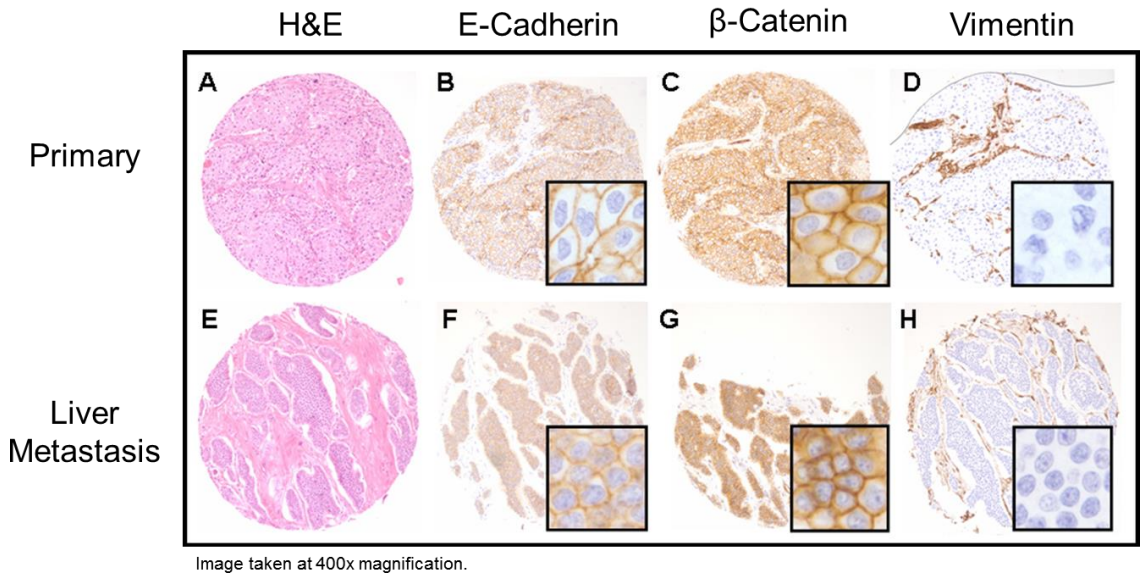

Figure 3.2. Representative case of non-EMT phenotype in SI-NETs.

Epithelial phenotype illustrated by membrane staining for E-cadherin and β-catenin in the absence of vimentin staining. Insets showing higher magnification.

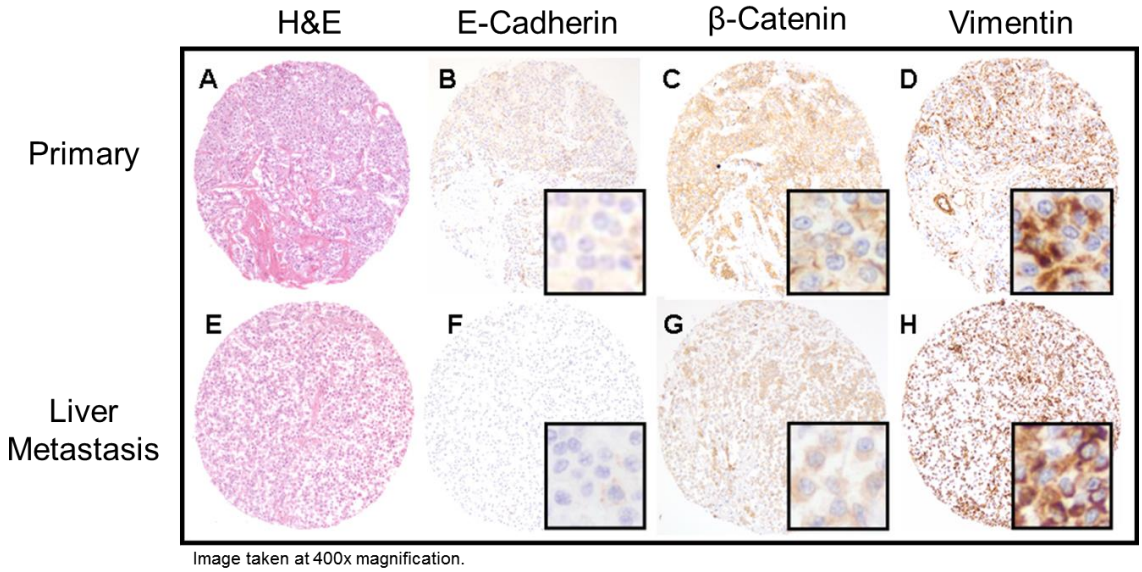

Figure 3.3. Representative case of EMT phenotype in SI-NETs.

Loss of membrane E-cadherin and β-catenin immunoreactivity and strong vimentin staining reflects a possible EMT event and is seen in both primary and liver metastasis. Insets showing higher magnification.

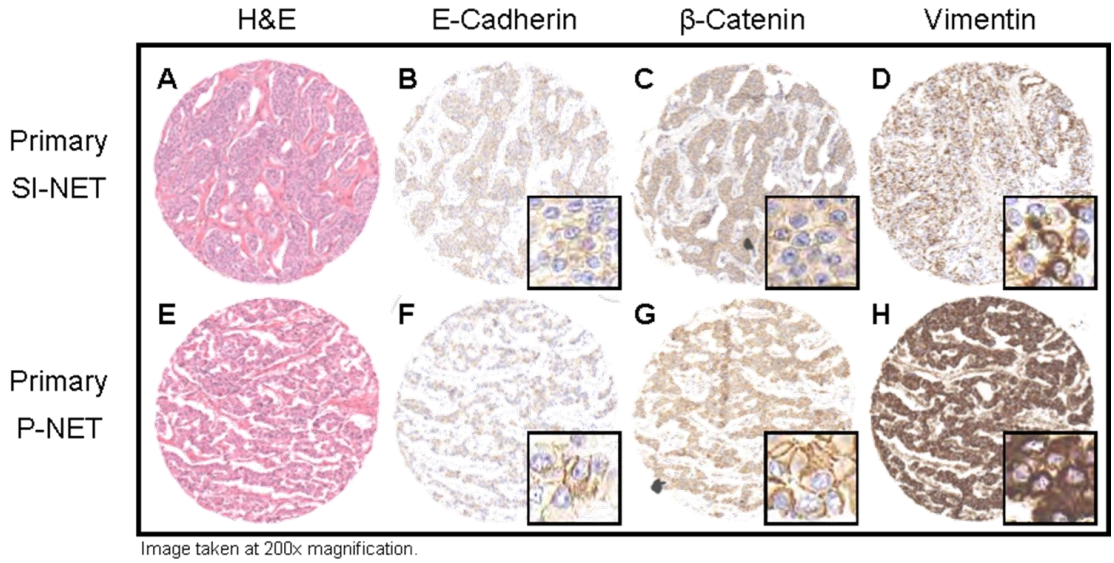

Figure 3.4. Representative cases of primary GEP-NETs in transition between an epithelial and mesenchymal phenotype.

Potential tumor cell phenotype change as illustrated by membrane staining of E-cadherin and β-catenin along with strong vimentin staining. Insets showing higher magnification.

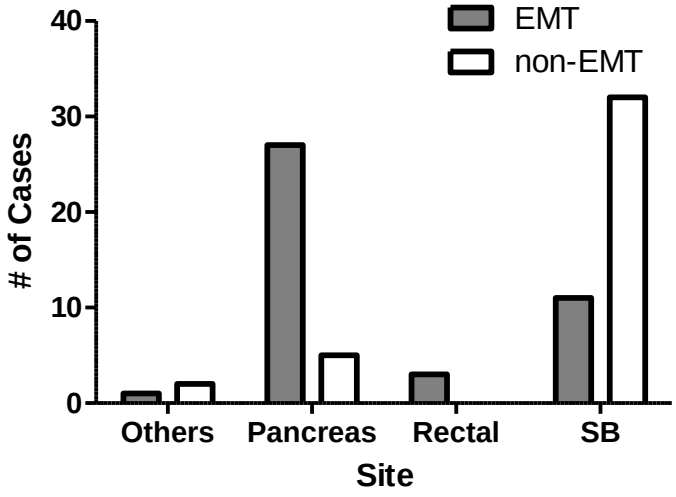

Figure 3.5. Breakdown of cases with or without an EMT phenotype by site of origin. [SB = small bowel/intestine]

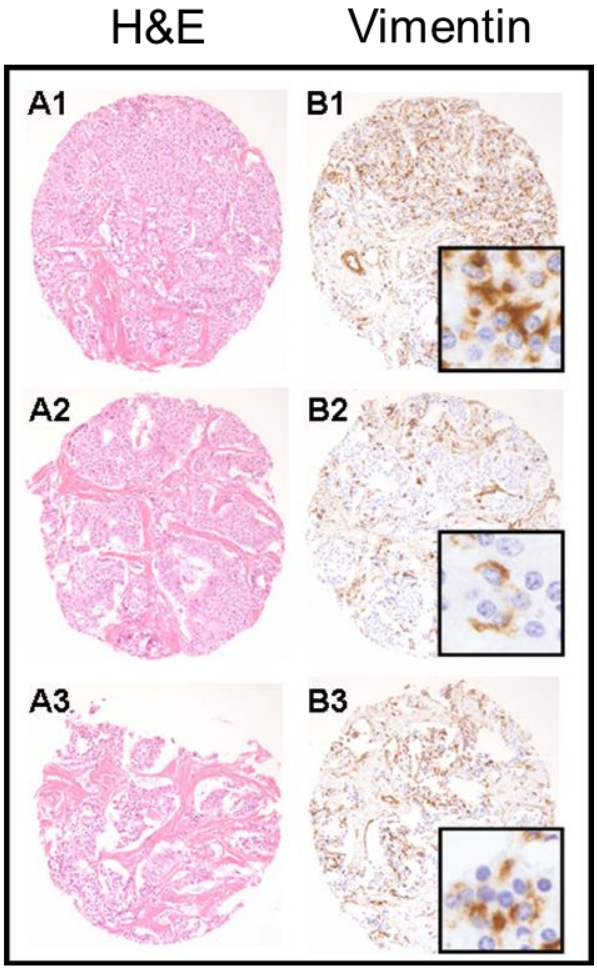

Figure 3.6. Core biopsy replicates within a given case showing variable levels of staining intensity and percentage of cells staining.

Differential expression levels of vimentin within a tumour mass demonstrates its heterogeneity and suggests that different areas of the tumour can undergo EMT at different stages in a given time point. Insets showing higher magnification.

3.2 EMT-associated gene expression pathways

To determine what pathways are involved in the EMT-phenotype we observed in our group of GEP-NETs, we decided to perform a comprehensive overview of gene expression studies in a number of related pathways known to be active in GEP-NETs or involved in EMT. In doing so, we were able to see differences in gene expression between primary and metastatic lesions as well as differences among GEP-NETs from different anatomical areas.

We followed up our results with a commercial EMT specific "profiler plate" (real-time RT-PCR panel) and expanded our scope to encompass GEP-NETs from different anatomical locations to determine whether EMT related genes were similarly upregulated at these sites (**Figure 3.7**). While all showed increased expression for certain EMT associated genes, the magnitude of change differed amongst the tumour groups. P-NETs consistently had the greatest fold change increases for genes such as ZEB1, TGF-β1, TGF-β3, MMP9, fibronectin 1 (FN1) and an assortment of collagens. Interestingly, there was an increase in BMP1 and BMP2 expression among SI-NETs which was not seen in P-NETs or R-NETs. High tissue inhibitor of metalloproteinase 1 (TIMP1) expression in these tumours was apparent and to be expected as a normal neuroendocrine trait according to literature.[64]

To round out our comprehensive overview of GEP-NETs, we included panels for genes associated with the mTOR and PI3K-AKT pathways (**Figure 3.8** and **Figure 3.9**). As previously mentioned in the introduction, the PI3K-AKT/mTOR pathway has been demonstrated to have a key role in GEP-NET tumorigenesis. Furthermore, recent studies have revealed that mTOR activation, via mTORC2, is responsible for the translational regulation leading to changes in cell size and invasion resulting from TGF-β-signalling pathway activation.[65, 66] Therefore, there certainly may be linkages between TGFβ and mTOR pathways. In genes that overlap these two panels, such as AKT1, 2, and 3, we see similar patterns of expression giving us confidence in assay consistency. Notable observations include the elevated expression level of hypoxia inducible factor 1 alpha (HIF1α) and insulin-like growth factor-binding protein 3 (IGFBP3) in the P-NETs.

These gene expression patterns corroborate with the EMT expression profile illustrated by the initial angiogenesis array. The EMT related gene panel points towards the TGF-β signaling pathway with upregulation of TGF-β1 ligand and SMAD2 expression, which relays TGF-β into the cell. The upregulation of ZEB1 transcription factor may be the link defining the effect of SMAD2 transcriptional influence and EMT action as ZEB proteins are known to both interact with SMAD proteins and repress genes responsible for E-cadherin expression leading to EMT. Elevated expression levels of HIF1α and IGFBP3, revealed by the mTOR pathway panels, offer other potential genes that can drive a cell towards EMT and regulate TGFβ-SMAD signalling respectively. Lastly, the expression of BMP proteins, a separate member of the TGFβ superfamily, in SI-NETs suggests that GEP-NETs from different sites could rely on different signalling pathways to drive their EMT progression. Overall these experiments have highlighted that genes belonging to the TGFβ/BMP/SMAD signalling axis are actively transcribed in GEP-NETs.

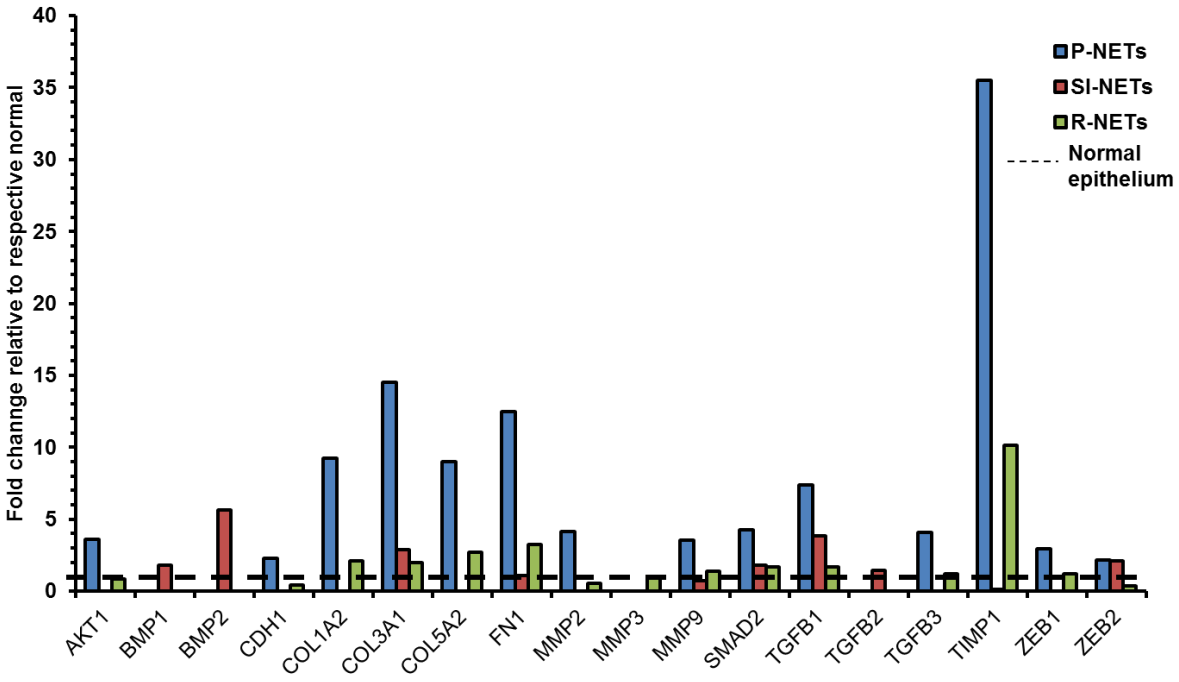

Figure 3.7. Expression of EMT associated genes in P-NETs, SI-NETs, and R-NETs compared against respective site specific normal epithelium.

[P-NET tumour n = 8, normal pancreas n = 8; SI-NET tumour n = 9, normal small intestine n = 9; R-NET tumour n = 8, normal colon/rectum epithelium n = 3].

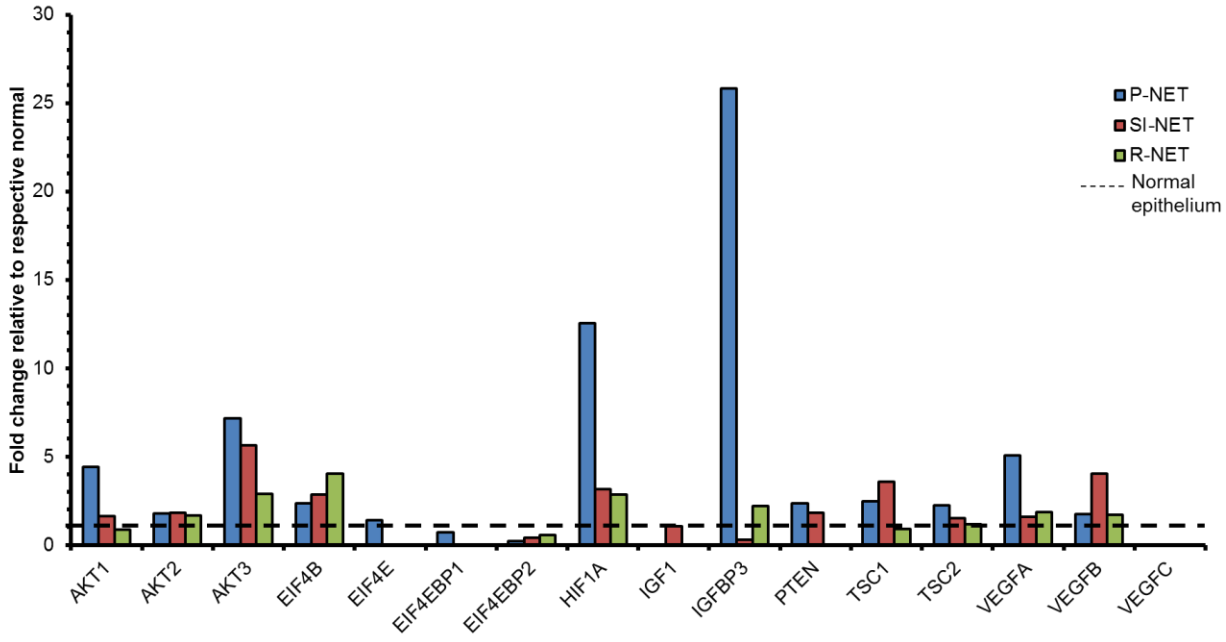

Figure 3.8. Expression of mTOR associated genes in P-NETs, SI-NETs, and R-NETs compared against respective site specific normal epithelium.

[P-NET tumour n = 8, normal pancreas n = 8; SI-NET tumour n = 9, normal small intestine n = 9; R-NET tumour n = 8, normal colon/rectum epithelium n = 3].

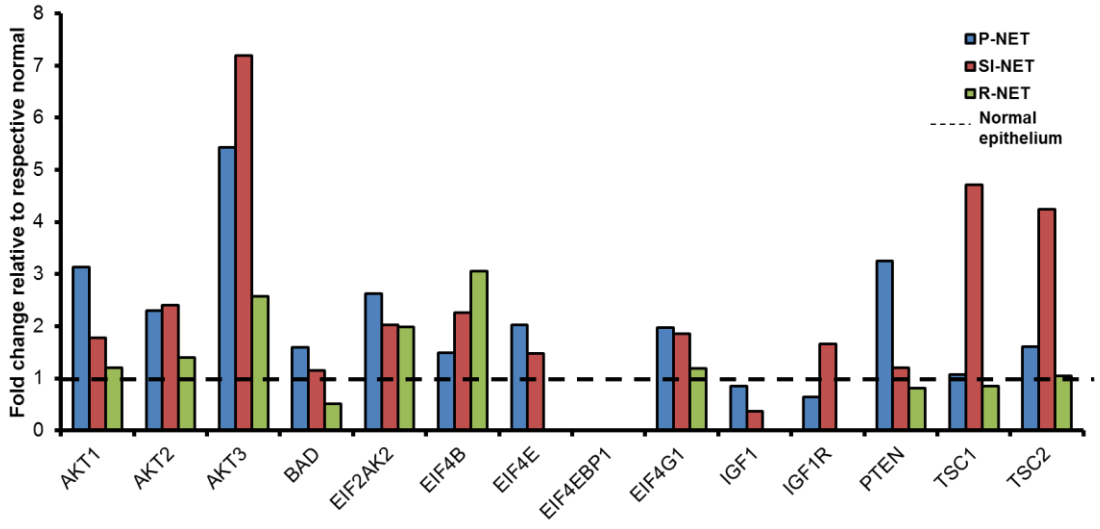

Figure 3.9. Expression of PI3K-AKT associated genes in P-NETs, SI-NETs, and R-NETs compared against respective site specific normal epithelium.

[P-NET tumour n = 8, normal pancreas n = 8; SI-NET tumour n = 9, normal small intestine n = 9; R-NET tumour n = 8, normal colon/rectum epithelium n = 3].

3.3 Correlating EMT gene expression with an EMT phenotype

In the next experiment, we sought to determine whether there was a relatable trend in gene expression with the EMT phenotype. For example, we would expect to see that those cases showing an EMT phenotype at the IHC level would have higher expression of genes related to the mesenchymal phenotype and a decreased expression level of genes related to the epithelial phenotype. Based on our primary data, we selected 17 genes related to EMT signalling to study on a group of 27 cases of P-NETs, some of which only had a primary lesion, and others with both primary and metastasis (**Table 2.5**). TGF-β/BMP receptor and ligand genes were selected to confirm our findings from the RT-PCR panels, along with EMT transcription factors and MMPs known to be associated with this pathway's activation. EMT markers E-cadherin and vimentin were also included as well. Clinical data regarding the grades, and metastatic status was correlated with these cases. We focused on pancreatic NETs due to results showing a higher percentage of an EMT phenotype occurring in these tumours (**Figure 3.5**) compared to GEP-NETs from other sites, as well as the greater magnitude of gene expression changes seen in this group in RT-PCR array studies.

Though most of these results do not reach significance when considering all unique cases of primary and secondary NETs, there is a trend in vimentin mRNA expression between EMT and non-EMT groups (**Figure 3.10**), with a higher expression in the EMT group which is to be expected in a cell transitioning towards a mesenchymal phenotype. This is consistent with transitioning towards a mesenchymal phenotype, and lends credibility to our IHC-based classification of these cases. Significantly higher expression of bone morphogenetic protein receptor 2 (BMPR2), which are part of the TGFβ/BMP superfamily, was observed in the EMT group compared to non-EMT group (**Figure 3.11**). When looking at the EMT phenotype subsets, the only significant difference is in gene expression for ZEB1, an EMT transcription factor linked with TGFβ/BMP downstream signalling, between cases with E-cadherin/β-catenin integrity lost, and the "in transition" subsets (**Figure 3.12**). A similar trend (not statistically significant) is seen with EMT transcription factor TWIST. No remarkable differences can be seen in the

remaining genes studied by their EMT phenotype subsets, including other EMT transcription factors SNAIL and TWIST (**Data not shown**).

When we exclude the metastatic NETs from the group and only consider the primary tumours in the group, BMPR2 appears to retain a significantly higher level of expression in the EMT group compared to the non-EMT group (**Figure 3.14, Figure 3.13**). Further dividing this group into the EMT phenotype subsets show no significant differences across the genes studied. (**Data not shown**).

Importantly, we also correlated gene expression differences based on clinical features, including tumour grade, presence or absence of metastasis, and type of metastasis (lymph node versus liver). With respect to grade, vimentin is significantly more highly expressed in G2 tumours, while BMPRIβ and MMP9 are more highly expressed in G1 tumours (**Figure 3.15, Figure 3.16**). E-cadherin expression is significantly elevated among cases with no known metastasis compared to those with some metastasis (**Figure 3.17**). No other differences were observed (**Figure 3.18**). When we further explore the type of metastasis into groupings of no metastasis, lymph node only metastasis, and liver metastasis (with or without lymph node involvement), the only difference in gene expression is seen in MMP2 where there is a higher expression in the no metastasis group compared to the liver metastasis group (**Figure 3.19, Figure 3.20**).

Although there were few differences in gene expression between EMT and non-EMT group, these experiments revealed several interesting findings. The significantly higher expression of EMT transcription factor ZEB1 among cases "in transition" compared to "integrity lost only", as well as similar trends in TWIST, suggests that gene transcriptional changes are more important prior to the full phenotypic onset of EMT, and that after EMT is achieved, their elevated expression is no longer necessary. The significantly elevated gene expression levels of vimentin, an intermediate filament typically expressed by mesenchymal cells, may indicate that as these tumours acquire more mesenchymal traits, they become more clinically aggressive. Finally, having robust E-cadherin gene expression seems to be a positive sign for tumours that have yet to

metastasize, possibly because the cell-cell contacts mediated by E-cadherin remain present in the tumour.

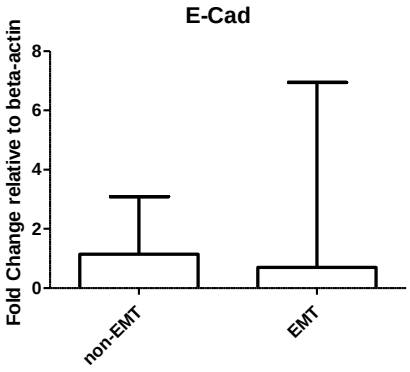
E-Cad
Fold Change relative to beta-actin
0
2
4
6
8
non-EMT
EMT

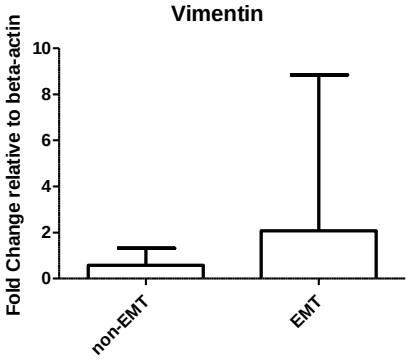
Vimentin
Fold Change relative to beta-actin
0
2
4
6
8
10
non-EMT
EMT

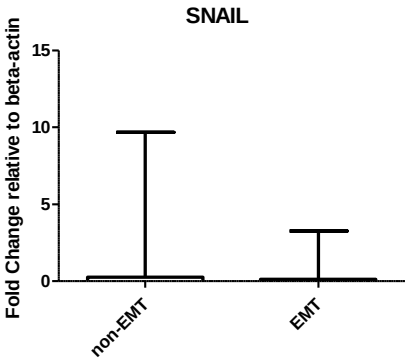
SNAIL
Fold Change relative to beta-actin
0
5
10
15
non-EMT
EMT

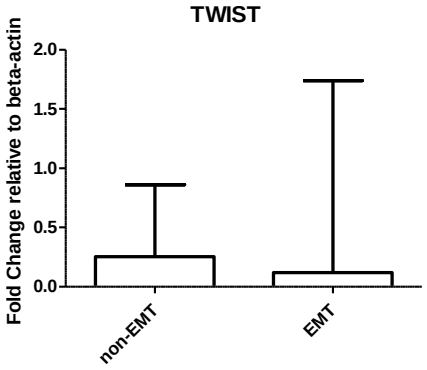
TWIST
Fold Change relative to beta-actin
0.0
0.5
1.0
1.5
2.0
non-EMT
EMT

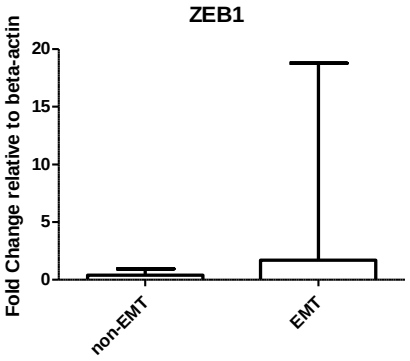
ZEB1
Fold Change relative to beta-actin
0
5
10
15
20
non-EMT
EMT

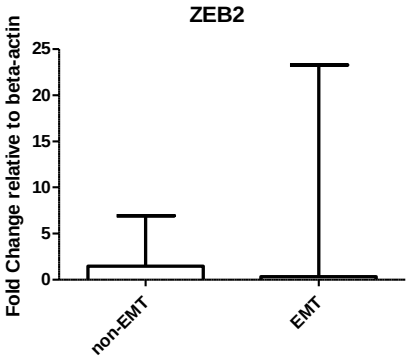
ZEB2
Fold Change relative to beta-actin
0
5
10
15
20
25
non-EMT
EMT

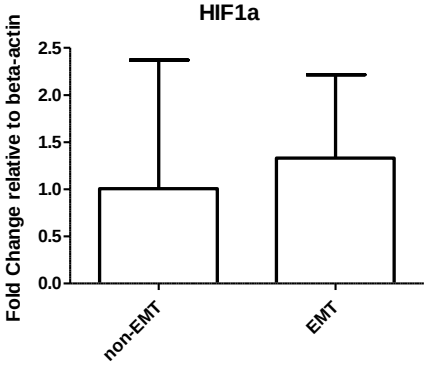
HIF1a
Fold Change relative to beta-actin
0.0
0.5
1.0
1.5
2.0
2.5
non-EMT
EMT

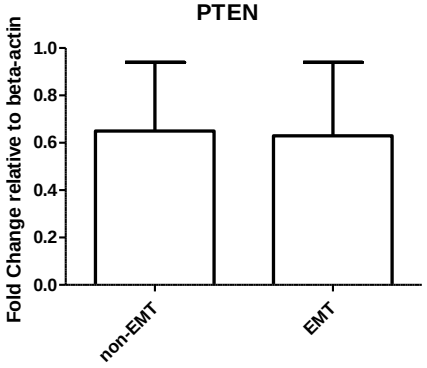
PTEN
Fold Change relative to beta-actin
0.0
0.2
0.4
0.6
0.8
1.0
non-EMT
EMT

Figure 3.10. Expression of EMT related genes in P-NETs based on their EMT phenotype defined by IHC.

Graphs show median with error bars representing interquartile range.
[“non-EMT” n = 8; “EMT” n = 17].

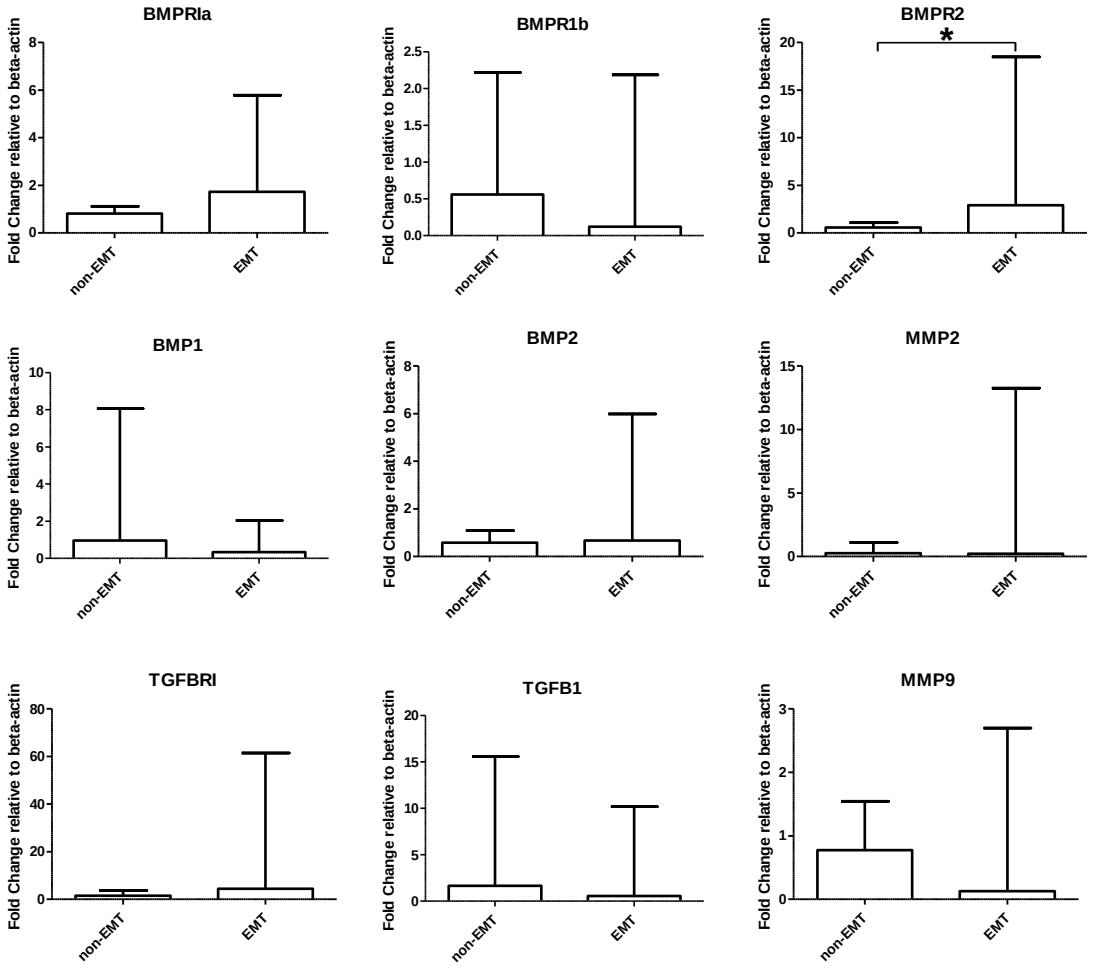

Figure 3.11. Expression of TGFβ/BMP signalling genes and select MMPs in P-NETs based on their EMT phenotype defined by IHC.

Graphs show median with error bars representing interquartile range. Asterisk (*) represents significance level of $p < 0.05$. ["non-EMT" n = 8; "EMT" n = 17].

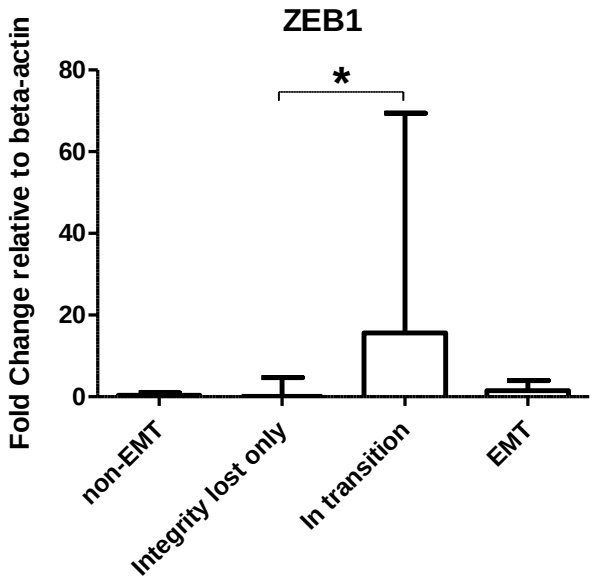

Figure 3.12. Expression of ZEB1 in P-NETs based on their EMT phenotype subset defined by IHC.

Graphs show median with error bars representing interquartile range. Asterisk (*) represents significance level of $p < 0.05$. [“non-EMT” n = 8; “Integrity lost only” n = 5; “In transition” n = 6; “EMT” n = 6].

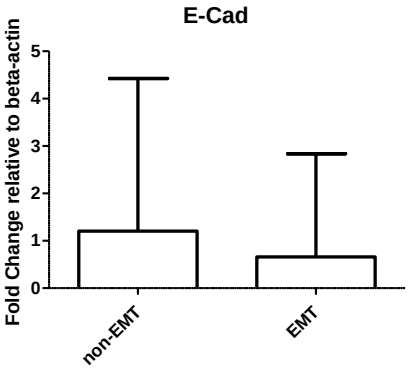
E-Cad
Fold Change relative to beta-actin
0
1
2
3
4
5
non-EMT
EMT

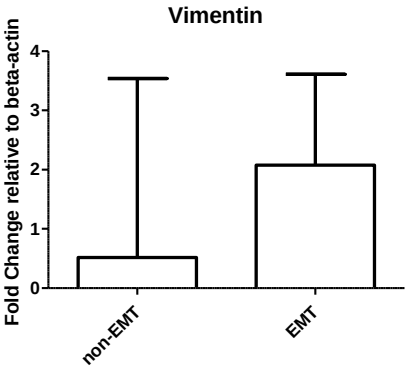
Vimentin
Fold Change relative to beta-actin
0
1
2
3
4
non-EMT
EMT

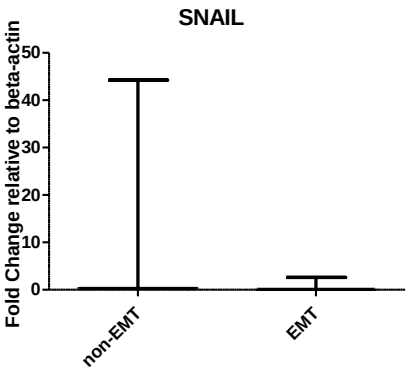
SNAIL
Fold Change relative to beta-actin
0
10
20
30
40
50
non-EMT
EMT

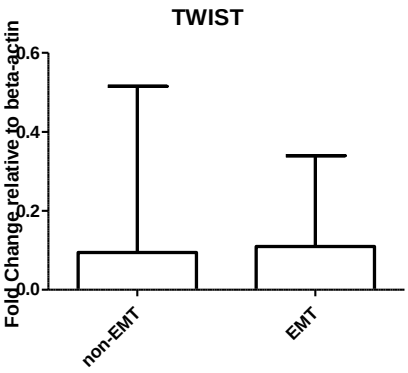
TWIST
Fold Change relative to beta-actin
0.0
0.2
0.4
0.6
non-EMT
EMT

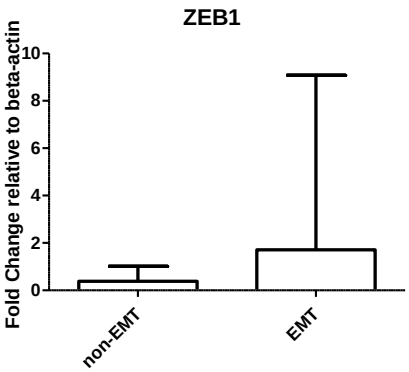
ZEB1
Fold Change relative to beta-actin
0
2
4
6
8
10
non-EMT
EMT

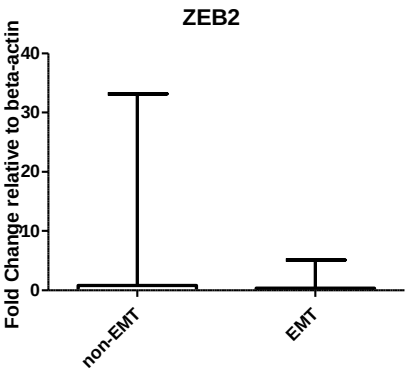
ZEB2
Fold Change relative to beta-actin
0
10
20
30
40
non-EMT
EMT

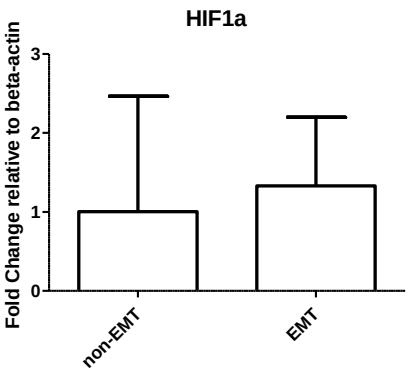
HIF1a
Fold Change relative to beta-actin
0
1
2
3
non-EMT
EMT

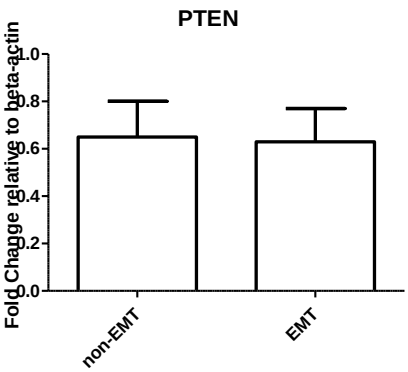
PTEN
Fold Change relative to beta-actin
0.0
0.2
0.4
0.6
0.8
1.0
non-EMT
EMT

Figure 3.13. Expression of EMT related genes in primary P-NETs based on their EMT phenotype defined by IHC.

Graphs show median with error bars representing interquartile range. [“non-EMT” n = 6; “EMT” n = 15].

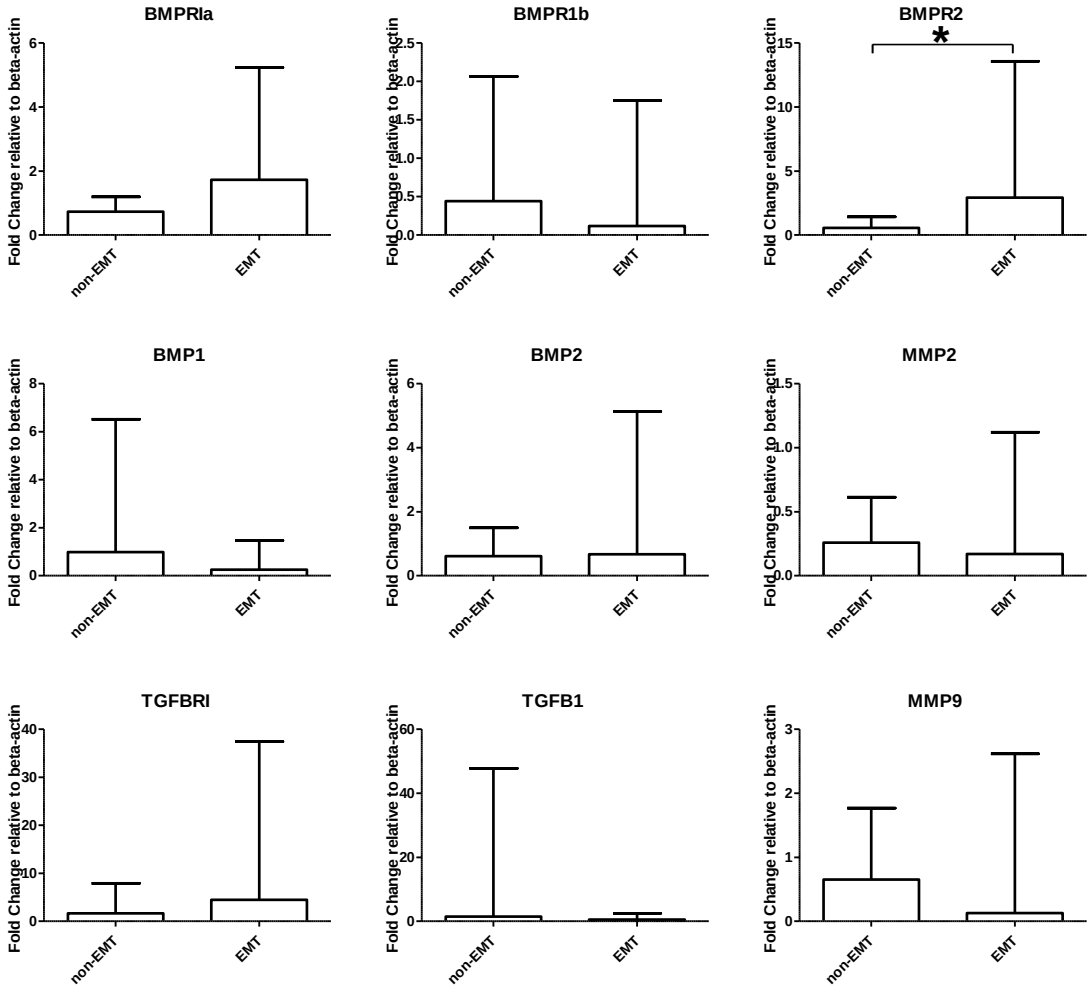

Figure 3.14. Expression of TGFβ/BMP signalling genes and select MMPs in primary P-NETs based on their EMT phenotype defined by IHC.

Graphs show median with error bars representing interquartile range. Asterisk (*) represents significance level of $p < 0.05$. ["non-EMT" n = 6; "EMT" n = 15].

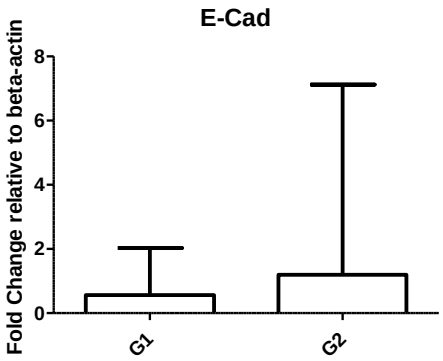
E-Cad
Fold Change relative to beta-actin
0
2
4
6
8
G1
G2

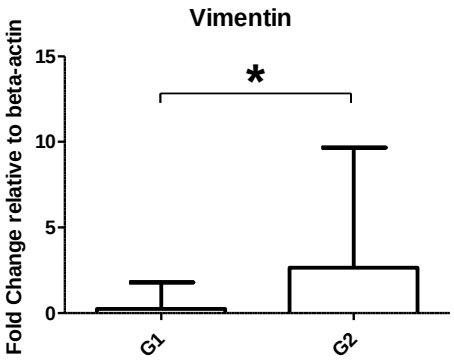
Vimentin
Fold Change relative to beta-actin
0
5
10
15
*
G1
G2

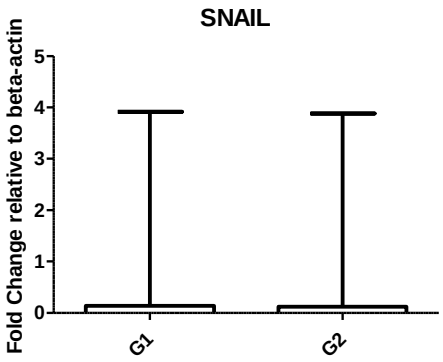
SNAIL
Fold Change relative to beta-actin
0
1
2
3
4
5
G1
G2

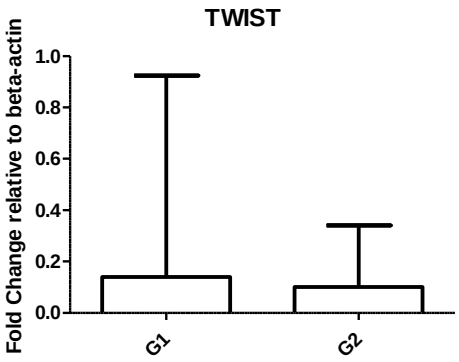
TWIST
Fold Change relative to beta-actin
0.0
0.2
0.4
0.6
0.8
1.0
G1
G2

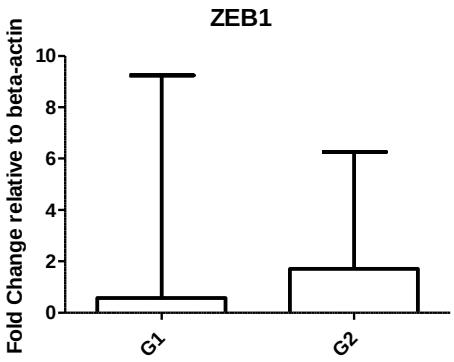
ZEB1
Fold Change relative to beta-actin
0
2
4
6
8
10
G1
G2

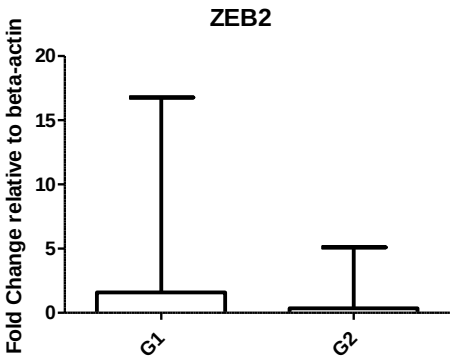
ZEB2
Fold Change relative to beta-actin
0
5
10
15
20
G1
G2

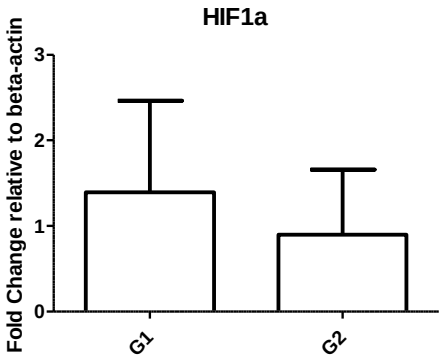
HIF1a
Fold Change relative to beta-actin
0
1
2
3
G1
G2

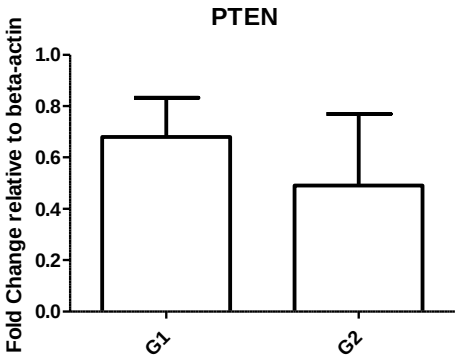
PTEN
Fold Change relative to beta-actin
0.0
0.2
0.4
0.6
0.8
1.0
G1
G2

Figure 3.15. Expression of EMT related genes in primary P-NETs based on grade. Graphs show median with error bars representing interquartile range. Asterisk (*) represents significance level of $p < 0.05$. ["G1" n = 10; "G2" n = 11].

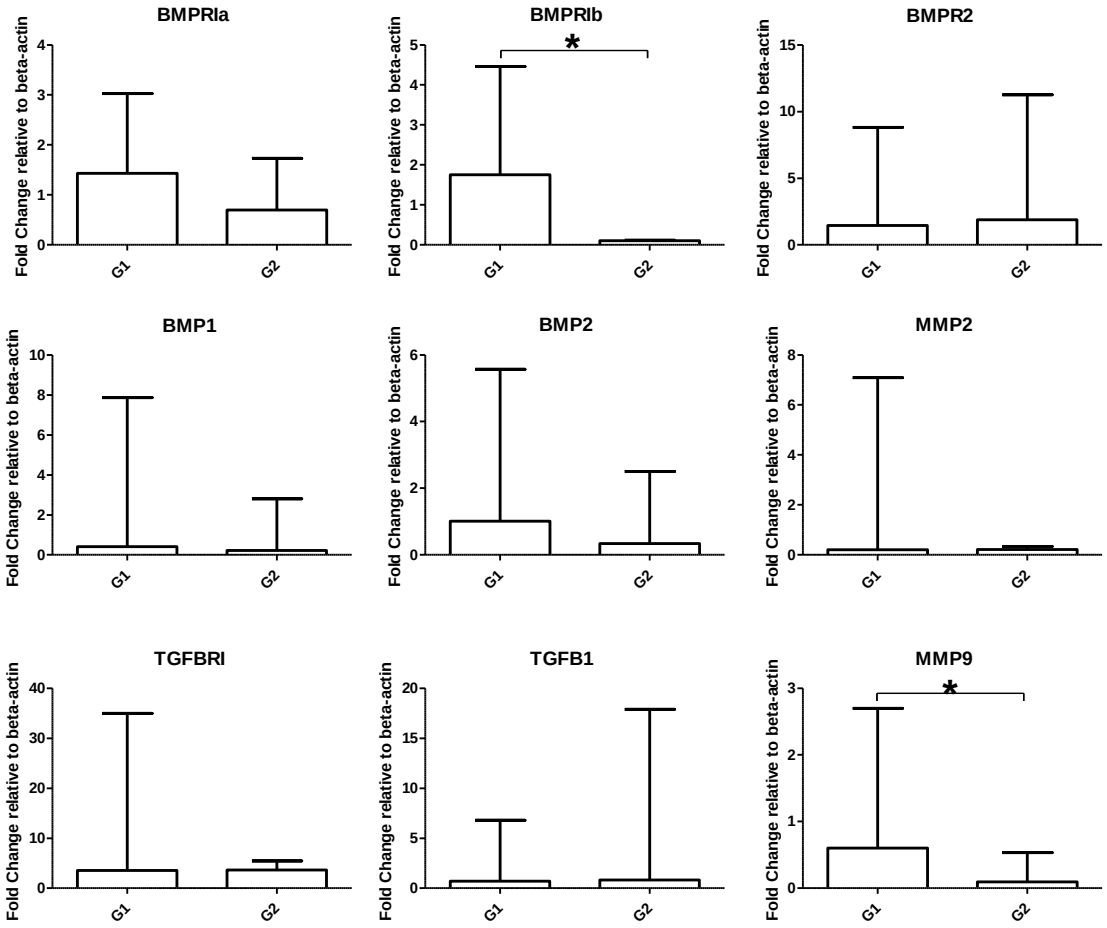

Figure 3.16. Expression of TGFβ/BMP signalling genes and select MMPs in primary P-NETs based on grade.

Graphs show median with error bars representing interquartile range. Asterisk (*) represents significance level of $p < 0.05$. ["G1" n = 10; "G2" n = 11].

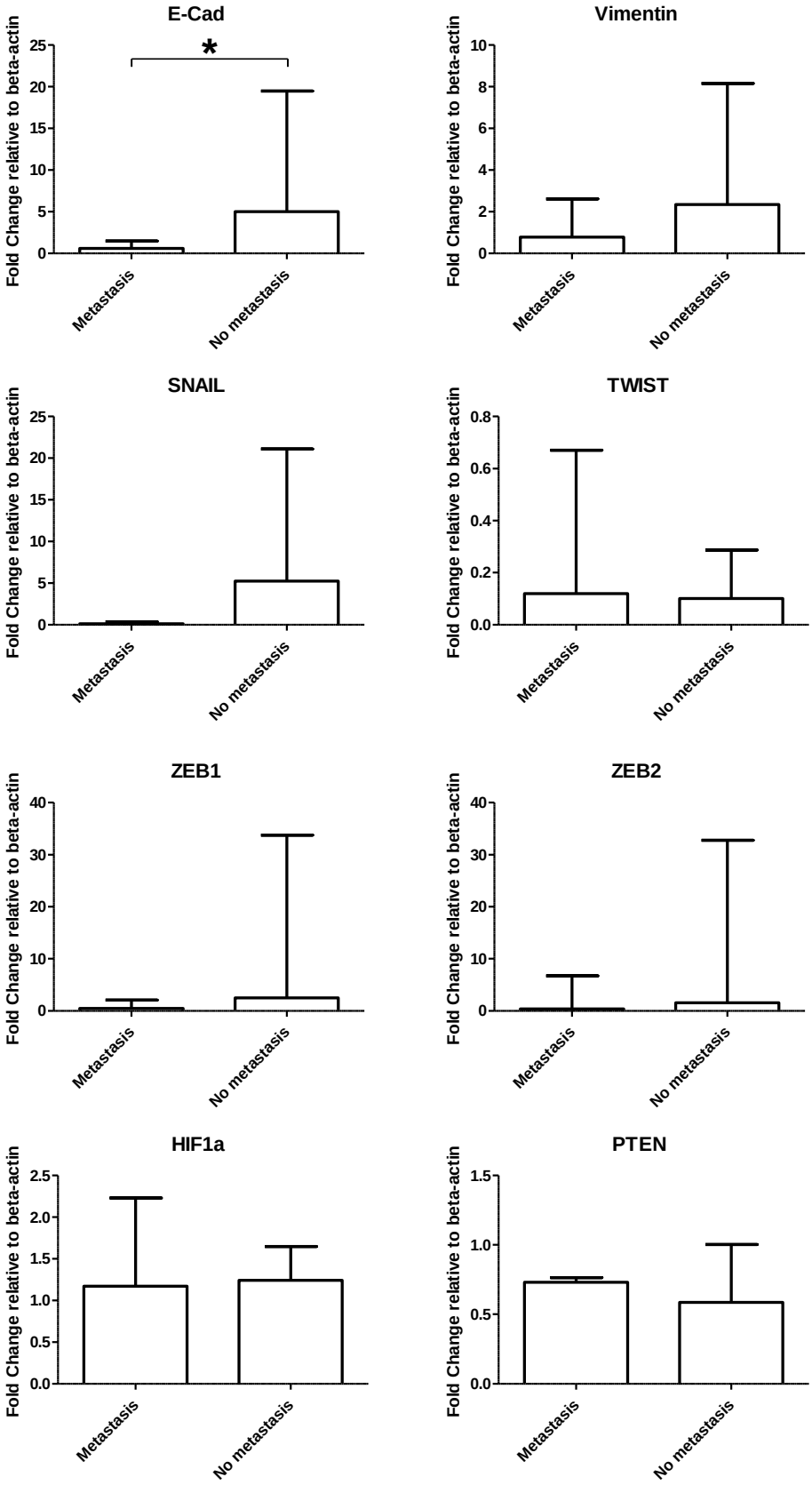
E-Cad
*
Fold Change relative to beta-actin
25
20
15
10
5
0
Metastasis
No metastasis
Vimentin
Fold Change relative to beta-actin
10
8
6
4
2
0
Metastasis
No metastasis
SNAIL
Fold Change relative to beta-actin
25
20
15
10
5
0
Metastasis
No metastasis
TWIST
Fold Change relative to beta-actin
0.8
0.6
0.4
0.2
0.0
Metastasis
No metastasis
ZEB1
Fold Change relative to beta-actin
40
30
20
10
0
Metastasis
No metastasis
ZEB2
Fold Change relative to beta-actin
40
30
20
10
0
Metastasis
No metastasis
HIF1a
Fold Change relative to beta-actin
2.5
2.0
1.5
1.0
0.5
0.0
Metastasis
No metastasis
PTEN
Fold Change relative to beta-actin
1.5
1.0
0.5
0.0
Metastasis
No metastasis

Figure 3.17. Expression of EMT related genes in primary P-NETs based on presence or absence of metastasis.

Graphs show median with error bars representing interquartile range. Asterisk (*) represents significance level of $p < 0.05$. ["Metastasis" n = 14; "No metastasis" n = 8].

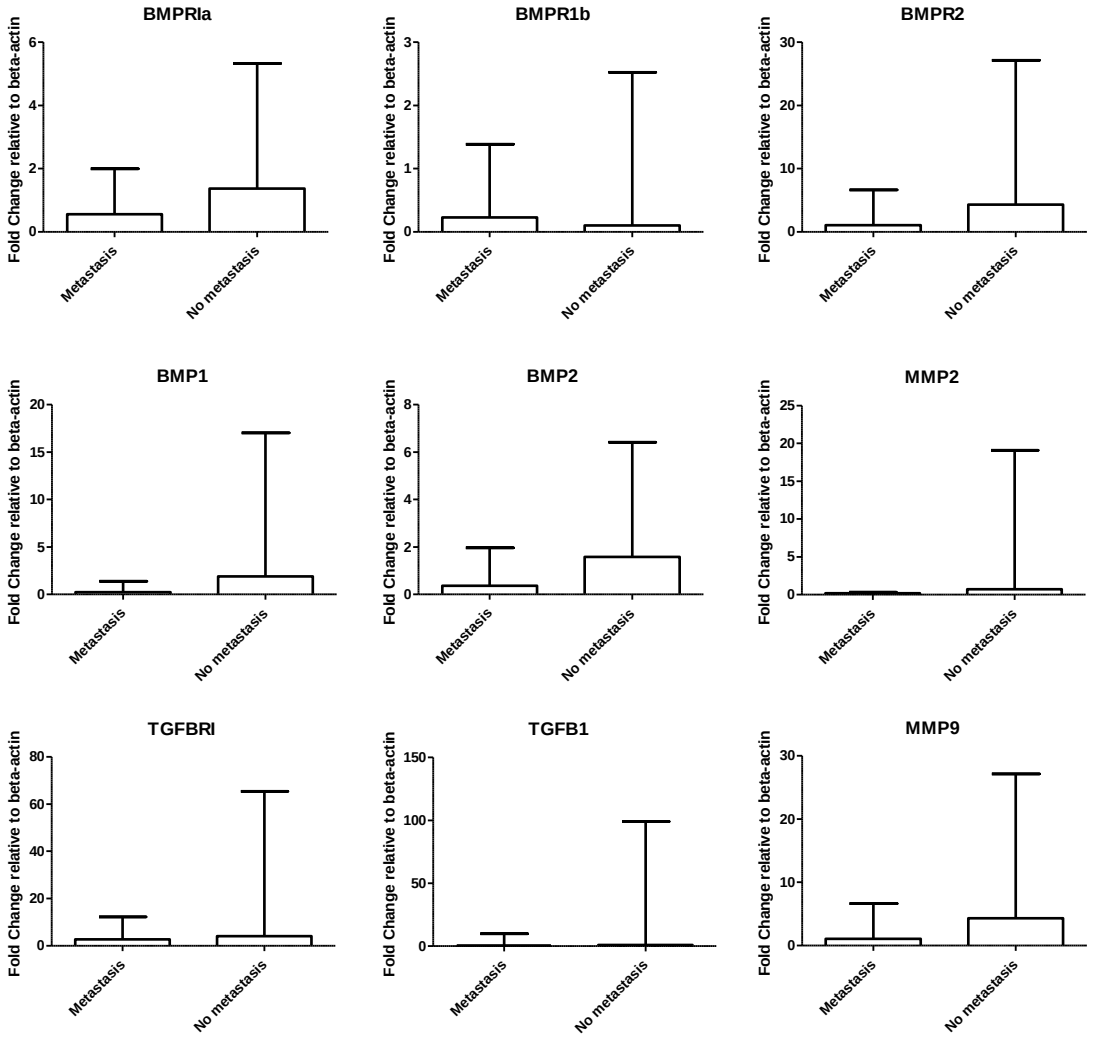

Figure 3.18. Expression of TGFβ/BMP signalling genes and select MMPs in primary P-NETs based on presence or absence of metastasis.

Graphs show median with error bars representing interquartile range. ["Metastasis" n = 14; "No metastasis" n = 8].

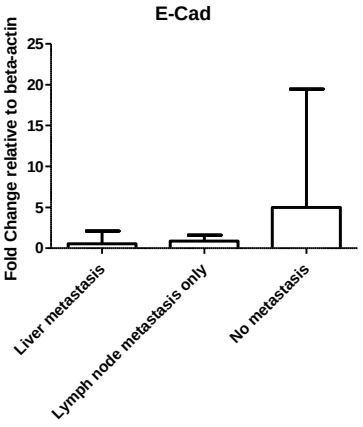
E-Cad
Fold Change relative to beta-actin
25
20
15
10
5
0
Liver metastasis
Lymph node metastasis only
No metastasis

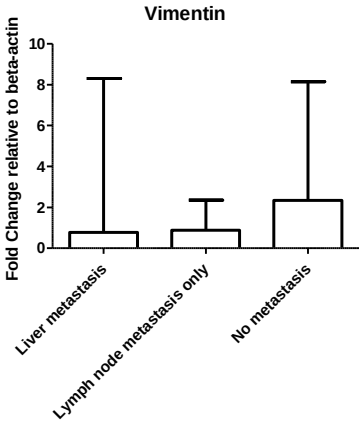
Vimentin
Fold Change relative to beta-actin
10
8
6
4
2
0
Liver metastasis
Lymph node metastasis only
No metastasis

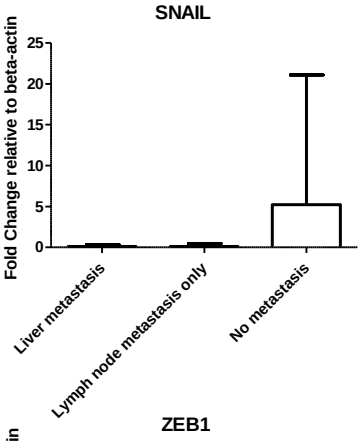
SNAIL
Fold Change relative to beta-actin
25
20
15
10
5
0
Liver metastasis
Lymph node metastasis only
No metastasis

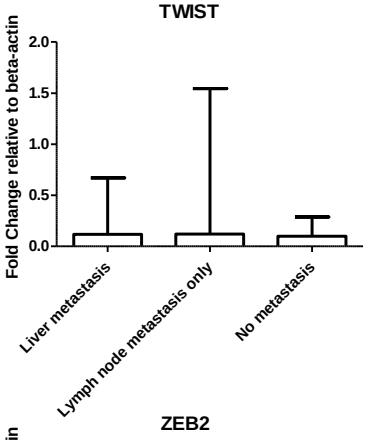
TWIST
Fold Change relative to beta-actin
2.0
1.5
1.0
0.5
0.0
Liver metastasis
Lymph node metastasis only
No metastasis

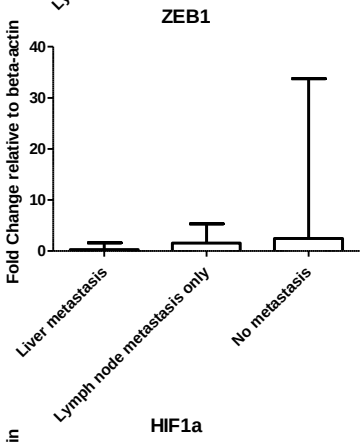
ZEB1
Fold Change relative to beta-actin
40
30
20
10
0
Liver metastasis
Lymph node metastasis only
No metastasis

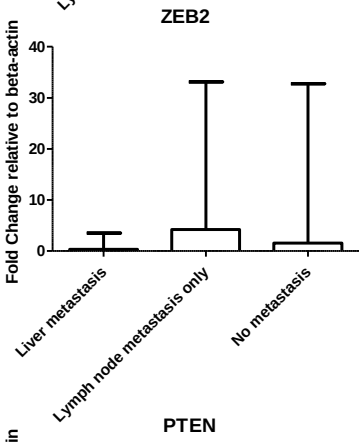
ZEB2
Fold Change relative to beta-actin
40
30
20
10
0
Liver metastasis
Lymph node metastasis only
No metastasis

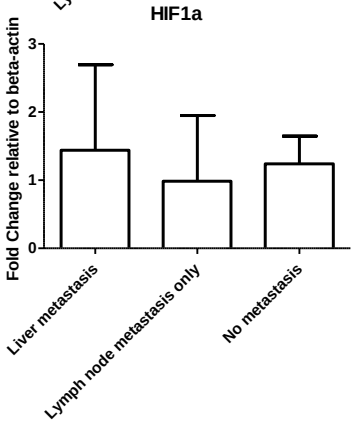
HIF1a
Fold Change relative to beta-actin
3
2
1
0
Liver metastasis
Lymph node metastasis only
No metastasis

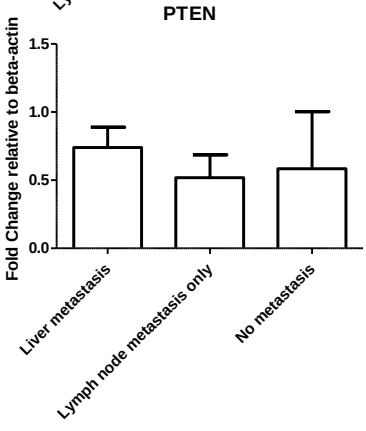
PTEN
Fold Change relative to beta-actin
1.5
1.0
0.5
0.0
Liver metastasis
Lymph node metastasis only
No metastasis

Figure 3.19. Expression of EMT related genes in primary P-NETs based on their metastatic subsets.

Graphs show median with error bars representing interquartile range. [“Liver metastasis” n = 9; “Lymph node metastasis only” n = 4; “No metastasis” n = 8].

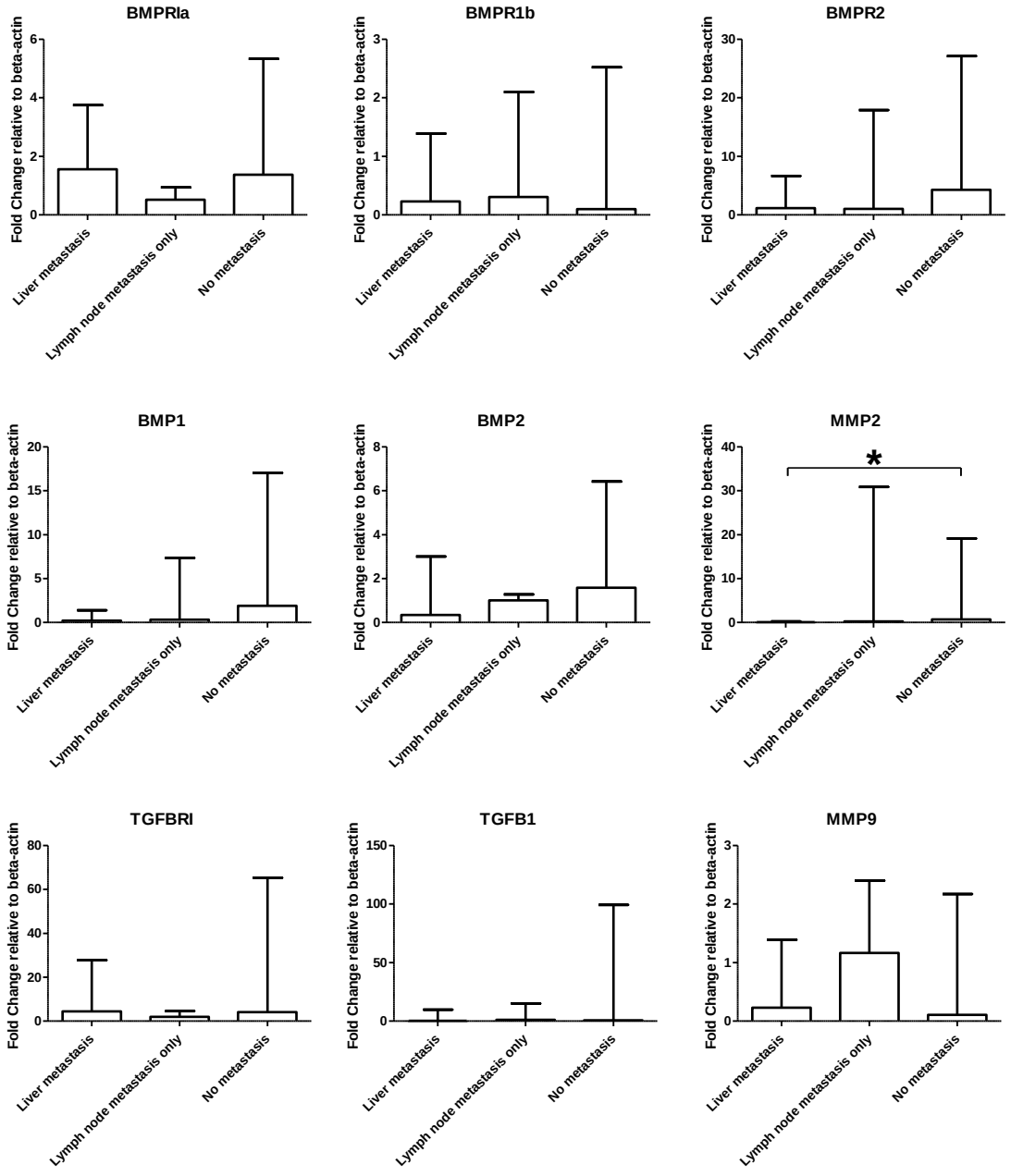

Figure 3.20. Expression of TGFβ/BMP signalling genes and select MMPs in primary P-NETs based on their metastatic subset.

Graphs show median with error bars representing interquartile range. Asterisk (*) represents significance level of $p < 0.05$. ["Liver metastasis" n = 9; "Lymph node metastasis only" n = 4; "No metastasis" n = 8].

3.4 SNAIL/SLUG protein expression among GEP-NETs

To support the involvement of EMT in GEP-NETs, we investigated to see whether well-established EMT transcription factors were detectable via IHC in the tumours represented in the TMAs. We also wanted to determine whether there was a relationship between EMT transcription factor expression with the EMT phenotype previously established or the clinical information retained. We set out to study the immunohistochemical profile of SNAIL/SLUG, TWIST, ZEB1 and ZEB2, but we were only able to validate and optimize the SNAIL/SLUG antibody for this study on the TMAs.

We considered the cytoplasmic and nuclear staining of this transcription factor separately when assigning IRS (**Figure 3.21**). There appears to be no correlation between cytoplasmic IRS and nuclear IRS (**Figure 3.22**). No significant differences were apparent for cytoplasmic SNAIL/SLUG staining among the different metastasis grouping, and different EMT phenotype groupings (**Figure 3.23**). However, there was a significantly higher expression of the transcription factor among primary and secondary rectal NETs when compared to their pancreatic and small bowel counterparts (**Figure 3.24**).

On the nuclear staining side, there was a significantly higher nuclear expression of SNAIL/SLUG in the non-EMT grouping within secondary NETs only (**Figure 3.25**). No significant differences are apparent when considering tumour type, site or grade (**Figure 3.26**).

In observing the immunohistochemical staining of a transcription factor, the nuclear staining is far more compelling than cytoplasmic presence given that the nucleus is where these proteins can influence further transcription. However, since there was no correlation between staining observed in the cytoplasm versus the nucleus, the possibility of different gene expression correlations existed. Indeed, it seems that R-NETs had the strongest cytoplasmic reactivity among the other GEP-NETs, but did not differ in nuclear staining. This site-specific difference may be a reflection of how different environments are from one another and how the external influences from each given site could

influence the expression and localization of transcription factor proteins such as SNAIL and SLUG.

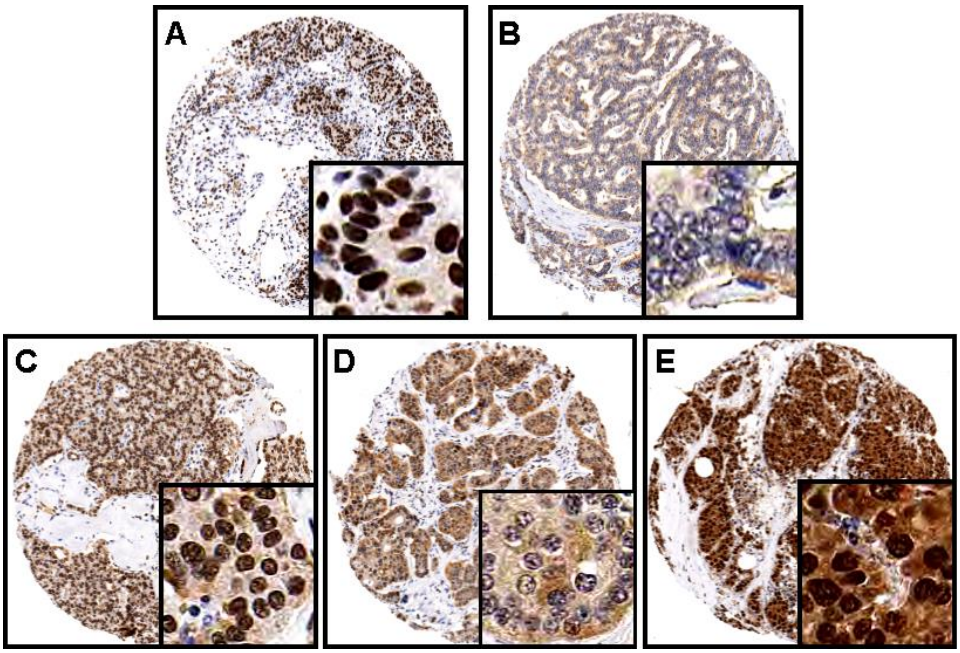

Figure 3.21. Representative images of TMA cores showing nuclear and cytoplasmic SNAIL/SLUG reactivity.

Cases showing strong nuclear but weak cytoplasmic staining (A), compared to those with moderate cytoplasmic staining with no nuclear involvement (B). Overall, R-NETs (E) showed strong reactivity to SNAIL/SLUG compared to SI-NETs (C) and P-NET (D). Insets showing higher magnification.

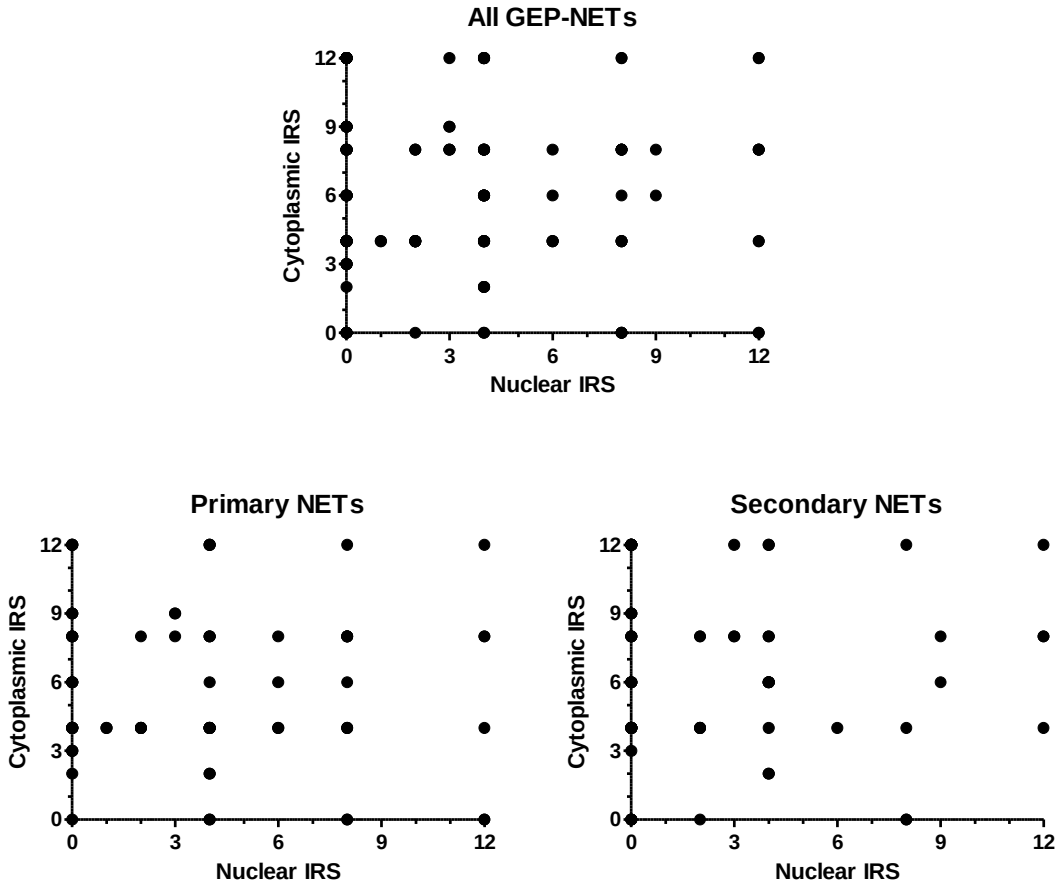

Figure 3.22. Scatterplot of SNAIL/SLUG nuclear expression versus cytosolic expression in primary and secondary NETs.

Pearson's correlation coefficient, r, for "All GEP-NETs", "Primary NETs" and "Secondary NETs" are -0.0479 [p = 0.5568, not significant, n = 149], -0.0564 [p = 0.6167, not significant, n= 76], -0.0066 [p = 0.964, not significant, n = 73] respectively.

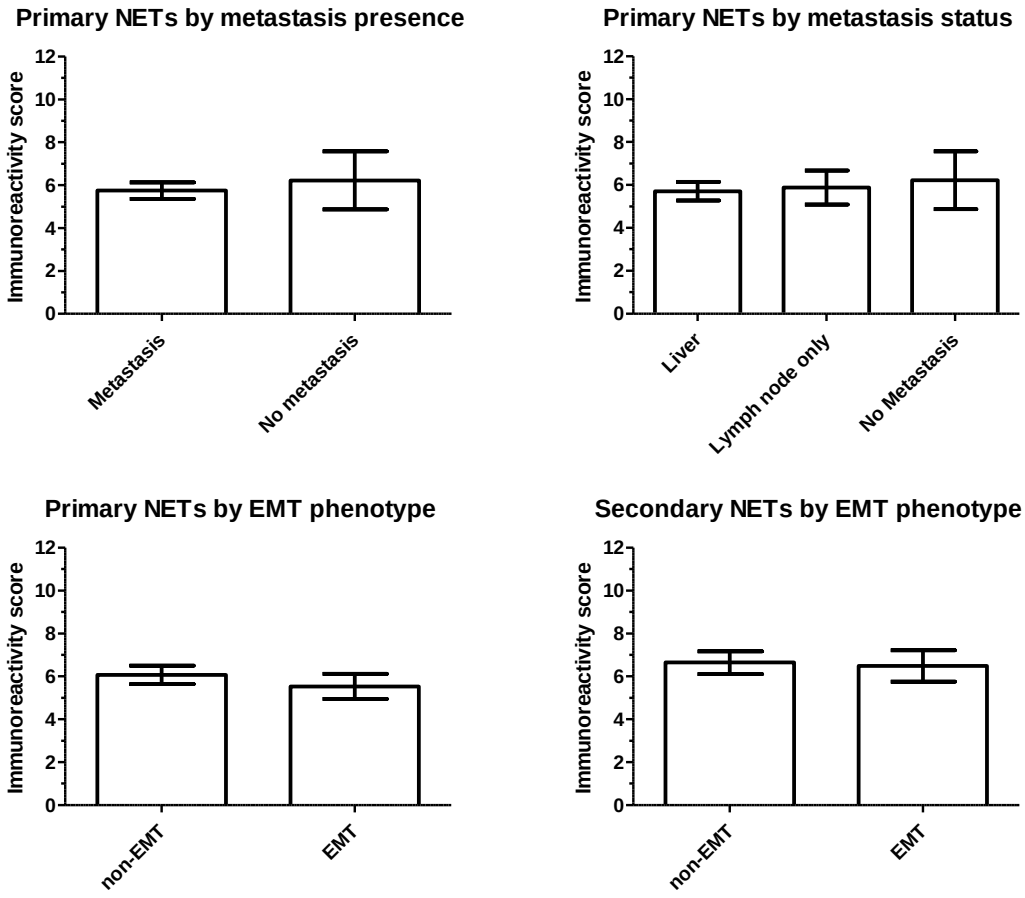

Figure 3.23. Cytoplasmic SNAIL/SLUG reactivity by metastasis status, and EMT phenotype.

Graphs show mean with error bars representing SEM.

[Primary NET "Metastasis" n = 67, "No metastasis" n = 9]

[Primary NET "Liver" n = 55, "Lymph node only" n = 12; "No metastasis" n = 9]

[Primary NET "non EMT" n = 37, "EMT" n = 39]

[Secondary NET "non-EMT" n = 39, "EMT" n = 33]

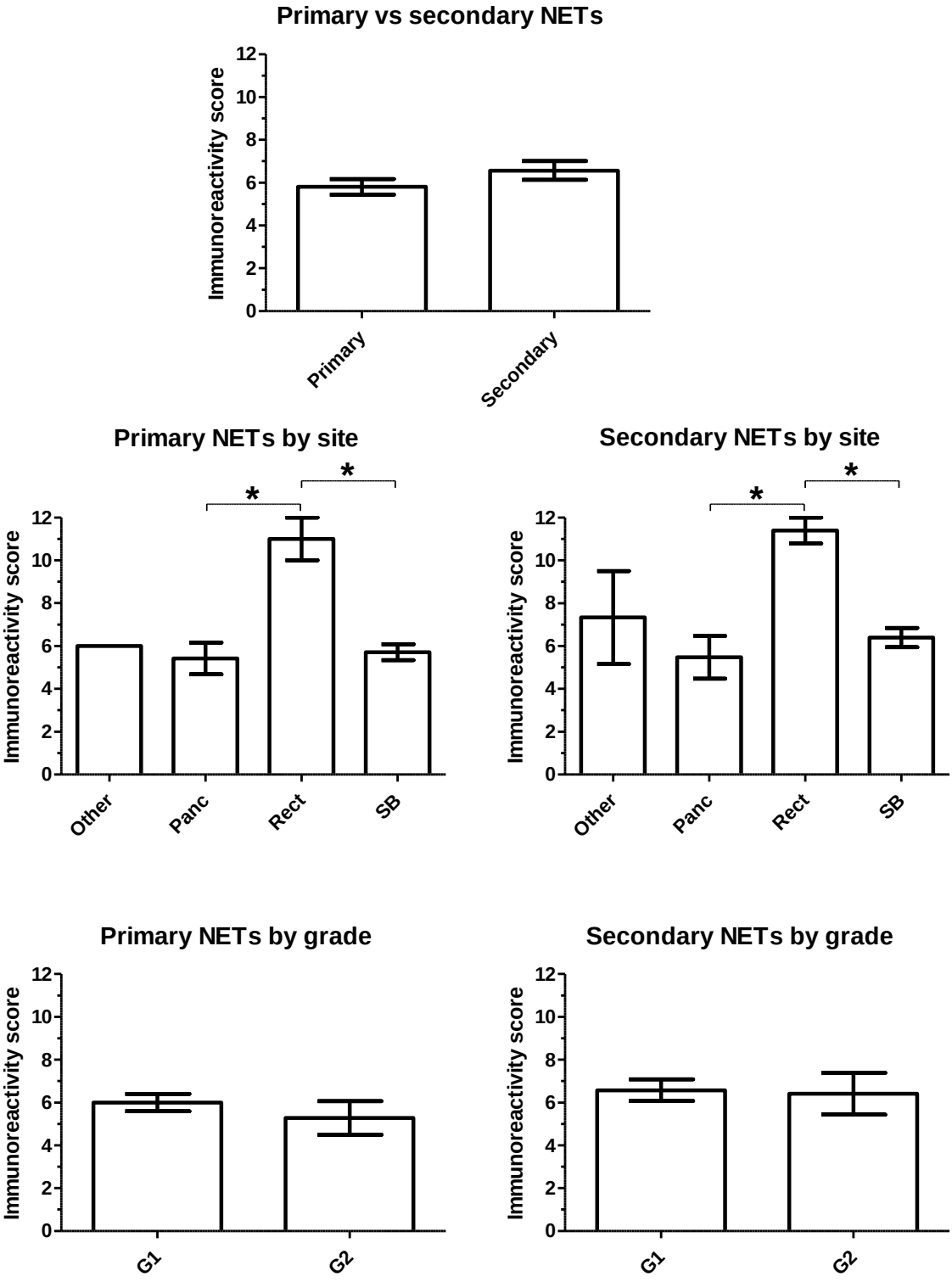
Primary vs secondary NETs
Immunoreactivity score
0
2
4
6
8
10
12
Primary
Secondary
Primary NETs by site
Secondary NETs by site
*
*
Other
Panc
Rect
SB
Primary NETs by grade
Secondary NETs by grade
G1
G2

Figure 3.24. Cytoplasmic SNAIL/SLUG reactivity by overall tumour type, site, and grade.

Graphs show mean with error bars representing SEM. Asterisk (*) represents significance level of $p < 0.05$. n = 76 for primary NETs; n = 73 for secondary NETs.

[Primary NET “Other” n = 2, “Panc” n = 26, “Rect” n = 3, “SB” n = 45]

[Primary NET “G1” n = 51, “G2” n = 21]

[Secondary NET “Other” n = 2, “Panc” n = 26, “Rect” n = 3, “SB” n = 45]

[Secondary NET “G1” n = 50, “G2” n = 18]

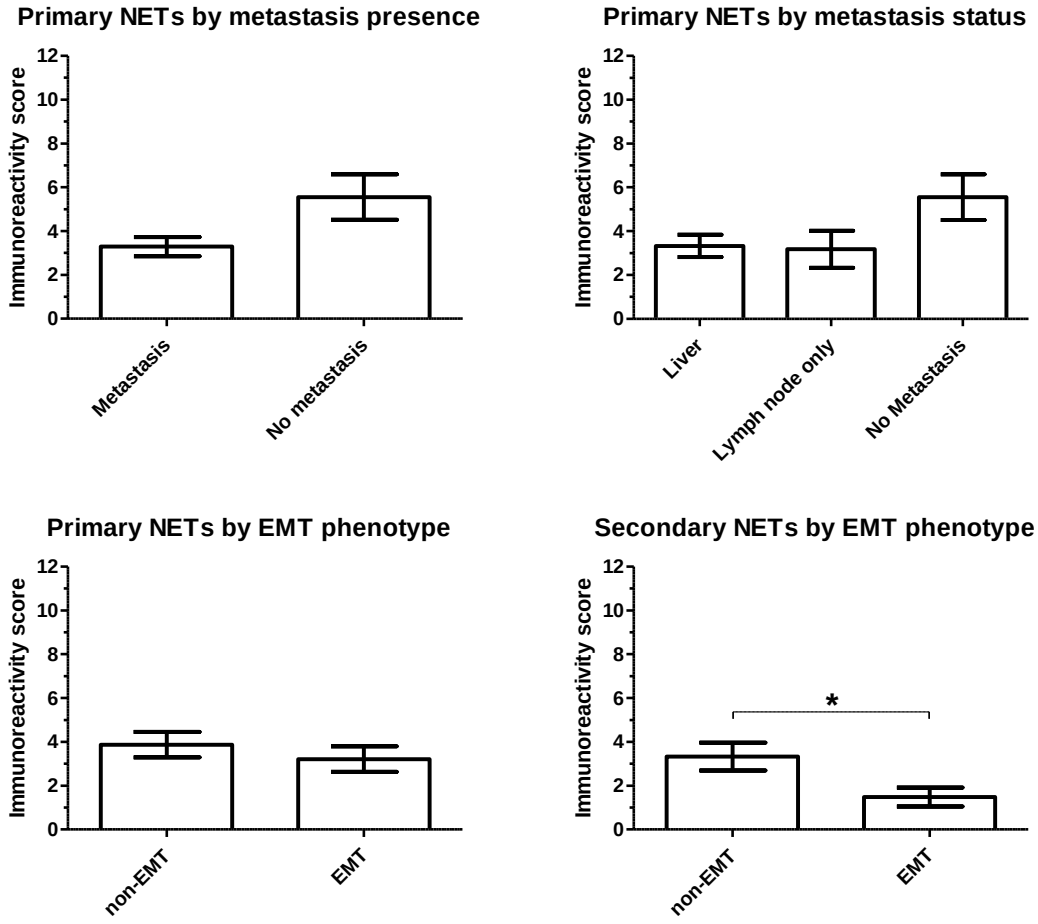

Figure 3.25. Nuclear SNAIL/SLUG reactivity by metastasis status, and EMT phenotype.

Graphs show mean with error bars representing SEM. Asterisk (*) represents significance level of $p < 0.05$.

[Primary NET "Metastasis" n = 67, "No metastasis" n = 9]

[Primary NET "Liver" n = 55, "Lymph node only" n = 12; "No metastasis" n = 9]

[Primary NET "non EMT" n = 37, "EMT" n = 39]

[Secondary NET "non-EMT" n = 39, "EMT" n = 33]

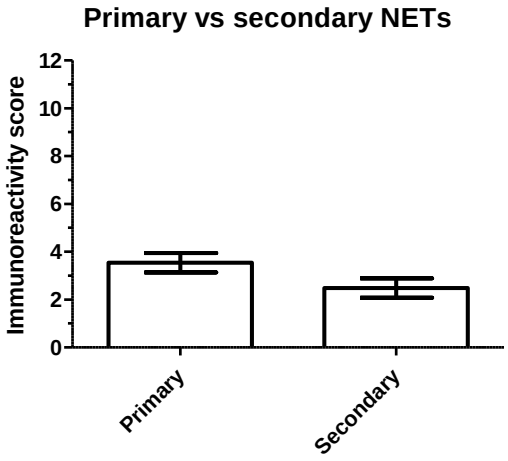
Primary vs secondary NETs
Immunoreactivity score
0
2
4
6
8
10
12
Primary
Secondary

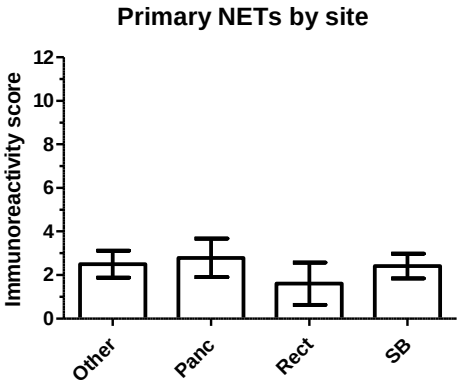
Primary NETs by site
Immunoreactivity score
0
2
4
6
8
10
12
Other
Panc
Rect
SB

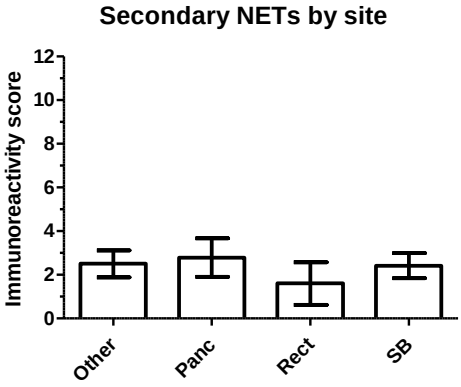
Secondary NETs by site
Immunoreactivity score
0
2
4
6
8
10
12
Other
Panc
Rect
SB

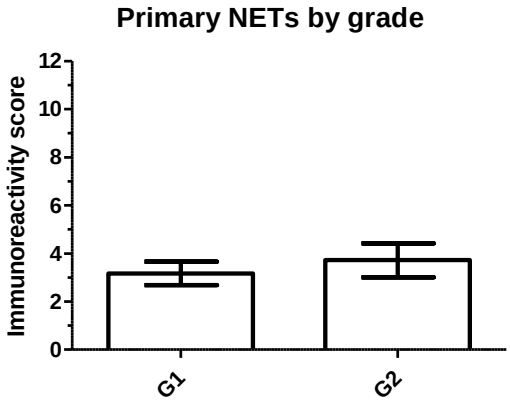
Primary NETs by grade
Immunoreactivity score
0
2
4
6
8
10
12
G1
G2

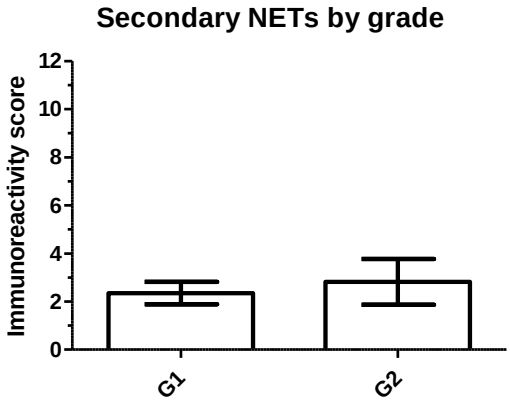
Secondary NETs by grade
Immunoreactivity score
0
2
4
6
8
10
12
G1
G2

Figure 3.26. Nuclear SNAIL/SLUG reactivity by overall tumour type, site, and grade.

Graphs show mean with error bars representing SEM.

[Primary NET “Other” n = 2, “Panc” n = 26, “Rect” n = 3, “SB” n = 45]

[Primary NET “G1” n = 51, “G2” n = 21]

[Secondary NET “Other” n = 2, “Panc” n = 26, “Rect” n = 3, “SB” n = 45]

[Secondary NET “G1” n = 50, “G2” n = 18]

3.5 SMAD immunohistochemistry profile in GEP-NETs

SMAD proteins are the link between the various signalling pathways associated with EMT and the upregulation in the expression of EMT transcription factors. Their presence in an active phosphorylated state and/or nuclear localization can indicate the activity of certain pathways initiating EMT. We looked at the immunoreactivity of several SMAD proteins to determine whether different SMADs, and thereby different signalling pathways, are active among different EMT phenotypes, site of origin, grade, and metastatic state. Specifically, p-SMAD2/3 is the phosphorylated product of TGFβ receptor activity, p-SMAD1/5/8 results from BMP signalling, and SMAD4 is the common SMAD that complexes with either of the other SMADs before translocating into the nucleus.

Phosphorylated SMAD2/3 (p-SMAD2/3) was exclusively reactive in the nucleus with very weak to completely negative reactivity in the cytoplasm uniformly across the cells represented in the TMA cores. Nuclear expression of p-SMAD2/3 is higher among cases with no metastasis (**Figure 3.27**). Although nuclear reactivity does not appear to differ between primary and secondary NETs, primary P-NETs have a significantly higher nuclear immunoreactivity score for p-SMAD2/3 compared to SI-NETs (**Figure 3.28**).

In p-SMAD1/5/8, both nuclear and cytosolic staining was seen among tumour cells and both staining patterns were evaluated. Correlating nuclear IRS with cytosolic IRS revealed a weakly positive relationship among all the GEP-NETs represented and a moderately positive relationship exists in the secondary NETs according to their Pearson's correlation coefficient (**Figure 3.29**). No differences in nuclear or cytosolic reactivity are apparent between metastasis and EMT phenotype groupings (**Figure 3.30**, **Figure 3.32**), although primary P-NETs appear to be more nuclear and cytosolically reactive than SI-NETs (**Figure 3.31, Figure 3.33**). Secondary NETs from other sites outside of the gastrointestinal tract appear to have higher cytosolic reactivity compared to P-NETs and SI-NETs **(Figure 3.33**).

SMAD4 nuclear and cytosolic staining also was seen among tumour cells. Correlating nuclear IRS with cytosolic IRS for this stain showed a very strong positive relationship

among all GEP-NETs even when separating primary and secondary NETs (**Figure 3.34**). SMAD4 nuclear reactivity is higher in cases with no metastasis compared to those with metastases, liver in particular (**Figure 3.35**). Cases with an EMT phenotype also have higher nuclear reactivity compared to non-EMT cases, particularly between cases "in transition" (**Figure 3.35**). Overall, the primary NETs are more nuclear reactive than secondary NETs. However, both show many significant differences in nuclear reactivity among the various sites of origins and grades (**Figure 3.36**). P-NETs and R-NETs have more SMAD4 nuclear reactivity than SI-NETs and miscellaneous NETs. G2 tumours are significantly more nuclear reactive than G1 tumours. The cytosolic reactivity follows a similar profile to their nuclear counterpart. Cases with no metastasis scored significantly higher IRS compared to those with metastases while no differences can be seen within EMT phenotype groupings (**Figure 3.37**). While the overall scores between primary and secondary NETs differ significantly, both demonstrate significantly higher IRS in P-NETs compared to SI-NETs, and G2 tumours compared to G1 tumours (**Figure 3.38**). P-NETs had higher SMAD reactivity across all the SMAD proteins investigated which may relate to the higher reactivity these tumours had for SNAIL/SLUG and greater fold change differences seen in ZEB1 and 2 compared to the other sites (**Figure 3.39**).

The SMAD protein expression patterns show that the SMAD proteins surveyed are localized in the nucleus, providing a readout for active signalling via TGFβ and BMP receptors which will presumably influence gene transcription. SMAD4 immunoreactivity appears to be higher in cases with an EMT phenotype and that have more clinically aggressive characteristics such as grade and site (pancreas and rectal). Although this does not appear to be reflected with respect to metastatic presence, as p-SMAD2/3 and SMAD4 proteins appear to be significantly elevated among cases that have no metastasis, it is possible that these tumours have yet had a chance to metastasize.

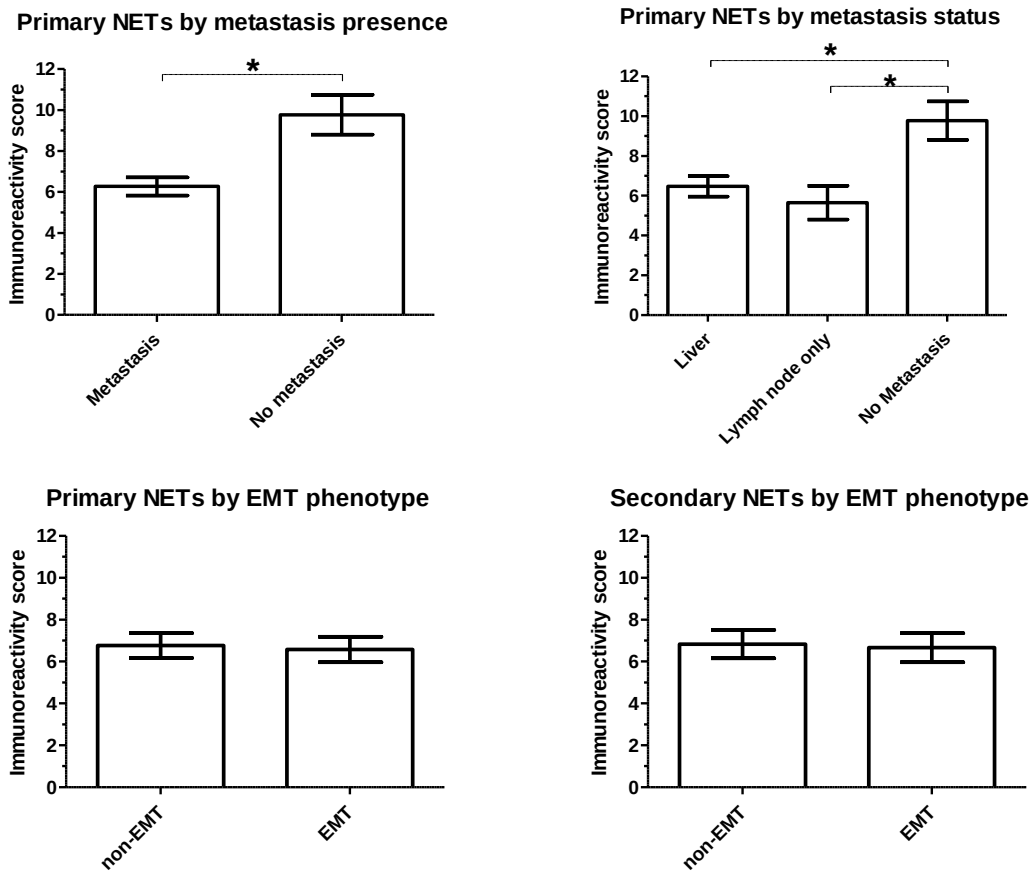

Figure 3.27. Phospho-SMAD2/3 nuclear reactivity by metastasis status, and EMT phenotype.

Graphs show mean with error bars representing SEM. Asterisk (*) represents significance level of $p < 0.05$.

[Primary NET "Metastasis" n = 67, "No metastasis" n = 9]

[Primary NET "Liver" n = 55, "Lymph node only" n = 12; "No metastasis" n = 9]

[Primary NET "non EMT" n = 37, "EMT" n = 39]

[Secondary NET "non-EMT" n = 39, "EMT" n = 33]

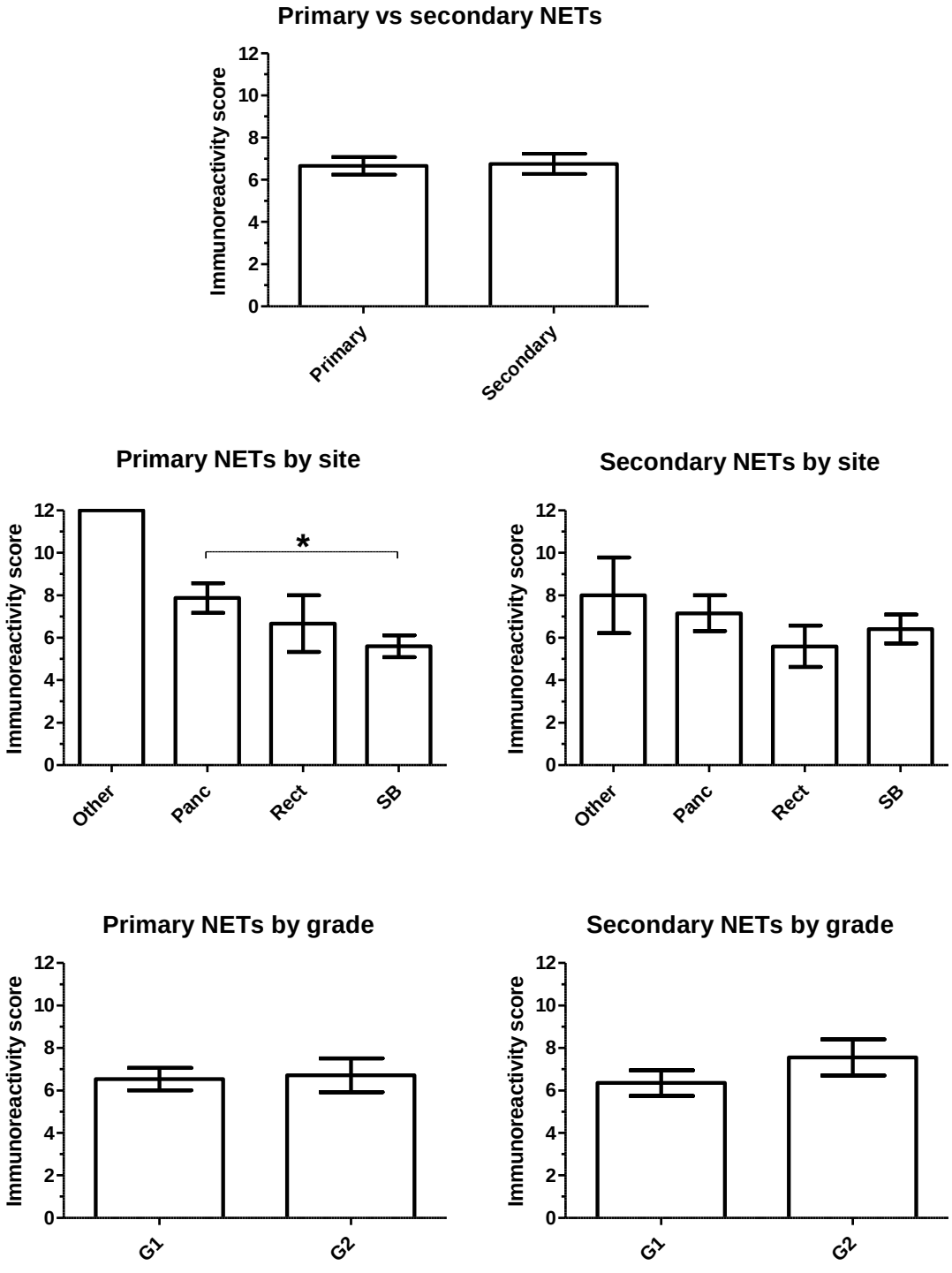
Primary vs secondary NETs
Immunoreactivity score
0
2
4
6
8
10
12
Primary
Secondary
Primary NETs by site
Immunoreactivity score
*
Other
Panc
Rect
SB
Secondary NETs by site
Immunoreactivity score
Other
Panc
Rect
SB
Primary NETs by grade
Immunoreactivity score
G1
G2
Secondary NETs by grade
Immunoreactivity score
G1
G2

Figure 3.28. Phospho-SMAD2/3 nuclear reactivity by overall tumour type, site, and grade.

Graphs show mean with error bars representing SEM. Asterisk (*) represents significance level of $p < 0.05$.

[Primary NET “Other” n = 2, “Panc” n = 26, “Rect” n = 3, “SB” n = 45]

[Primary NET “G1” n = 51, “G2” n = 21]

[Secondary NET “Other” n = 2, “Panc” n = 26, “Rect” n = 3, “SB” n = 45]

[Secondary NET “G1” n = 50, “G2” n = 18]

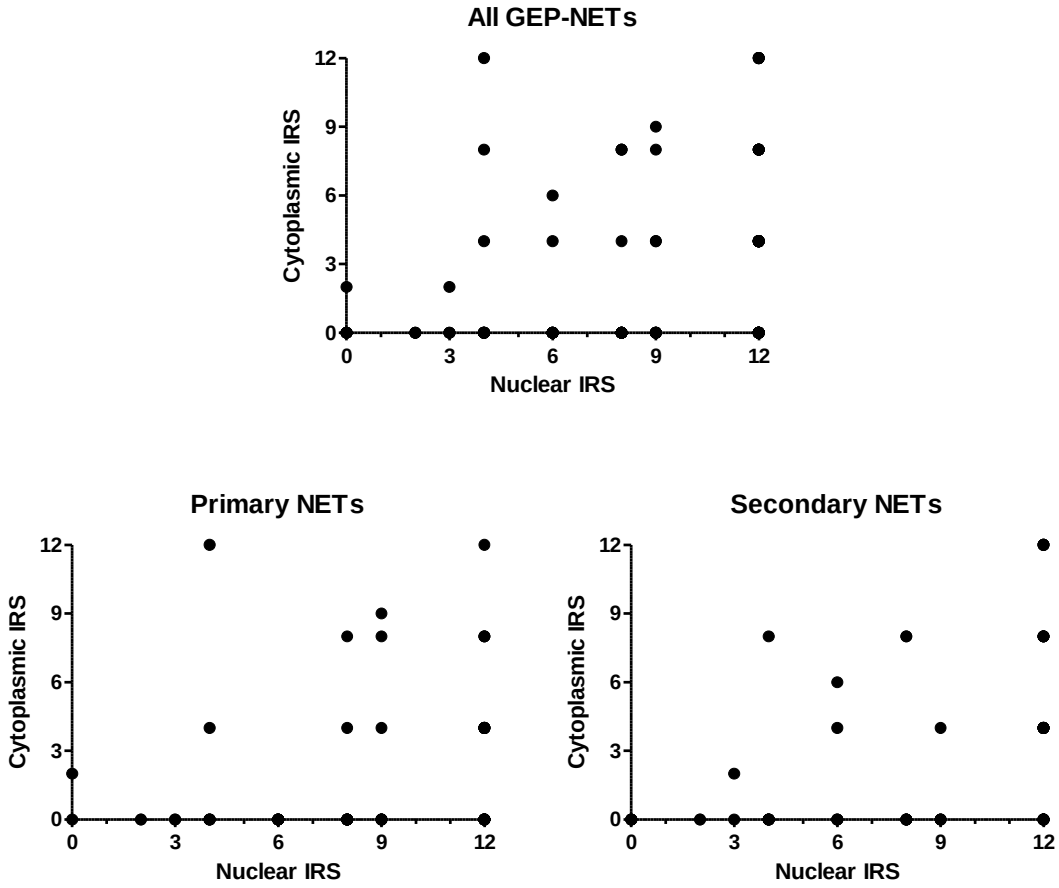

Figure 3.29. Scatterplot of p-SMAD1/5/8 nuclear versus cytosolic expression in primary and secondary NETs.

Pearson's correlation coefficient, r, for "All GEP-NETs", "Primary NETs" and "Secondary NETS" are 0.2661 [p = 0.0009, significant, n = 153], 0.1816 [p = 0.1091, not significant, n = 79], and 0.3325 [p = 0.0038, significant, n = 74] respectively.

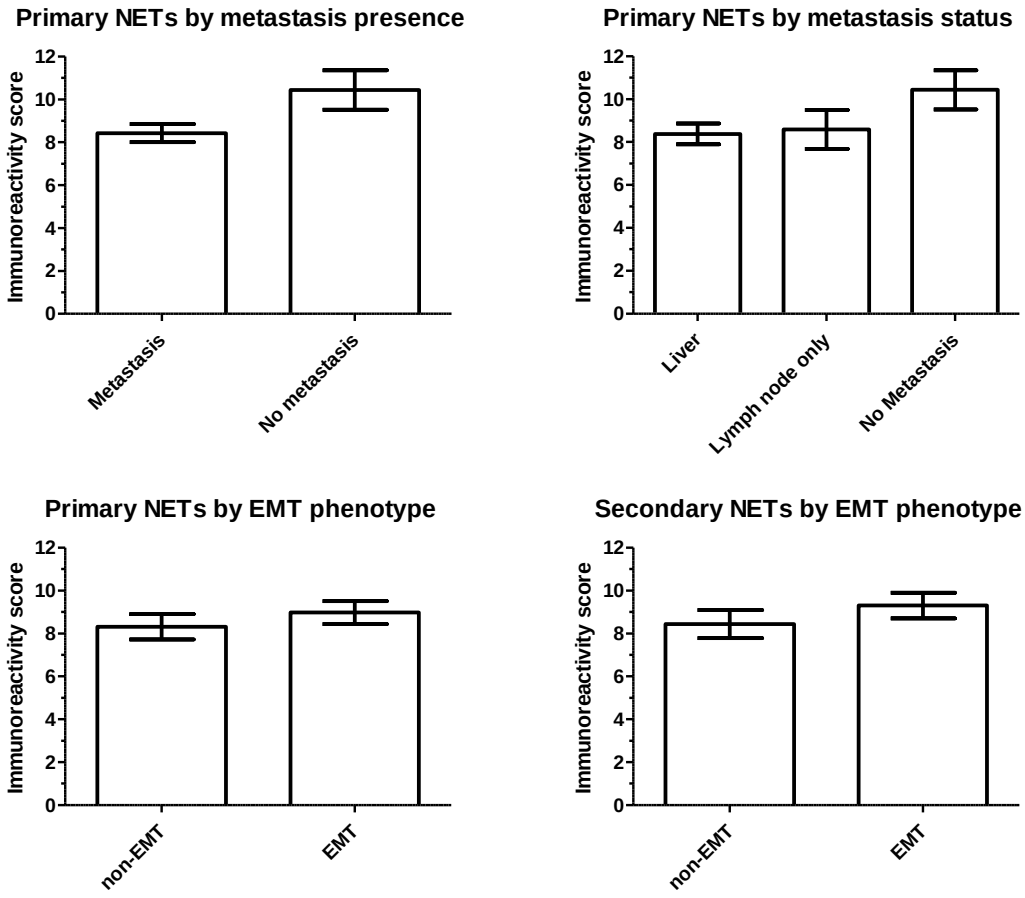

Figure 3.30. Phospho-SMAD1/5/8 nuclear reactivity by metastasis status, EMT phenotype and EMT phenotype subsets.

Graphs show mean with error bars representing SEM.

[Primary NET "Metastasis" n = 67, "No metastasis" n = 9]

[Primary NET "Liver" n = 55, "Lymph node only" n = 12; "No metastasis" n = 9]

[Primary NET "non EMT" n = 37, "EMT" n = 39]

[Secondary NET "non-EMT" n = 39, "EMT" n = 33]

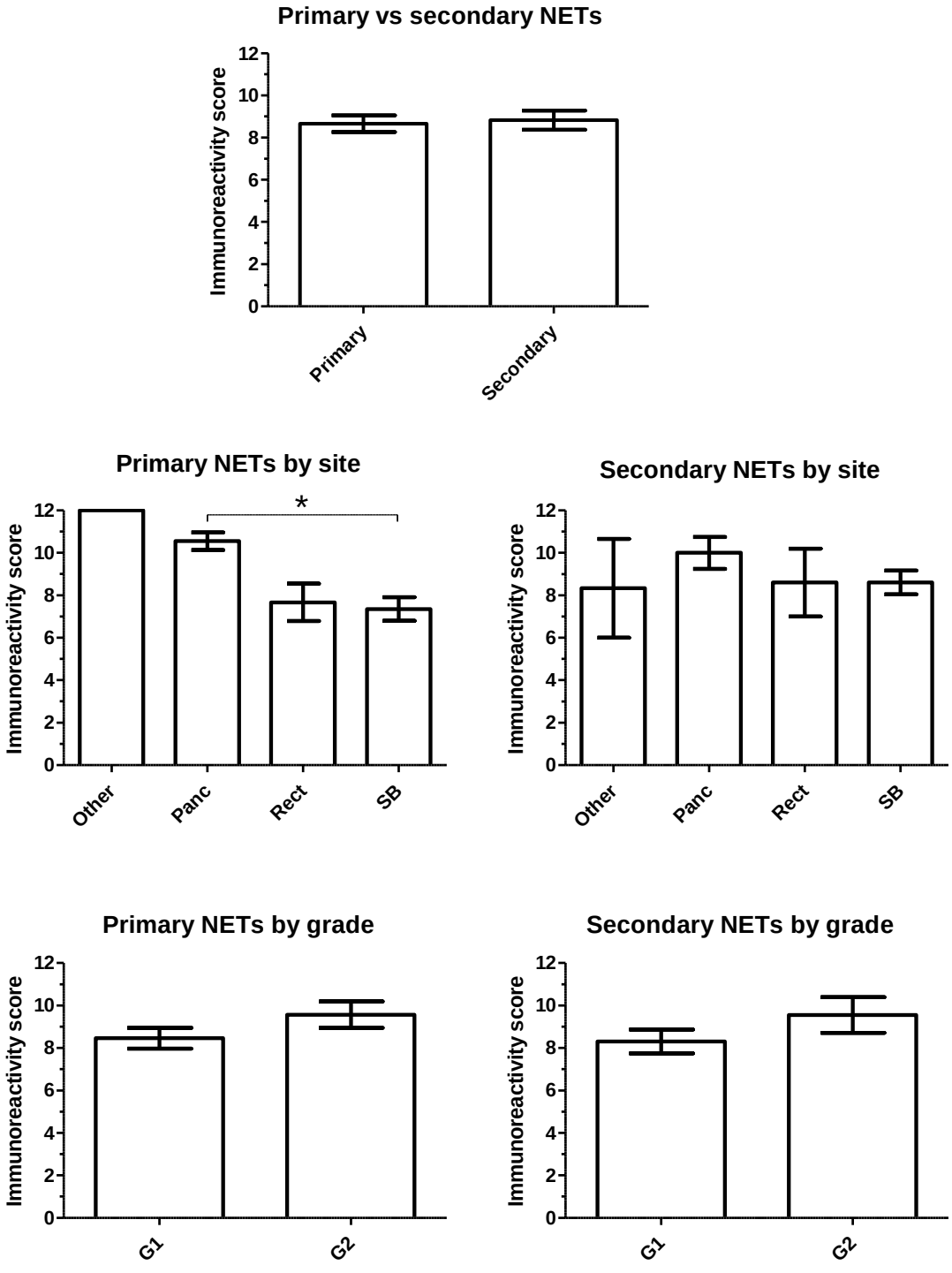
Primary vs secondary NETs
Immunoreactivity score
0
2
4
6
8
10
12
Primary
Secondary
Primary NETs by site
*
Other
Panc
Rect
SB
Secondary NETs by site
Other
Panc
Rect
SB
Primary NETs by grade
G1
G2
Secondary NETs by grade
G1
G2

Figure 3.31. Phospho-SMAD1/5/8 nuclear reactivity by overall tumour type, site, and grade.

Graphs show mean with error bars representing SEM. Asterisk (*) represents significance level of $p < 0.05$.

Graphs show mean with error bars representing SEM.

[Primary NET “Other” n = 2, “Panc” n = 26, “Rect” n = 3, “SB” n = 45]

[Primary NET “G1” n = 51, “G2” n = 21]

[Secondary NET “Other” n = 2, “Panc” n = 26, “Rect” n = 3, “SB” n = 45]

[Secondary NET “G1” n = 50, “G2” n = 18]

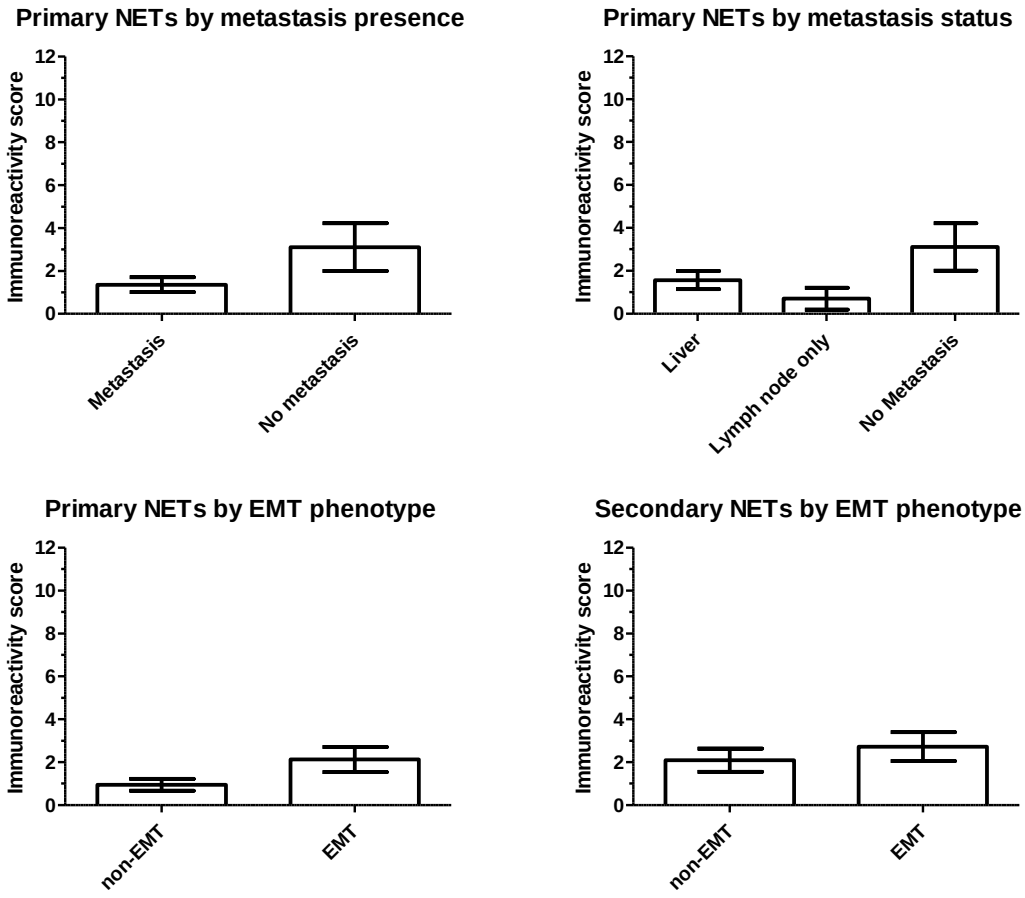

Figure 3.32. Phospho-SMAD1/5/8 cytosolic reactivity by metastasis status, EMT phenotype and EMT phenotype subsets.

Graphs show mean with error bars representing SEM.

[Primary NET "Metastasis" n = 67, "No metastasis" n = 9]

[Primary NET "Liver" n = 55, "Lymph node only" n = 12; "No metastasis" n = 9]

[Primary NET "non EMT" n = 37, "EMT" n = 39]

[Secondary NET "non-EMT" n = 39, "EMT" n = 33]

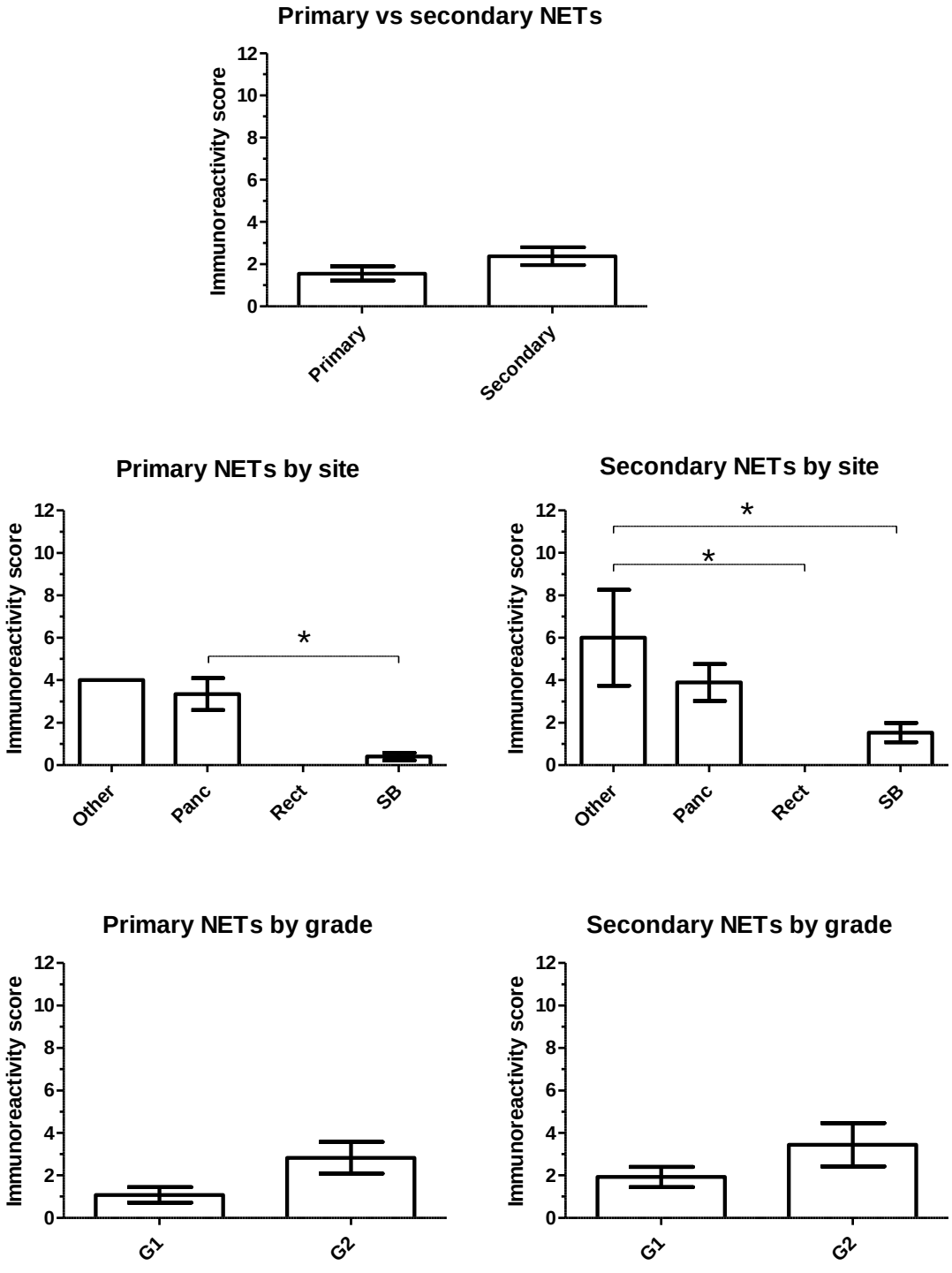
Primary vs secondary NETs
Immunoreactivity score
0
2
4
6
8
10
12
Primary
Secondary
Primary NETs by site
Immunoreactivity score
*
Other
Panc
Rect
SB
Secondary NETs by site
Immunoreactivity score
*
*
Other
Panc
Rect
SB
Primary NETs by grade
Immunoreactivity score
G1
G2
Secondary NETs by grade
Immunoreactivity score
G1
G2

Figure 3.33. Phospho-SMAD1/5/8 cytosolic reactivity by overall tumour type, site, and grade.

Graphs show mean with error bars representing SEM. Asterisk (*) represents significance level of $p < 0.05$.

[Primary NET “Other” n = 2, “Panc” n = 26, “Rect” n = 3, “SB” n = 45]

[Primary NET “G1” n = 51, “G2” n = 21]

[Secondary NET “Other” n = 2, “Panc” n = 26, “Rect” n = 3, “SB” n = 45]

[Secondary NET “G1” n = 50, “G2” n = 18]

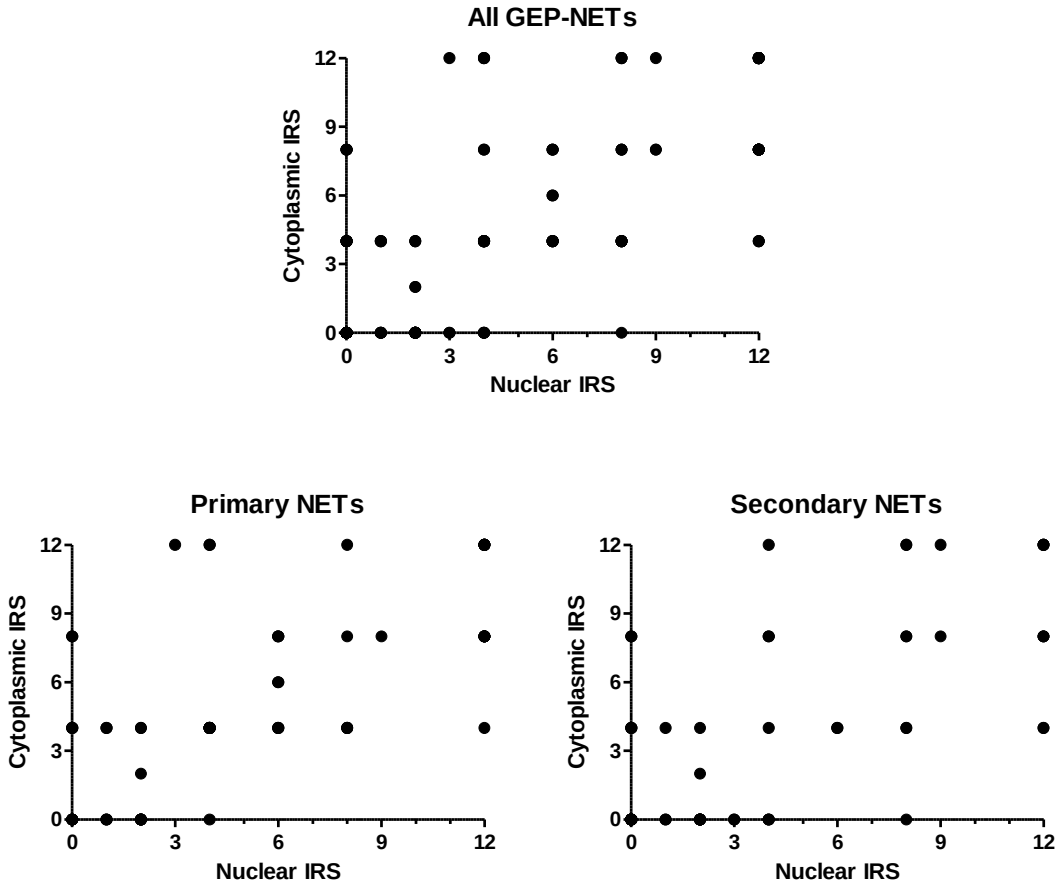

Figure 3.34. Scatterplot of SMAD4 nuclear versus cytosolic expression in primary and secondary NETs.

Pearson's correlation coefficient, r, for "All GEP-NETs", "Primary NETs" and "Secondary NETS" are 0.07353 [$p < 0.0001$, significant, n = 153], 0.7198 [$p < 0.0001$, significant, n = 79], and 0.7195 [$p < 0.0001$, significant, n = 74] respectively.

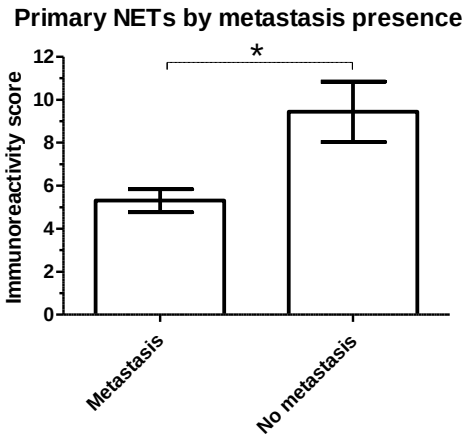
Primary NETs by metastasis presence
Immunoreactivity score
0
2
4
6
8
10
12
*
Metastasis
No metastasis

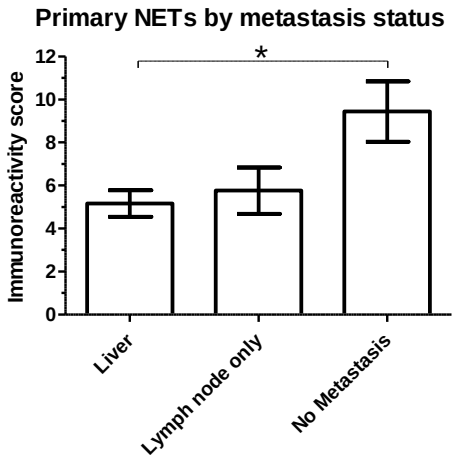
Primary NETs by metastasis status
Immunoreactivity score
0
2
4
6
8
10
12
*
Liver
Lymph node only
No Metastasis

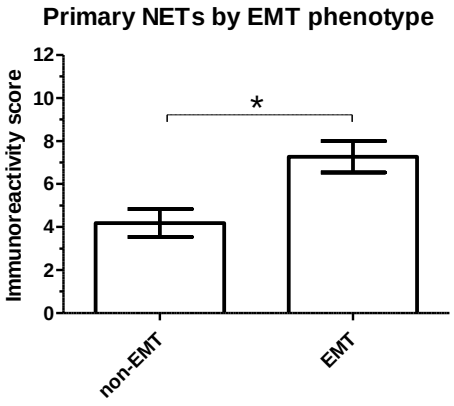
Primary NETs by EMT phenotype
Immunoreactivity score
0
2
4
6
8
10
12
*
non-EMT
EMT

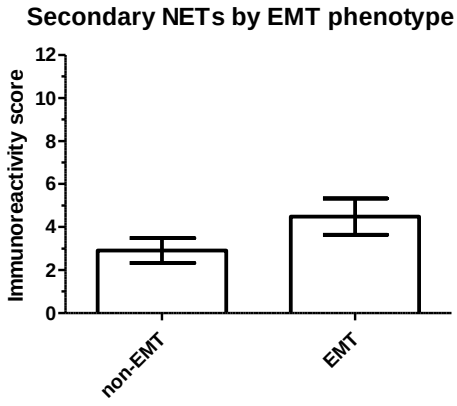
Secondary NETs by EMT phenotype
Immunoreactivity score
0
2
4
6
8
10
12
non-EMT
EMT

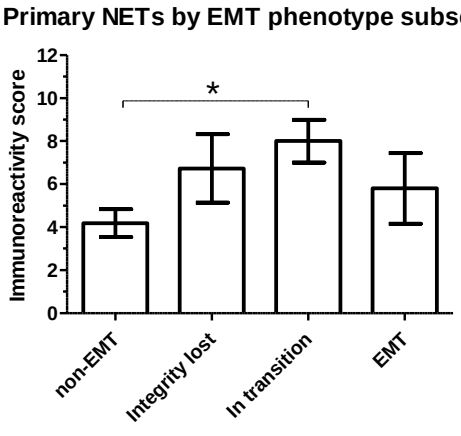
Primary NETs by EMT phenotype subset
Immunoreactivity score
0
2
4
6
8
10
12
*
non-EMT
Integrity lost
In transition
EMT

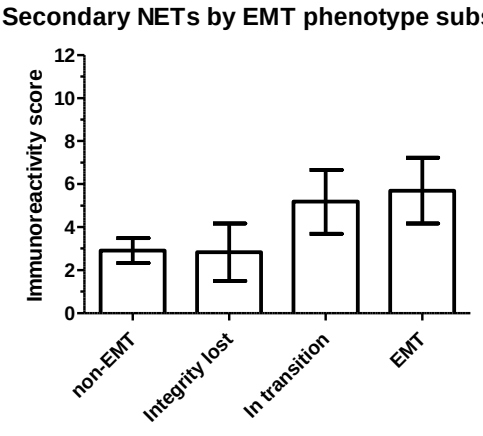
Secondary NETs by EMT phenotype subset
Immunoreactivity score
0
2
4
6
8
10
12
non-EMT
Integrity lost
In transition
EMT

Figure 3.35. SMAD4 nuclear reactivity by metastasis status, EMT phenotype and EMT phenotype subsets.

Graphs show mean with error bars representing SEM. Asterisk (*) represents significance level of $p < 0.05$.

[Primary NET "Metastasis" n = 67, "No metastasis" n = 9]

[Primary NET "Liver" n = 55, "Lymph node only" n = 12; "No metastasis" n = 9]

[Primary NET "non EMT" n = 37, "EMT" n = 39]

[Primary NET "non-EMT" n = 37, "Integrity lost" n = 12, "In transition" n = 17, "EMT" n = 10]

[Secondary NET "non-EMT" n = 39, "EMT" n = 33]

[Secondary NET "non-EMT" n = 39, "Integrity lost" n = 12, "In transition" n = 12, "EMT" n = 10]

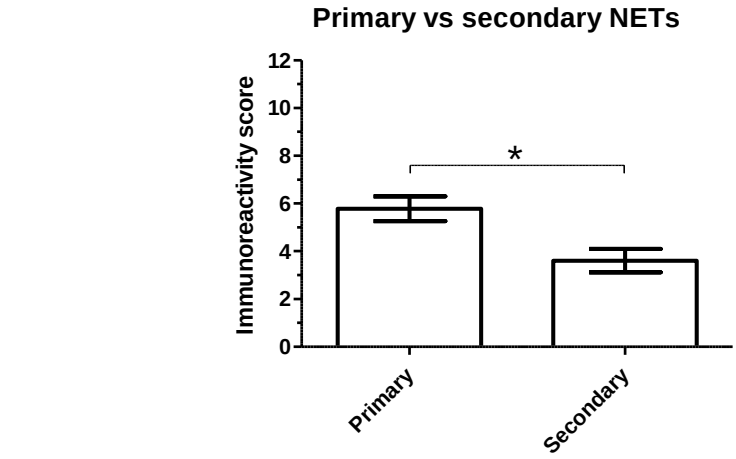
Primary vs secondary NETs
Immunoreactivity score
0
2
4
6
8
10
12
*
Primary
Secondary

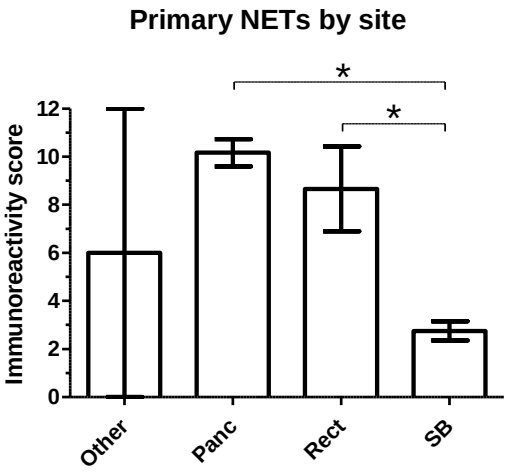
Primary NETs by site
Immunoreactivity score
0
2
4
6
8
10
12
*
*
Other
Panc
Rect
SB

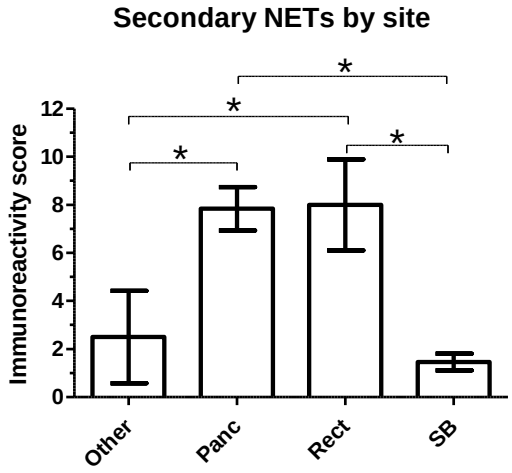
Secondary NETs by site
Immunoreactivity score
0
2
4
6
8
10
12
*
*
*
Other
Panc
Rect
SB

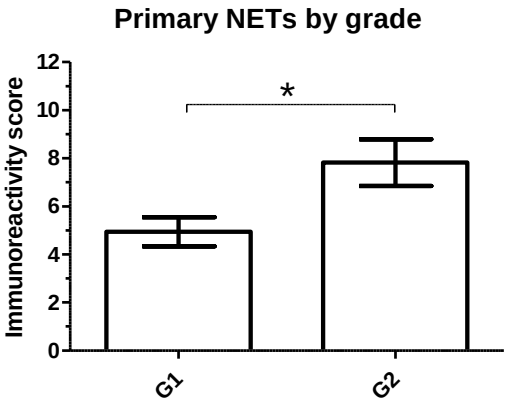
Primary NETs by grade
Immunoreactivity score
0
2
4
6
8
10
12
*
G1
G2

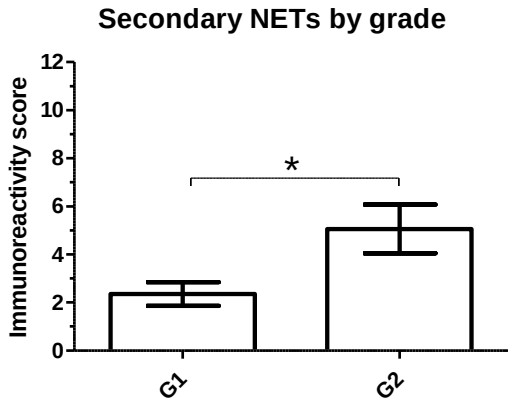
Secondary NETs by grade
Immunoreactivity score
0
2
4
6
8
10
12
*
G1
G2

Figure 3.36. SMAD4 nuclear reactivity by overall tumour type, site, and grade.
Graphs show mean with error bars representing SEM. Asterisk (*) represents significance level of $p < 0.05$.
[Primary NET "Other" n = 2, "Panc" n = 26, "Rect" n = 3, "SB" n = 45]
[Primary NET "G1" n = 51, "G2" n = 21]
[Secondary NET "Other" n = 2, "Panc" n = 26, "Rect" n = 3, "SB" n = 45]
[Secondary NET "G1" n = 50, "G2" n = 18]

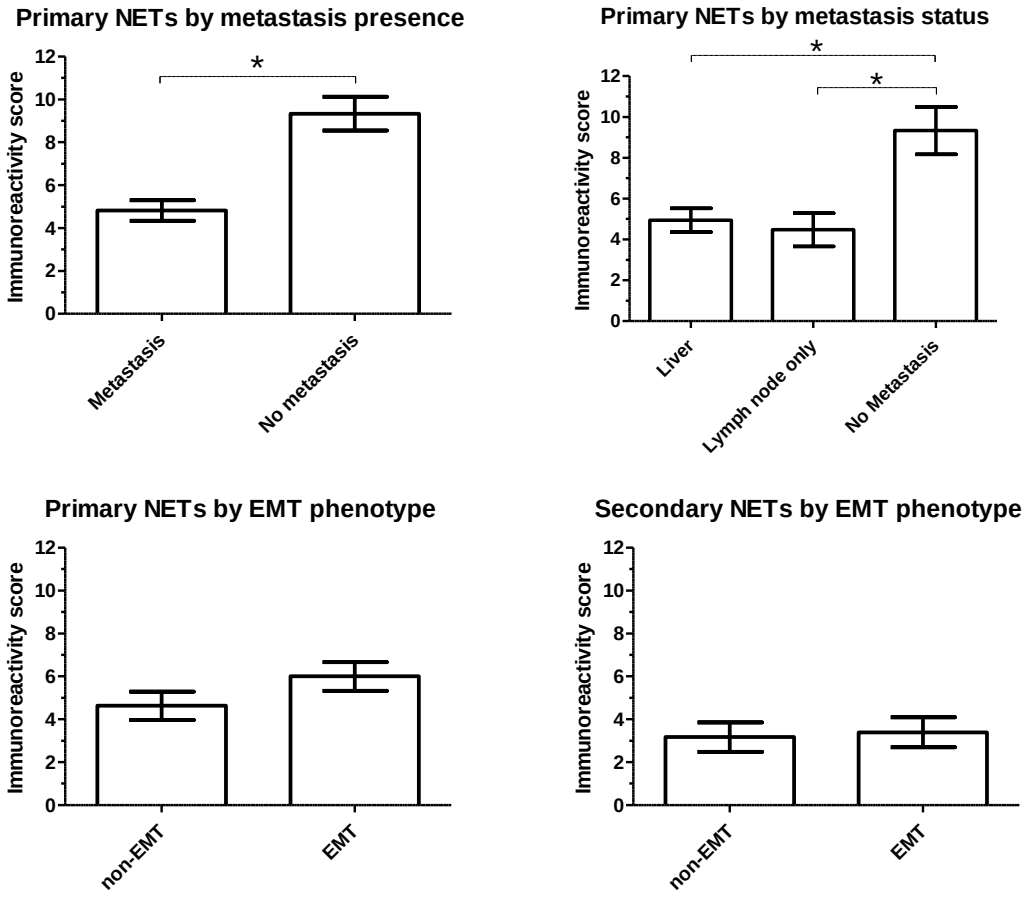

Figure 3.37. SMAD4 cytosolic reactivity by metastasis status, EMT phenotype and EMT phenotype subsets.

Graphs show mean with error bars representing SEM. Asterisk (*) represents significance level of $p < 0.05$.

[Primary NET "Metastasis" n = 67, "No metastasis" n = 9]

[Primary NET "Liver" n = 55, "Lymph node only" n = 12; "No metastasis" n = 9]

[Primary NET "non EMT" n = 37, "EMT" n = 39]

[Secondary NET "non-EMT" n = 39, "EMT" n = 33]

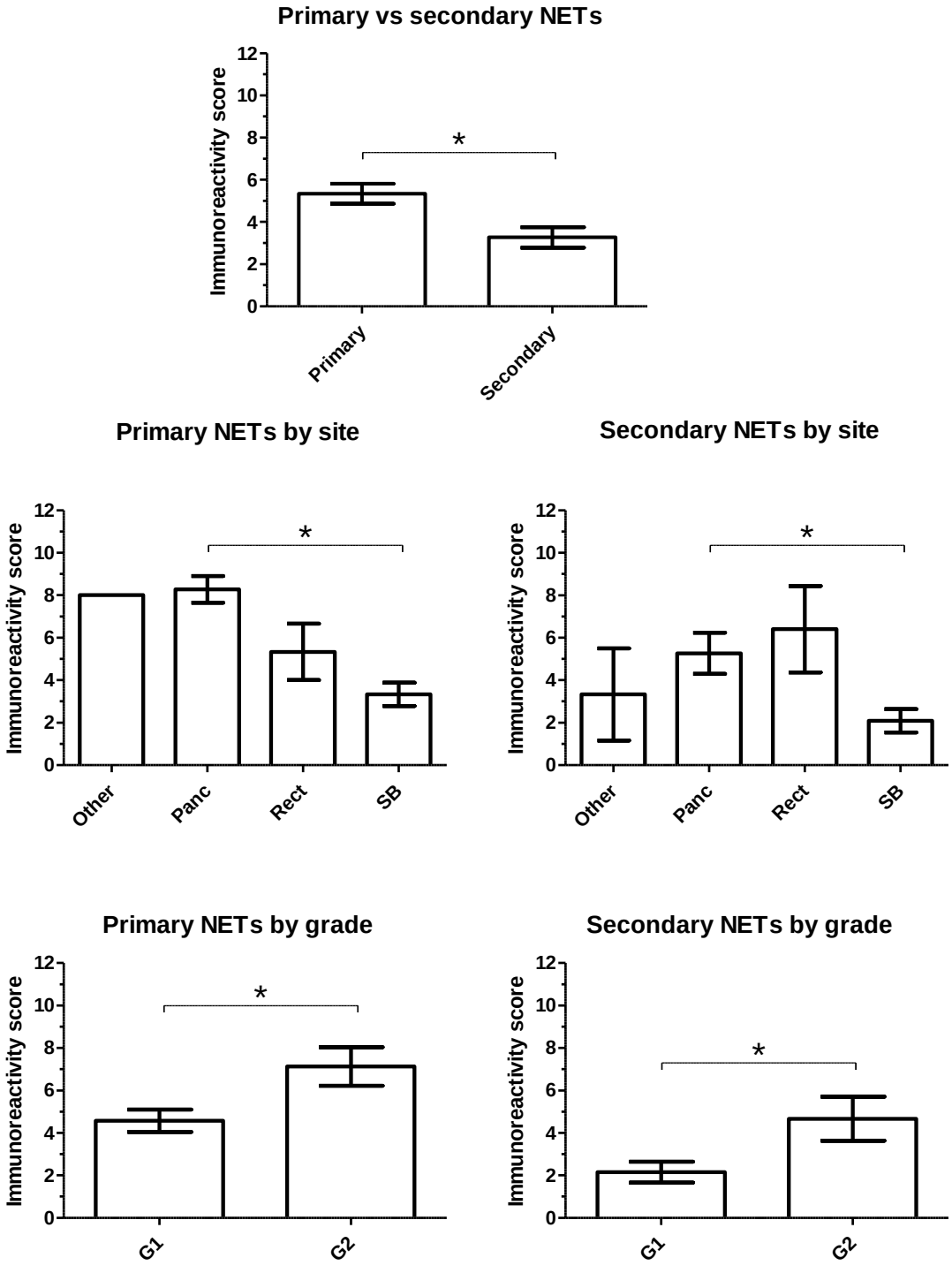
Primary vs secondary NETs
Immunoreactivity score
12
10
8
6
4
2
0
*
Primary
Secondary
Primary NETs by site
Immunoreactivity score
*
Other
Panc
Rect
SB
Secondary NETs by site
Immunoreactivity score
*
Other
Panc
Rect
SB
Primary NETs by grade
Immunoreactivity score
*
G1
G2
Secondary NETs by grade
Immunoreactivity score
*
G1
G2

Figure 3.38. SMAD4 cytosolic reactivity by overall tumour type, site, and grade. Graphs show mean with error bars representing SEM. Asterisk (*) represents significance level of $p < 0.05$.

[Primary NET "Metastasis" n = 67, "No metastasis" n = 9]

[Primary NET "Liver" n = 55, "Lymph node only" n = 12; "No metastasis" n = 9]

[Primary NET "non EMT" n = 37, "EMT" n = 39]

[Primary NET "non-EMT" n = 37, "Integrity lost" n = 12, "In transition" n = 17, "EMT" n = 10]

[Secondary NET "non-EMT" n = 39, "EMT" n = 33]

[Secondary NET "non-EMT" n = 39, "Integrity lost" n = 12, "In transition" n = 12, "EMT" n = 10]

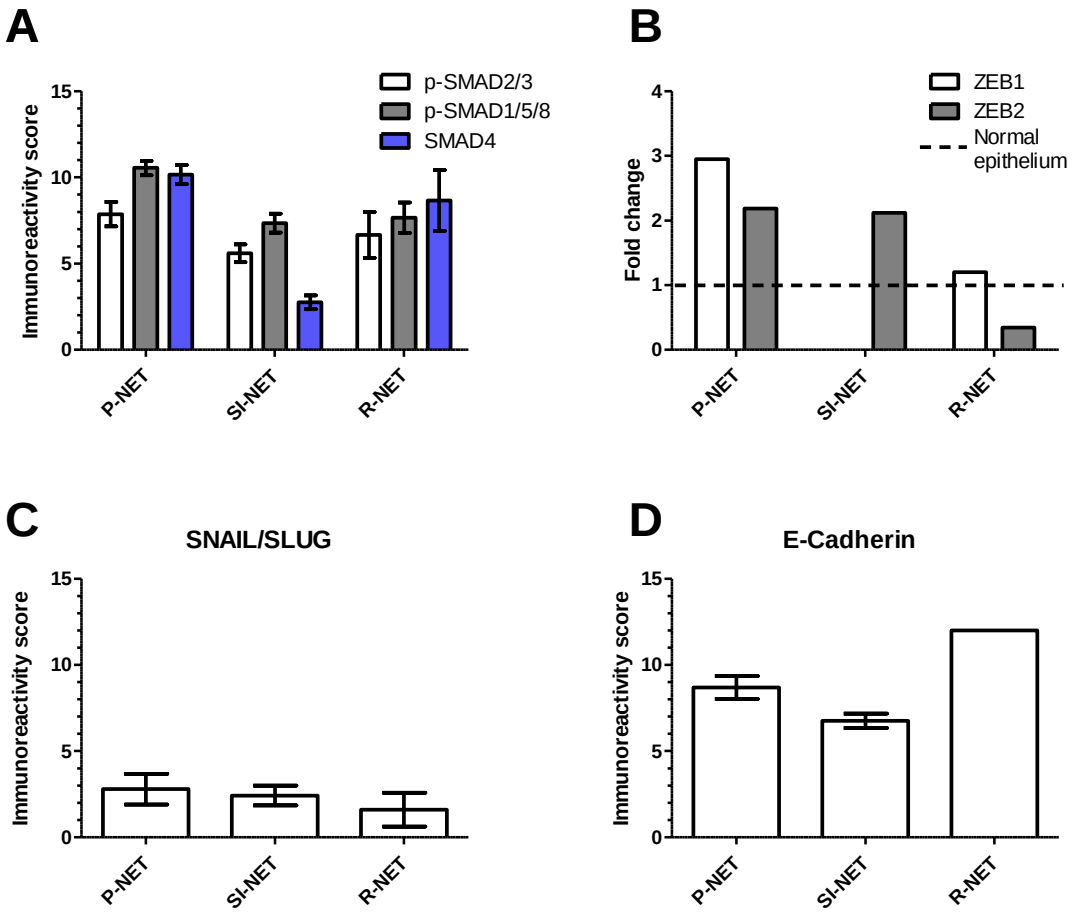

Figure 3.39. Overview summary of different select stains and gene expression among GEP-NETs from different sites.

Immunoreactivity scores for TGFβ/BMP downstream effectors SMADs (**A**) and their associated targets of transcription SNAIL/SLUG (**C**) across different GEP-NETs. Nuclear IRS scores shown. Gene expression data for ZEB proteins which are also induced by TGFβ signalling across various sites shown (**B**). SNAIL/SLUG and ZEB proteins act to repress genes expressing E-cadherin (**D**). Graphs showing mean ± SEM. Data summarized from previous figures.

3.6 EMT phenotype and mTOR signalling in GEP-NETs

The mTOR pathway and its pathogenic involvement in GEP-NETs have become more prominent as research uncovers its contribution, especially since genes along the mTOR signalling axis were shown to be frequently mutated among P-NETs.[20] Clinical trials demonstrating prolonged progression-free survival in advanced P-NETs for patients on mTOR inhibitor, Everolimus, prompted USA Food and Drug Administration, and Health Canada approval.[67] Since then, the relative success with the use of mTOR inhibitors for patients with advanced P-NETs who have exhausted other therapeutic options provides evidence that this pathway is likely to have a role in GEP-NET pathogenesis. [68] Recent studies linking mTOR to TGFβ induced EMT,[66] prompted us to study whether there may be a correlation with an EMT phenotype and the activation of the mTOR pathway through immunohistochemistry on our TMA sets. As with our other experiments, we also looked at whether tumour site, grade, and metastatic status corresponded with mTOR pathway activation.

We looked at three mTOR related genes: phosphorylated mammalian target of rampamycin (p-mTOR), phosphorylated eukaryotic translation initiation factor 4E-binding protein 1 (p-4EBP1), and phosphatase and tensin homolog (PTEN) (**Figure 3.40**). Phosphorylated mTOR reactivity is significantly higher in non-EMT groups than EMT groups in both overall and subset phenotypes within primary NETs but not secondary NETs (**Figure 3.41**). It also appears that p-mTOR is more reactive in primary small bowel NETs than rectal NETs, and that G1 primary NETs are more p-mTOR reactive than G2 NETs (**Figure 3.42**). No significant differences are apparent in p-4EBP1 staining reactivity among all parameters checked (**Figure 3.43, Figure 3.44**). PTEN immunoreactivity appears to be significantly higher in the "no metastasis" grouping than the "liver metastasis" group, and in no other group parameter (**Figure 3.45**, **Figure 3.46**).

To assess possible correlations, we conservatively set cases with an IRS score of 3 or above as staining positive, while those with an IRS score of 2 and below were negative. This would ensure that cases which were organized into "mTOR pathway activated" (cases with either p-mTOR or p-4EBP1 staining positive) had robust staining versus

cases sorted into “mTOR pathway inactive” (p-mTOR and p-4EBP1 negative) categories. No correlations were apparent based on a simple chi-squared and Fisher’s exact test except in primary tumours where there is an association with PTEN staining (**Figure 3.47**, **Figure 3.48**).

This experiment shows that the mTOR pathway appears to be more active among GEP-NETs that are less clinically aggressive, given that G1 tumours, non-EMT NETs and SI-NETs had higher immunoreactivity to p-mTOR. Possibly of greater importance, it appears that PTEN is significantly more reactive among cases that have no metastasis, suggesting that PTEN may play a key role in suppression of aggressive behaviour. These two observations together suggest that mTOR signaling is active in GEP-NETs, and that disease progression could occur when there is mTOR dysregulation at the PTEN level.

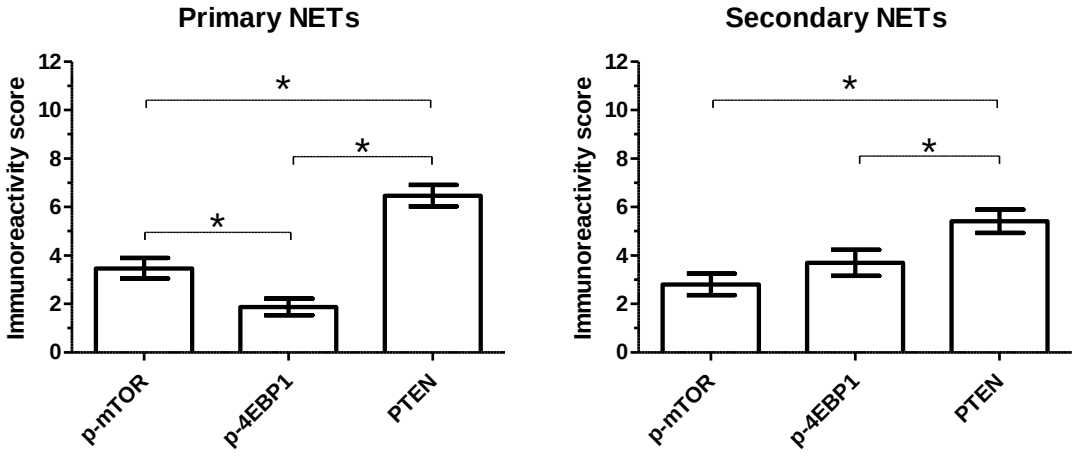

Figure 3.40. Immunoreactivity scores of mTOR pathway related stains.

Graphs showing mean with SEM. Asterisk (*) represents significance level of $p < 0.05$. . [n = 76 for primary NETs and n = 73 for secondary NETs for each stain].

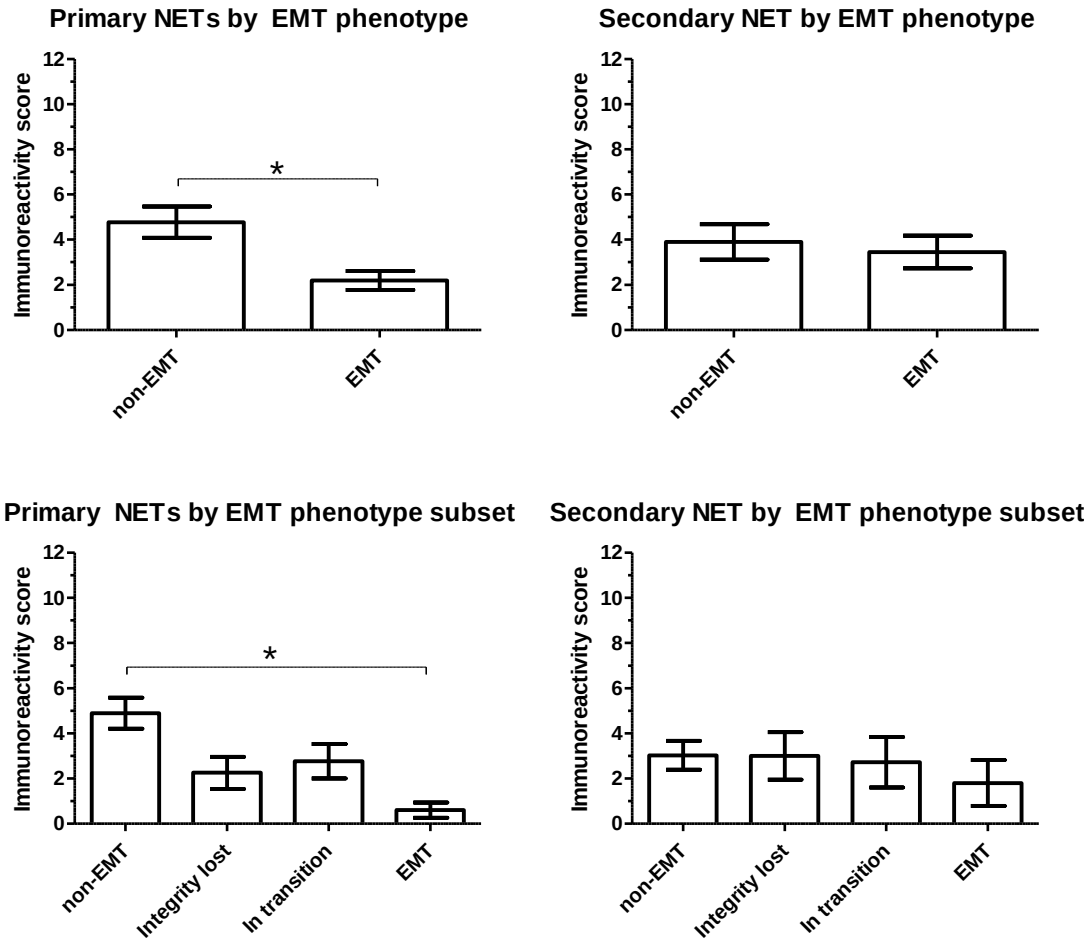

Figure 3.41. Immunoreactivity score of p-mTOR based on EMT phenotype and subsets.

Graphs showing mean with SEM. Asterisk (*) represents significance level of $p < 0.05$.

[Primary NET "non EMT" n = 37, "EMT" n = 39]

[Primary NET "non-EMT" n = 37, "Integrity lost" n = 12, "In transition" n = 17, "EMT" n = 10]

[Secondary NET "non-EMT" n = 39, "EMT" n = 33]

[Secondary NET "non-EMT" n = 39, "Integrity lost" n = 12, "In transition" n = 12, "EMT" n = 10]

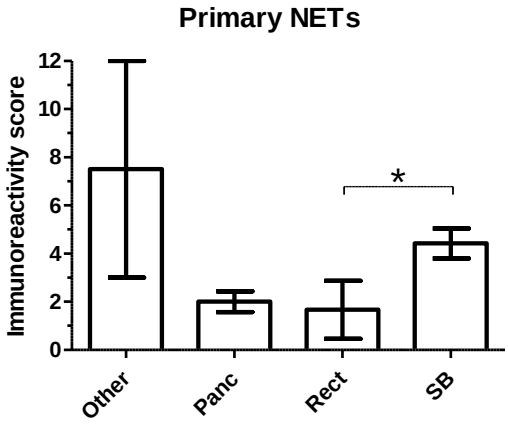
Primary NETs
Immunoreactivity score
0
2
4
6
8
10
12
*
Other
Panc
Rect
SB

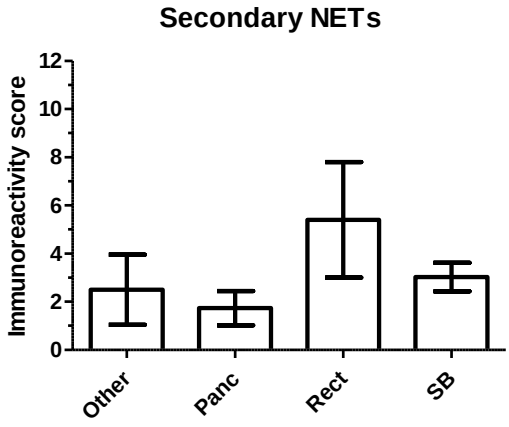
Secondary NETs
Immunoreactivity score
0
2
4
6
8
10
12
Other
Panc
Rect
SB

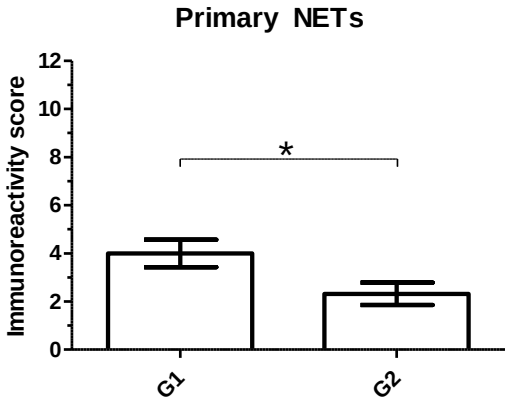
Primary NETs
Immunoreactivity score
0
2
4
6
8
10
12
*
G1
G2

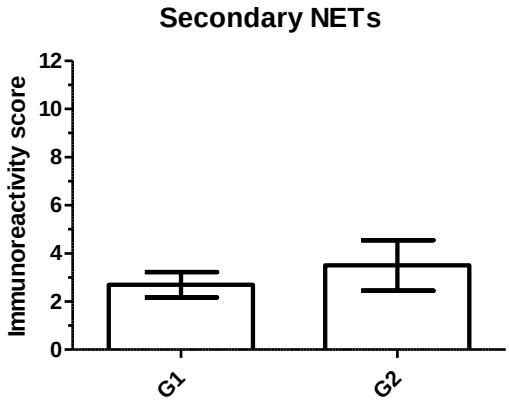
Secondary NETs
Immunoreactivity score
0
2
4
6
8
10
12
G1
G2

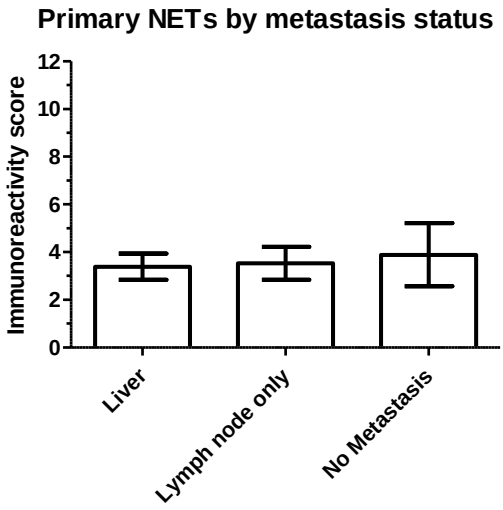
Primary NETs by metastasis status
Immunoreactivity score
0
2
4
6
8
10
12
Liver
Lymph node only
No Metastasis

Figure 3.42. Immunoreactivity score of p-mTOR based on site of origin, grade, and metastasis status.

Graphs showing mean with SEM. Asterisk (*) represents significance level of $p < 0.05$.

[Primary NET “Other” n = 2, “Panc” n = 26, “Rect” n = 3, “SB” n = 45]

[Primary NET “G1” n = 51, “G2” n = 21]

[Secondary NET “Other” n = 2, “Panc” n = 26, “Rect” n = 3, “SB” n = 45]

[Secondary NET “G1” n = 50, “G2” n = 18]

[Primary NET “Metastasis” n = 67, “No metastasis” n = 9]

[Primary NET “Liver” n = 55, “Lymph node only” n = 12; “No metastasis” n = 9]

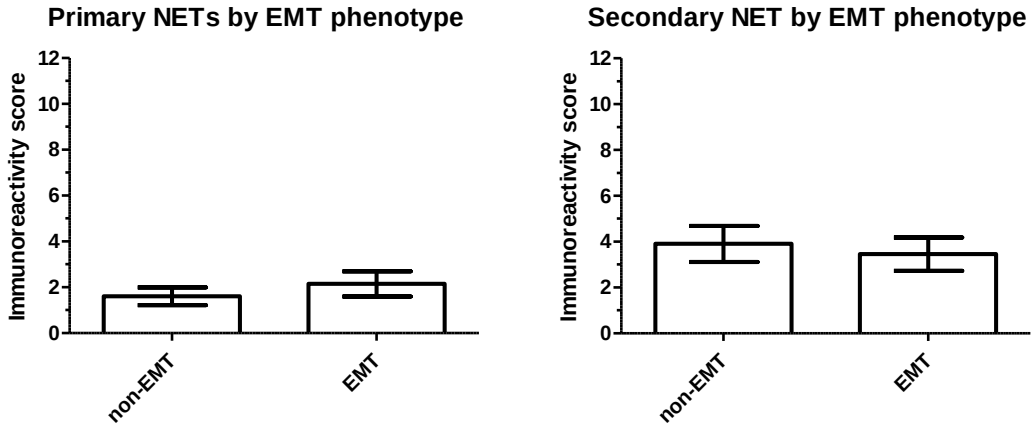

Figure 3.43. Immunoreactivity score for p-4EBP1 based on EMT phenotype.

Graphs showing mean with SEM.

[Primary NET "non EMT" n = 37, "EMT" n = 39]

[Secondary NET "non-EMT" n = 39, "EMT" n = 33]

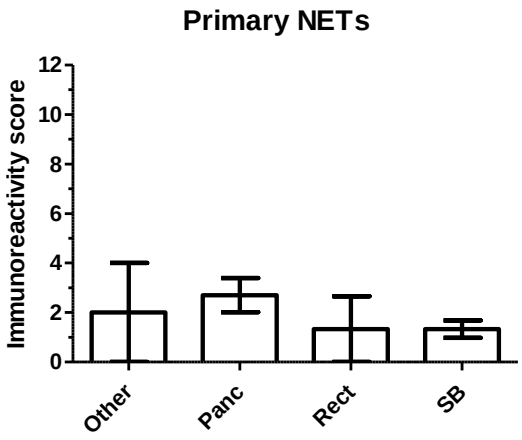
Primary NETs
Immunoreactivity score
12
10
8
6
4
2
0
Other
Panc
Rect
SB

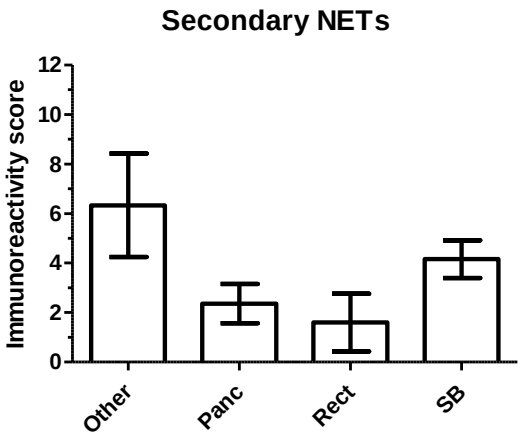
Secondary NETs
Immunoreactivity score
12
10
8
6
4
2
0
Other
Panc
Rect
SB

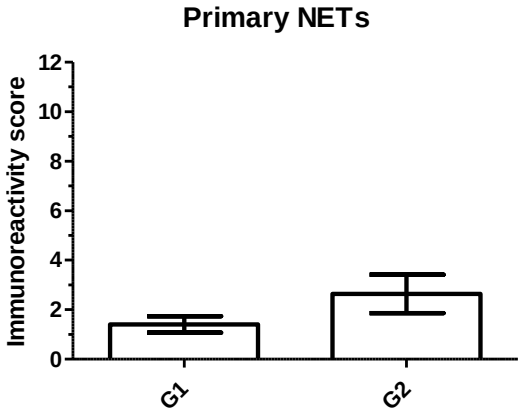
Primary NETs
Immunoreactivity score
12
10
8
6
4
2
0
G1
G2

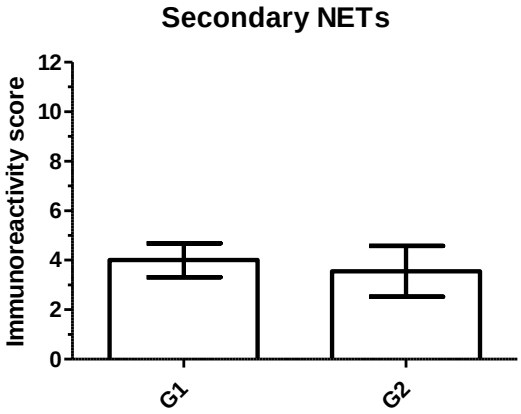
Secondary NETs
Immunoreactivity score
12
10
8
6
4
2
0
G1
G2

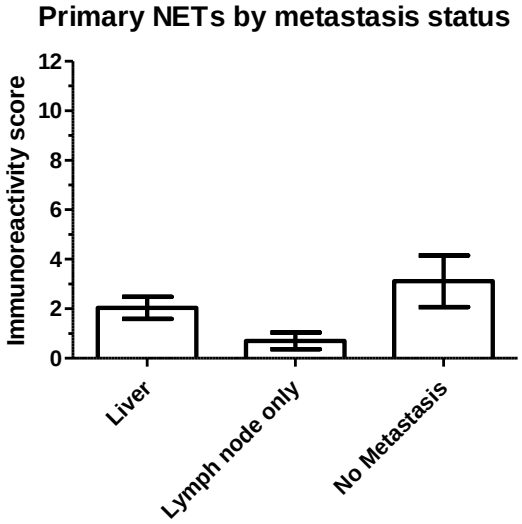
Primary NETs by metastasis status
Immunoreactivity score
12
10
8
6
4
2
0
Liver
Lymph node only
No Metastasis

Figure 3.44. Immunoreactivity score of p-4EBP1 based on site of origin, grade, and metastasis status.

Graphs showing mean with SEM.

[Primary NET “Other” n = 2, “Panc” n = 26, “Rect” n = 3, “SB” n = 45]

[Primary NET “G1” n = 51, “G2” n = 21]

[Secondary NET “Other” n = 2, “Panc” n = 26, “Rect” n = 3, “SB” n = 45]

[Secondary NET “G1” n = 50, “G2” n = 18]

[Primary NET “Metastasis” n = 67, “No metastasis” n = 9]

[Primary NET “Liver” n = 55, “Lymph node only” n = 12; “No metastasis” n = 9]

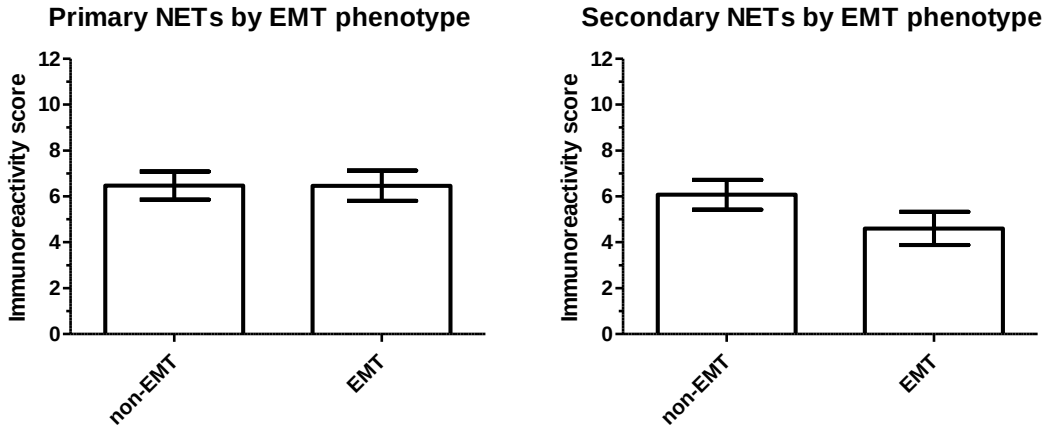

Figure 3.45. Immunoreactivity score for PTEN based on EMT phenotype.

Graphs showing mean with SEM.

[Primary NET "non EMT" n = 37, "EMT" n = 39]

[Secondary NET "non-EMT" n = 39, "EMT" n = 33]

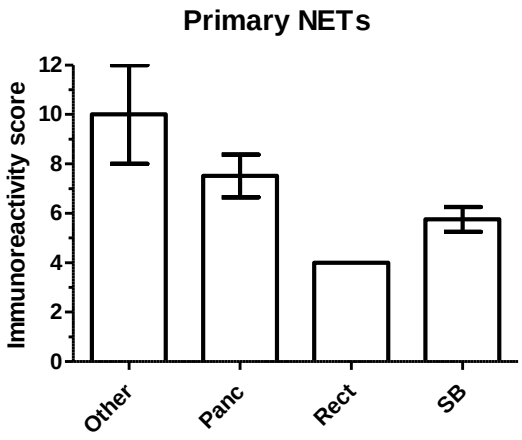
Primary NETs
Immunoreactivity score
0
2
4
6
8
10
12
Other
Panc
Rect
SB

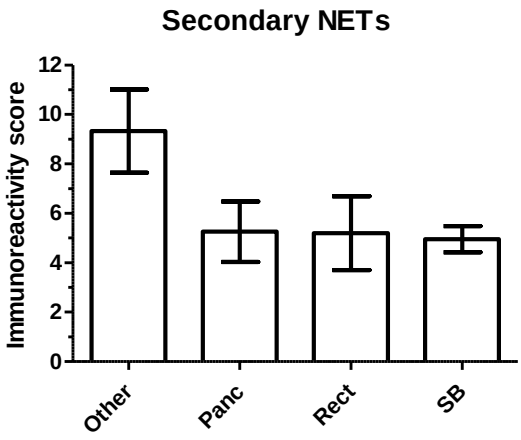
Secondary NETs
Immunoreactivity score
0
2
4
6
8
10
12
Other
Panc
Rect
SB

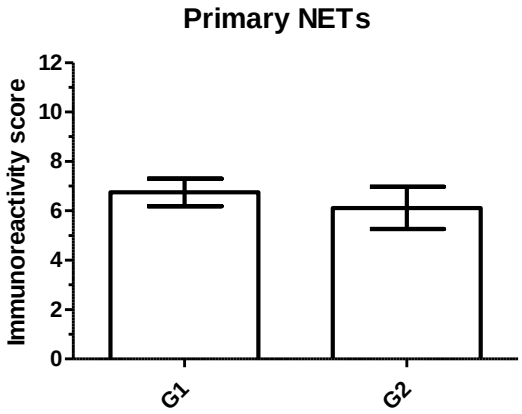
Primary NETs
Immunoreactivity score
0
2
4
6
8
10
12
G1
G2

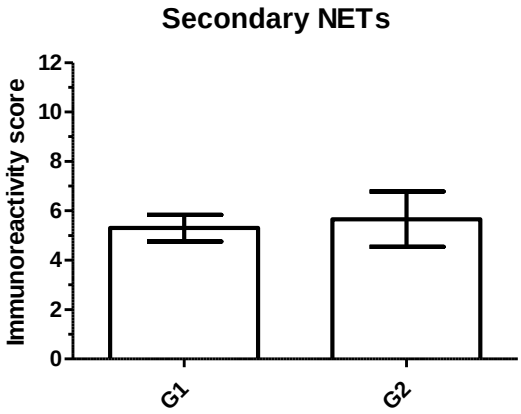
Secondary NETs
Immunoreactivity score
0
2
4
6
8
10
12
G1
G2

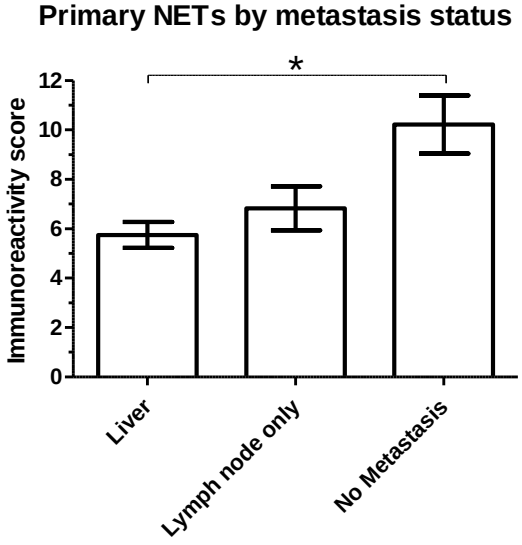
Primary NETs by metastasis status
*
Immunoreactivity score
0
2
4
6
8
10
12
Liver
Lymph node only
No Metastasis

Figure 3.46. Immunoreactivity score of PTEN based on site of origin, grade, and metastasis status.

Graphs showing mean with SEM. Asterisk (*) represents significance level of $p < 0.05$.

[Primary NET “Other” n = 2, “Panc” n = 26, “Rect” n = 3, “SB” n = 45]

[Primary NET “G1” n = 51, “G2” n = 21]

[Secondary NET “Other” n = 2, “Panc” n = 26, “Rect” n = 3, “SB” n = 45]

[Secondary NET “G1” n = 50, “G2” n = 18]

[Primary NET “Metastasis” n = 67, “No metastasis” n = 9]

[Primary NET “Liver” n = 55, “Lymph node only” n = 12; “No metastasis” n = 9]

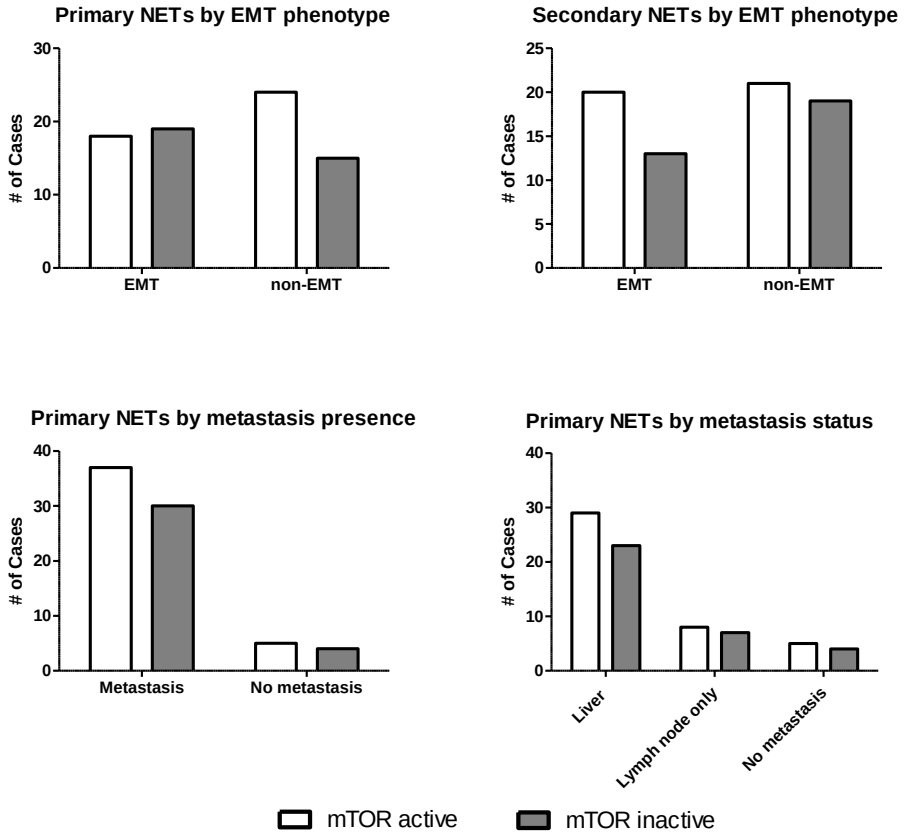

Figure 3.47. Contingency graphs for mTOR pathway activity in EMT phenotypes and metastasis status.

Chi-squared and Fisher's exact test show no significant correlations.

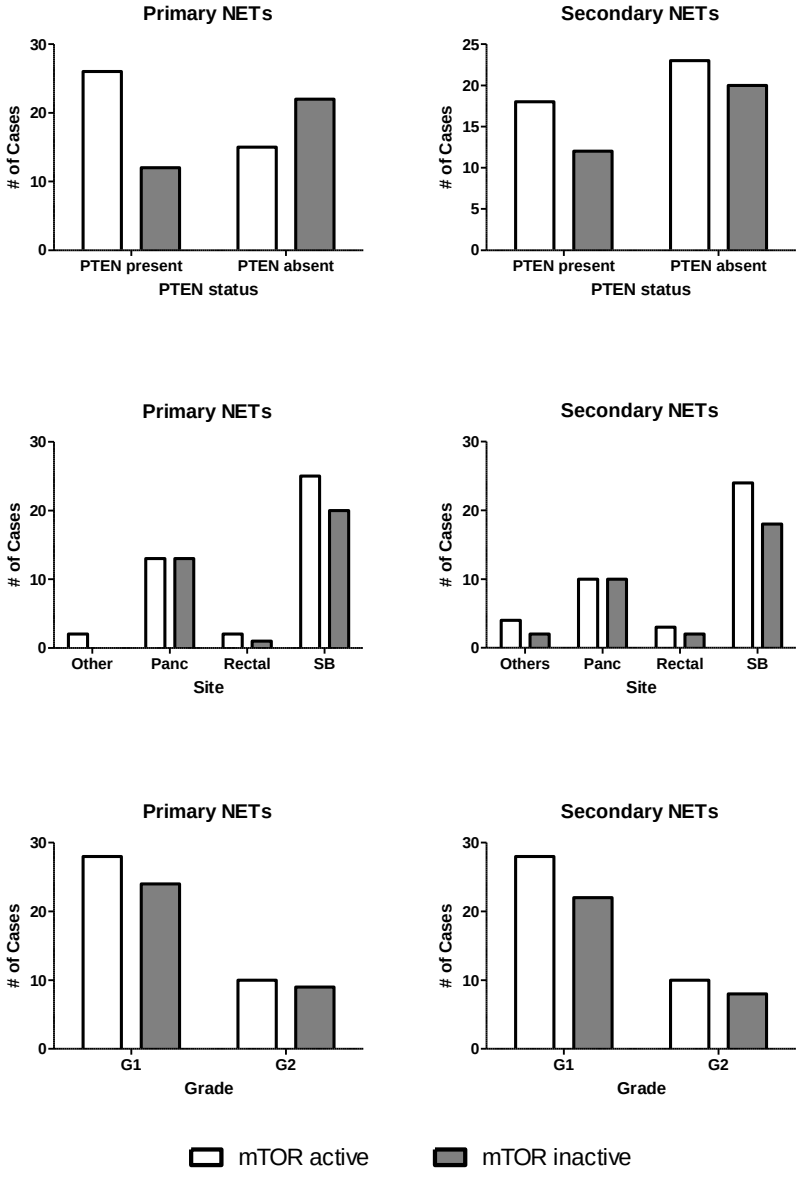

Figure 3.48. Contingency graphs for mTOR pathway activity in PTEN status, site of origin, and grade.

Chi-squared and Fisher's exact tests show no significant correlations except in primary tumours where there is an association with PTEN status.

Chapter 4

4 Conclusions

4.1 Discussion

Although EMT has been demonstrated in vitro for other epithelial tumours, this study is the first to show that EMT is involved in the pathogenic progression of GEP-NETs. We established the presence of an EMT phenotype using epithelial and mesenchymal markers and in doing so, discovered interesting expression patterns and trends among the cases represented in our group of GEP-NETs. Although alterations of E-cadherin and β-catenin have been noted in GEP-NETs within literature,[61, 69] this is the first to show concomitant expression of mesenchymal marker, vimentin. Previous studies have attempted, but failed to demonstrate vimentin expression within GEP-NETs outside of the stromal cells.[70] Vimentin is a well-known intermediate filament present in mesenchymal cells that aids in anchoring organelles within the cytoplasm during any sort of mechanical stress, be it external or for self-propulsion. Among the cases with E-cadherin/β-catenin loss of integrity and membrane staining, the majority of this group showed β-catenin sequestered in the cytoplasm. β-catenin is typically expected to either translocate into the nucleus to act as a transcription factor, or be subjected to ubiquitin-mediated protein degradation when it loses its association with E-cadherin.[71] The presence of β-catenin remaining in the cytoplasm suggests that another signalling pathway, Wnt, may be active in stabilizing the protein.[40] Wnt signalling is a pathway commonly associated with EMT and the preservation of a stem cell phenotype.[72]

The high proportion of P-NETs and all of the R-NETs displaying an EMT phenotype comparted to SI-NETs is interesting, given that NETs from these sites tend to behave more aggressively.[73-75] Knowing this, it is possible that part of their aggression comes from a tendency towards an EMT occurrence allowing for greater opportunity for metastasis which is ultimately what patients succumb to.

Heterogeneity of these tumours was apparent in our IHC staining analyses. A number of cases showed markedly different staining patterns and intensity across core replicates

from the same tumour using various immunohistochemical stains used in the study. This is not necessarily surprising, as EMT is likely not occurring simultaneously across all tumour cells at a given time. In fact, it seems more likely that a few single or clustered cells may transition to an EMT phenotype at a certain point in time.[70] The location of these cells may influence the likelihood of EMT. For instance, EMT could be more frequent in cells at the leading edge of a tumour or in cells immediately adjacent to blood vessels that would facilitate its eventual dissemination and metastasis. Indeed, studies have shown differential expression levels of key genes such as β-catenin within tumours where the cells from leading edges have elevated mRNA expression compared to those from the inner parts.[76] The heterogeneity of staining that we have observed may also mean that some cases with no evidence of an EMT immunophenotype may be misrepresented due to sampling artifact. Interestingly, staining differences were apparent among cases with paired primary and secondary lesions as well, although this might be expected as research reveals that despite sharing similar origins, primary tumour and their metastases may not share the same characteristics.[77, 78] Despite all of this, validation studies employing the use of TMAs on FFPE breast and ovarian cancer specimens have shown that a single 0.6 mm core is sufficient to represent a tumour for protein expression studies, with increasing accuracy with greater replicates.[79, 80] Emphasis was placed in sampling different areas, especially from areas of the edges and core were essential when taking replicate cores for an immunohistochemical profile.[81]

TGFβ has been shown to reduce E-cadherin expression as a result of upregulating promoter activity on EMT transcription factors SNAIL/SLUG via downstream effector SMAD complexes.[47, 49] Our SNAIL/SLUG and SMAD series of immunohistochemical stains help highlight the significance of identifying nuclear staining as these proteins are relevant for their ability to regulate cellular transcription. The immunohistochemistry shows us that not only are EMT transcription factors and downstream signalling molecules present in the GEP-NETs, but they are also localized to the nucleus where they actively influence transcription. Although few differences were seen among the SNAIL/SLUG staining, the SMAD proteins investigated seem to suggest that SMAD activity is particularly active among P-NETs relative to SI-NETs overall. Cases that had not metastasized had higher p-SMAD2/3 and SMAD4 reactivity than those with

metastases, but with no difference in p-SMAD1/5/8 reactivity, seem to suggest a more active role of TGFβ signalling over BMP signalling among primary NETs. SMAD4 reactivity patterns fall in line with its tumour suppressor properties as it has been shown the absence of it is seen in higher frequency among colorectal cancers with distant metastases, and later associated with worse overall survival.[82, 83] The immunoreactivity patterns observed in these stains suggest that TGFβ signalling is needed early in the EMT process but after EMT and metastasis are achieved, its dysregulation may be more advantageous.

One of the caveats to our gene expression studies is the quality of starting genetic material used. Although we extracted our RNA from FFPE tissue, we are satisfied by the quality and consistency of the results yielded in our gene expression studies. Other studies have also demonstrated the feasibility and potential to use DNA and RNA extracted from FFPE specimens with success.[84] Certain features, such as the high expression of TIMP1, which has been cited in literature as a normal neuroendocrine cell expression tendency, help reassure the reliability of our results.[64] The consistency in relative expression among overlapping genes represented across the various profiler plates such as the VEGF ligands, AKT1/2/3, and TSC1 further supports this. Ultimately, we treated our profiler plate gene expression studies as a way to obtain a general overview of what is happening in the collective of GEP-NETs in order to aid in selecting specific genes and signalling pathways to focus future studies on.

The individual case based PCR reaction experiments helped show that cases with an EMT phenotype at the protein level also have elevated vimentin mRNA expression, at least among all samples of GEP-NETs. The lack of changes seen in EMT versus non-EMT groups specifically may be a reflection on the focal nature of the EMT phenotype seen in many cases. Additionally, changes in subcellular localization of key EMT-related proteins, like E-cadherin or β-catenin, may not necessarily be reflected at the mRNA level as decreased expression. Going forward, adding additional cases to our series may help some of the results reach statistical significance. However, certain significant differences were discovered. Elevated expression of BMPRIα and BMPR2 in the overall EMT group suggest the involvement of the BMP branch of the TGFβ superfamily. The

expression of ZEB1 being significantly higher in cases “in transition” versus those with “integrity lost” only suggests that the expression of these transcription factors precedes the full onset of EMT and taper off after the transition begins. The potential clinical correlation of vimentin being more highly expressed in G2 tumours versus G1 suggest vimentin could be a biomarker for aggressive tumour behaviour. E-cadherin was seen to be more highly expressed in cases with no known metastases verses those that had some which further highlights the importance of retaining cell-cell contacts when maintaining an epithelial phenotype. This fits with the EMT process as the loss of E-cadherin is a key hallmark of the transition and the suppression of intercellular interactions mediated by E-cadherin may be a separate trigger of EMT on its own. Elevated MMP expression levels seen in G1 tumours for MMP9 and tumours without metastases for MMP2 could provide the means of initiating EMT as these MMPs can cleave latent TGFβ ligands sequestered in the ECM.[30]

Our mTOR pathway related immunohistochemistry suggests that mTOR signalling plays a larger role among non-EMT cases, small bowel NETs and G1 tumours overall, characteristics commonly associated with less aggressive clinical behaviour. This activation may be strictly regulated with higher PTEN expression since cases that remain non-aggressive as primary NETs with no metastasis had elevated PTEN expression. This upstream control seems to be reduced in cases with known liver metastasis. Indeed, PTEN loss has been associated with poorer outcomes and higher grade in prostate cancer[85, 86] Early PTEN dysregulation may be an early step in overall elevated mTOR activity in cases that have yet to show aggressiveness. Lack of correlation between p-4EBP1 expression with any of our clinical parameters appears to agree with similar studies done immunohistochemically profiling mTOR pathway proteins in P-NETs.[87] The mTOR pathway seems to be more active in cases that retain their epithelial phenotype, have yet to metastasize, or overall appear to be clinically less aggressive which seems counter-intuitive to the cases of advanced P-NETs that have benefitted from mTOR inhibitor therapies.

4.2 Future Directions

Overall, this study demonstrates there is EMT associated with GEP-NETs. It is difficult to definitively say which of the many potential pathways are inducing this process. However given our observations, TGFβ/BMP signalling pathway and EMT transcription factors associated with its activation are present and could be related to the EMT described. Certain elements in the EMT process may be useful as biomarkers indicating aggressive clinical behaviour such as loss of membrane E-cadherin or gain of vimentin expression. Molecularly, to further appreciate the role of EMT in GEP-NETs, a living model system needs to be used. Currently, several human cell lines exist for the disease, including the CNDT2[88], GOT-1[89], and KRJ-I cell lines[90], as well as the STS[91] cell line series. However, the utility of each have their own problems when replicating the neuroendocrine phenotype which has cast doubt on their appropriateness in replicating disease. A cell model is needed to test whether cells respond to certain ligands of specific signalling systems to see if they recapitulate an EMT event.

The notably high gene expressions of HIF1α and IGFBP3 from the real-time RT-PCR panels remains to be investigated in future studies as well. It is known that HIF1α is a transcription factor upregulated in the hypoxic environment frequently found in cancers.[92] Similarly, IGFBP3 expression has been noted in hypoxic tumour environments of esophageal cancer and shown to contribute to tumour progression with growth stimulation.[93] Additional studies have shown that IGFBP3 is a hypoxia-inducible gene and that HIF1α is capable of inducing its mRNA expression.[94] This environment enhancing IGFBP3 has been found to facilitate TGFβ1-mediated EMT, independent of its IGF-binding capacity, by stabilizing SMAD2/3 phosphorylation.[95] This gives motivation that given the expression patterns seen in HIF1α and IGFBP3, it is possible that they contribute towards EMT by allowing persistent phosphorylation of SMAD2/3, subsequently upregulating EMT transcription factors. Investigating these leads may expand on the interplay between mTOR and TGFβ/BMP signalling in these tumours.

Chapter 5

5 References

1. Pearse, A.G. The cytochemistry and ultrastructure of polypeptide hormone-producing cells of the APUD series and the embryologic, physiologic and pathologic implications of the concept. *The journal of histochemistry and cytochemistry : official journal of the Histochemistry Society* **17**, 303-313 (1969).

2. Fujita, T., Kobayashi, S. & Yui, R. Paraneuron concept and its current implications. *Advances in biochemical psychopharmacology* **25**, 321-325 (1980).

3. Day, R. & Salzet, M. The neuroendocrine phenotype, cellular plasticity, and the search for genetic switches: redefining the diffuse neuroendocrine system. *Neuro endocrinology letters* **23**, 447-451 (2002).

4. Cheng, H. & Leblond, C.P. Origin, differentiation and renewal of the four main epithelial cell types in the mouse small intestine. III. Entero-endocrine cells. *The American journal of anatomy* **141**, 503-519 (1974).

5. Rosai, J. The origin of neuroendocrine tumors and the neural crest saga. *Modern pathology : an official journal of the United States and Canadian Academy of Pathology, Inc* **24 Suppl 2**, S53-57 (2011).

6. Yao, J.C. *et al.* One hundred years after "carcinoid": epidemiology of and prognostic factors for neuroendocrine tumors in 35,825 cases in the United States. *J Clin Oncol* **26**, 3063-3072 (2008).

7. Frilling, A. *et al.* Neuroendocrine tumor disease: an evolving landscape. *Endocr Relat Cancer* **19**, R163-185 (2012).

8. Modlin, I.M. *et al.* Gastrointestinal neuroendocrine (carcinoid) tumours: current diagnosis and management. *The Medical journal of Australia* **193**, 46-52 (2010).

9. Khan, M.S. *et al.* A comparison of Ki-67 and mitotic count as prognostic markers for metastatic pancreatic and midgut neuroendocrine neoplasms. *British journal of cancer* **108**, 1838-1845 (2013).

10. Tang, L.H., Gonen, M., Hedvat, C., Modlin, I.M. & Klimstra, D.S. Objective quantification of the Ki67 proliferative index in neuroendocrine tumors of the gastroenteropancreatic system: a comparison of digital image analysis with manual methods. *The American journal of surgical pathology* **36**, 1761-1770 (2012).

11. Klimstra, D.S., Modlin, I.R., Coppola, D., Lloyd, R.V. & Suster, S. The pathologic classification of neuroendocrine tumors: a review of nomenclature, grading, and staging systems. *Pancreas* **39**, 707-712 (2010).

12. Hirabayashi, K. *et al.* Histopathology of gastrointestinal neuroendocrine neoplasms. *Frontiers in oncology* **3**, 2 (2013).

13. Kloppel, G. Classification and pathology of gastroenteropancreatic neuroendocrine neoplasms. *Endocrine-related cancer* **18 Suppl 1**, S1-16 (2011).

14. Alexiev, B.A., Drachenberg, C.B. & Papadimitriou, J.C. Endocrine tumors of the gastrointestinal tract and pancreas: grading, tumor size and proliferation index do not predict malignant behavior. *Diagnostic pathology* **2**, 28 (2007).

15. Modlin, I.M. *et al.* Gastroenteropancreatic neuroendocrine tumours. *Lancet Oncol* **9**, 61-72 (2008).

16. Kloppel, G. Tumour biology and histopathology of neuroendocrine tumours. *Best practice & research. Clinical endocrinology & metabolism* **21**, 15-31 (2007).

17. Thompson, L.A., Kim, M., Wenger, S.D. & O'Bryant, C.L. Everolimus: a new treatment option for advanced pancreatic neuroendocrine tumors. *Ann Pharmacother* **46**, 1212-1219 (2012).

18. Raymond, E. *et al.* Sunitinib malate for the treatment of pancreatic neuroendocrine tumors. *N Engl J Med* **364**, 501-513 (2011).

19. Strosberg, J. Neuroendocrine tumours of the small intestine. *Best Pract Res Clin Gastroenterol* **26**, 755-773 (2012).

20. Jiao, Y. *et al.* DAXX/ATRX, MEN1, and mTOR pathway genes are frequently altered in pancreatic neuroendocrine tumors. *Science* **331**, 1199-1203 (2011).

21. Banck, M.S. *et al.* The genomic landscape of small intestine neuroendocrine tumors. *J Clin Invest* **123**, 2502-2508 (2013).

22. Shida, T. *et al.* Expression of an activated mammalian target of rapamycin (mTOR) in gastroenteropancreatic neuroendocrine tumors. *Cancer Chemother Pharmacol* **65**, 889-893 (2010).

23. Kasajima, A. *et al.* mTOR expression and activity patterns in gastroenteropancreatic neuroendocrine tumours. *Endocr Relat Cancer* **18**, 181-192 (2011).

24. Missiaglia, E. *et al.* Pancreatic endocrine tumors: expression profiling evidences a role for AKT-mTOR pathway. *J Clin Oncol* **28**, 245-255 (2010).

25. Heldin, C.H., Vanlandewijck, M. & Moustakas, A. Regulation of EMT by TGFbeta in cancer. *FEBS Lett* **586**, 1959-1970 (2012).

26. Katsuno, Y., Lamouille, S. & Derynck, R. TGF-beta signalling and epithelial-mesenchymal transition in cancer progression. *Curr Opin Oncol* **25**, 76-84 (2013).

27. Ahmed, S., Liu, C.C. & Nawshad, A. Mechanisms of palatal epithelial seam disintegration by transforming growth factor (TGF) beta3. *Developmental biology* **309**, 193-207 (2007).

28. Laverty, H.G., Wakefield, L.M., Occleston, N.L., O'Kane, S. & Ferguson, M.W. TGF-beta3 and cancer: a review. *Cytokine & growth factor reviews* **20**, 305-317 (2009).

29. Finnson, K.W., McLean, S., Di Guglielmo, G.M. & Philip, A. Dynamics of Transforming Growth Factor Beta Signalling in Wound Healing and Scarring. *Advances in wound care* **2**, 195-214 (2013).

30. Yu, Q. & Stamenkovic, I. Cell surface-localized matrix metalloproteinase-9 proteolytically activates TGF-beta and promotes tumor invasion and angiogenesis. *Genes & development* **14**, 163-176 (2000).

31. Sato, Y. & Rifkin, D.B. Inhibition of endothelial cell movement by pericytes and smooth muscle cells: activation of a latent transforming growth factor-beta 1-like molecule by plasmin during co-culture. *The Journal of cell biology* **109**, 309-315 (1989).

32. Pircher, R., Jullien, P. & Lawrence, D.A. Beta-transforming growth factor is stored in human blood platelets as a latent high molecular weight complex. *Biochemical and biophysical research communications* **136**, 30-37 (1986).

33. Brunner, G. & Blakytny, R. Extracellular regulation of TGF-beta activity in wound repair: growth factor latency as a sensor mechanism for injury. *Thrombosis and haemostasis* **92**, 253-261 (2004).

34. Derynck, R. & Zhang, Y.E. Smad-dependent and Smad-independent pathways in TGF-beta family signalling. *Nature* **425**, 577-584 (2003).

35. Xu, J., Lamouille, S. & Derynck, R. TGF-beta-induced epithelial to mesenchymal transition. *Cell research* **19**, 156-172 (2009).

36. Biernacka, A., Dobaczewski, M. & Frangogiannis, N.G. TGF-beta signalling in fibrosis. *Growth factors* **29**, 196-202 (2011).

37. Greenburg, G. & Hay, E.D. Epithelia suspended in collagen gels can lose polarity and express characteristics of migrating mesenchymal cells. *The Journal of cell biology* **95**, 333-339 (1982).

38. Yap, A.S., Brieher, W.M. & Gumbiner, B.M. Molecular and functional analysis of cadherin-based adherens junctions. *Annual review of cell and developmental biology* **13**, 119-146 (1997).

39. Onder, T.T. *et al.* Loss of E-cadherin promotes metastasis via multiple downstream transcriptional pathways. *Cancer Res* **68**, 3645-3654 (2008).

40. Shimizu, H. *et al.* Transformation by Wnt family proteins correlates with regulation of beta-catenin. *Cell growth & differentiation : the molecular biology journal of the American Association for Cancer Research* **8**, 1349-1358 (1997).

41. Huang, R.Y. *et al.* An EMT spectrum defines an anoikis-resistant and spheroidogenic intermediate mesenchymal state that is sensitive to e-cadherin restoration by a src-kinase inhibitor, saracatinib (AZD0530). *Cell death & disease* **4**, e915 (2013).

42. Schliekelman, M.J. *et al.* Molecular portraits of epithelial, mesenchymal, and hybrid States in lung adenocarcinoma and their relevance to survival. *Cancer research* **75**, 1789-1800 (2015).

43. Kalluri, R. & Weinberg, R.A. The basics of epithelial-mesenchymal transition. *The Journal of clinical investigation* **119**, 1420-1428 (2009).

44. Peinado, H., Olmeda, D. & Cano, A. Snail, Zeb and bHLH factors in tumour progression: an alliance against the epithelial phenotype? *Nature reviews. Cancer* **7**, 415-428 (2007).

45. Bolos, V. *et al.* The transcription factor Slug represses E-cadherin expression and induces epithelial to mesenchymal transitions: a comparison with Snail and E47 repressors. *Journal of cell science* **116**, 499-511 (2003).

46. Moreno-Bueno, G. *et al.* Genetic profiling of epithelial cells expressing E-cadherin repressors reveals a distinct role for Snail, Slug, and E47 factors in epithelial-mesenchymal transition. *Cancer research* **66**, 9543-9556 (2006).

47. Medici, D., Hay, E.D. & Olsen, B.R. Snail and Slug promote epithelial-mesenchymal transition through beta-catenin-T-cell factor-4-dependent expression of transforming growth factor-beta3. *Molecular biology of the cell* **19**, 4875-4887 (2008).

48. Cho, H.J., Baek, K.E., Saika, S., Jeong, M.J. & Yoo, J. Snail is required for transforming growth factor-beta-induced epithelial-mesenchymal transition by activating PI3 kinase/Akt signal pathway. *Biochemical and biophysical research communications* **353**, 337-343 (2007).

49. Herfs, M. *et al.* Transforming growth factor-beta1-mediated Slug and Snail transcription factor up-regulation reduces the density of Langerhans cells in

epithelial metaplasia by affecting E-cadherin expression. *The American journal of pathology* **172**, 1391-1402 (2008).

50. Sakai, D. *et al.* Regulation of Slug transcription in embryonic ectoderm by beta-catenin-Lef/Tcf and BMP-Smad signalling. *Development, growth & differentiation* **47**, 471-482 (2005).

51. Carver, E.A., Jiang, R., Lan, Y., Oram, K.F. & Gridley, T. The mouse snail gene encodes a key regulator of the epithelial-mesenchymal transition. *Molecular and cellular biology* **21**, 8184-8188 (2001).

52. Nieto, M.A., Sargent, M.G., Wilkinson, D.G. & Cooke, J. Control of cell behavior during vertebrate development by Slug, a zinc finger gene. *Science* **264**, 835-839 (1994).

53. Postigo, A.A., Depp, J.L., Taylor, J.J. & Kroll, K.L. Regulation of Smad signalling through a differential recruitment of coactivators and corepressors by ZEB proteins. *The EMBO journal* **22**, 2453-2462 (2003).

54. Aigner, K. *et al.* The transcription factor ZEB1 (deltaEF1) promotes tumour cell dedifferentiation by repressing master regulators of epithelial polarity. *Oncogene* **26**, 6979-6988 (2007).

55. Gregory, P.A. *et al.* The miR-200 family and miR-205 regulate epithelial to mesenchymal transition by targeting ZEB1 and SIP1. *Nature cell biology* **10**, 593-601 (2008).

56. Soo, K. *et al.* Twist function is required for the morphogenesis of the cephalic neural tube and the differentiation of the cranial neural crest cells in the mouse embryo. *Developmental biology* **247**, 251-270 (2002).

57. Yang, J. *et al.* Twist, a master regulator of morphogenesis, plays an essential role in tumor metastasis. *Cell* **117**, 927-939 (2004).

58. Rosivatz, E. *et al.* Differential expression of the epithelial-mesenchymal transition regulators snail, SIP1, and twist in gastric cancer. *The American journal of pathology* **161**, 1881-1891 (2002).

59. Hoek, K. *et al.* Expression profiling reveals novel pathways in the transformation of melanocytes to melanomas. *Cancer research* **64**, 5270-5282 (2004).

60. Thuault, S. *et al.* Transforming growth factor-beta employs HMGA2 to elicit epithelial-mesenchymal transition. *The Journal of cell biology* **174**, 175-183 (2006).

61. Galvan, J.A. *et al.* Epithelial-mesenchymal transition markers in the differential diagnosis of gastroenteropancreatic neuroendocrine tumors. *American journal of clinical pathology* **140**, 61-72 (2013).

62. Walter, R.F. *et al.* FFPE tissue as a feasible source for gene expression analysis--a comparison of three reference genes and one tumor marker. *Pathology, research and practice* **209**, 784-789 (2013).

63. Livak, K.J. & Schmittgen, T.D. Analysis of relative gene expression data using real-time quantitative PCR and the 2(-Delta Delta C(T)) Method. *Methods* **25**, 402-408 (2001).

64. Sorensen, I.V. *et al.* Characterization of anti-TIMP-1 monoclonal antibodies for immunohistochemical localization in formalin-fixed, paraffin-embedded tissue. *The journal of histochemistry and cytochemistry : official journal of the Histochemistry Society* **54**, 1075-1086 (2006).

65. Lamouille, S. & Derynck, R. Cell size and invasion in TGF-beta-induced epithelial to mesenchymal transition is regulated by activation of the mTOR pathway. *J Cell Biol* **178**, 437-451 (2007).

66. Lamouille, S., Connolly, E., Smyth, J.W., Akhurst, R.J. & Derynck, R. TGF-beta-induced activation of mTOR complex 2 drives epithelial-mesenchymal transition and cell invasion. *J Cell Sci* **125**, 1259-1273 (2012).

67. Yao, J.C. *et al.* Everolimus for advanced pancreatic neuroendocrine tumors. *The New England journal of medicine* **364**, 514-523 (2011).

68. Yao, J.C., Phan, A.T., Jehl, V., Shah, G. & Meric-Bernstam, F. Everolimus in advanced pancreatic neuroendocrine tumors: the clinical experience. *Cancer research* **73**, 1449-1453 (2013).

69. Li, C.C. *et al.* Alterations of E-cadherin, alpha-catenin and beta-catenin expression in neuroendocrine tumors of the gastrointestinal tract. *Virchows Arch* **440**, 145-154 (2002).

70. Fendrich, V. *et al.* Epithelial-mesenchymal transition is a critical step in tumorgenesis of pancreatic neuroendocrine tumors. *Cancers (Basel)* **4**, 281-294 (2012).

71. Clevers, H. Wnt/beta-catenin signalling in development and disease. *Cell* **127**, 469-480 (2006).

72. Wend, P., Holland, J.D., Ziebold, U. & Birchmeier, W. Wnt signalling in stem and cancer stem cells. *Seminars in cell & developmental biology* **21**, 855-863 (2010).

73. Panzuto, F. *et al.* Prognostic factors and survival in endocrine tumor patients: comparison between gastrointestinal and pancreatic localization. *Endocr Relat Cancer* **12**, 1083-1092 (2005).

74. Bernick, P.E. *et al.* Neuroendocrine carcinomas of the colon and rectum. *Diseases of the colon and rectum* **47**, 163-169 (2004).

75. Kim, S.J. *et al.* Clinical course of neuroendocrine tumors with different origins (the pancreas, gastrointestinal tract, and lung). *Am J Clin Oncol* **35**, 549-556 (2012).

76. Bandapalli, O.R. *et al.* Transcriptional activation of the beta-catenin gene at the invasion front of colorectal liver metastases. *The Journal of pathology* **218**, 370-379 (2009).

77. Zen, Y. & Heaton, N. Elevated Ki-67 labeling index in 'synchronous liver metastases' of well differentiated enteropancreatic neuroendocrine tumor. *Pathol Int* **63**, 532-538 (2013).

78. Lindholm, E.B. *et al.* Do primary neuroendocrine tumors and metastasis have the same characteristics? *J Surg Res* **174**, 200-206 (2012).

79. Zhang, D., Salto-Tellez, M., Putti, T.C., Do, E. & Koay, E.S. Reliability of tissue microarrays in detecting protein expression and gene amplification in breast cancer. *Modern pathology : an official journal of the United States and Canadian Academy of Pathology, Inc* **16**, 79-84 (2003).

80. Rosen, D.G. *et al.* Validation of tissue microarray technology in ovarian carcinoma. *Modern pathology : an official journal of the United States and Canadian Academy of Pathology, Inc* **17**, 790-797 (2004).

81. Camp, R.L., Charette, L.A. & Rimm, D.L. Validation of tissue microarray technology in breast carcinoma. *Laboratory investigation; a journal of technical methods and pathology* **80**, 1943-1949 (2000).

82. Miyaki, M. *et al.* Higher frequency of Smad4 gene mutation in human colorectal cancer with distant metastasis. *Oncogene* **18**, 3098-3103 (1999).

83. Kozak, M.M. *et al.* Smad4 inactivation predicts for worse prognosis and response to fluorouracil-based treatment in colorectal cancer. *Journal of clinical pathology* **68**, 341-345 (2015).

84. Lehmann, U. & Kreipe, H. Real-time PCR analysis of DNA and RNA extracted from formalin-fixed and paraffin-embedded biopsies. *Methods* **25**, 409-418 (2001).

85. Sircar, K. *et al.* PTEN genomic deletion is associated with p-Akt and AR signalling in poorer outcome, hormone refractory prostate cancer. *The Journal of pathology* **218**, 505-513 (2009).

86. Yoshimoto, M. *et al.* PTEN losses exhibit heterogeneity in multifocal prostatic adenocarcinoma and are associated with higher Gleason grade. *Mod Pathol* **26**, 435-447 (2013).

87. Komori, Y. *et al.* Mammalian target of rapamycin signalling activation patterns in pancreatic neuroendocrine tumors. *Journal of hepato-biliary-pancreatic sciences* **21**, 288-295 (2014).

88. Van Buren, G., 2nd *et al.* The development and characterization of a human midgut carcinoid cell line. *Clinical cancer research : an official journal of the American Association for Cancer Research* **13**, 4704-4712 (2007).

89. Kolby, L. *et al.* A transplantable human carcinoid as model for somatostatin receptor-mediated and amine transporter-mediated radionuclide uptake. *The American journal of pathology* **158**, 745-755 (2001).

90. Modlin, I.M., Kidd, M., Pfragner, R., Eick, G.N. & Champaneria, M.C. The functional characterization of normal and neoplastic human enterochromaffin cells. *The Journal of clinical endocrinology and metabolism* **91**, 2340-2348 (2006).

91. Pfragner, R. *et al.* Establishment and characterization of three novel cell lines - P-STS, L-STS, H-STS - derived from a human metastatic midgut carcinoid. *Anticancer research* **29**, 1951-1961 (2009).

92. Semenza, G.L. HIF-1 mediates metabolic responses to intratumoral hypoxia and oncogenic mutations. *The Journal of clinical investigation* **123**, 3664-3671 (2013).

93. Natsuizaka, M. *et al.* IGFBP3 promotes esophageal cancer growth by suppressing oxidative stress in hypoxic tumor microenvironment. *American journal of cancer research* **4**, 29-41 (2014).

94. Natsuizaka, M. *et al.* Hypoxia induces IGFBP3 in esophageal squamous cancer cells through HIF-1 alpha-mediated mRNA transcription and continuous protein synthesis. *Faseb J* **26**, 2620-2630 (2012).

95. Natsuizaka, M. *et al.* Insulin-like growth factor-binding protein-3 promotes transforming growth factor-beta 1-mediated epithelial-to-mesenchymal transition and motility in transformed human esophageal cells. *Carcinogenesis* **31**, 1344-1353 (2010).

Curriculum Vitae

STEPHANIE MOK

Education

2013 - 2015 **Masters of Science**, Pathology and Laboratory Medicine, University of Western Ontario

2009 - 2013 **Bachelor of Medical Sciences with Distinction**, Honours Specialization in Pathology and Toxicology, University of Western Ontario

Work/Teaching Experience

2015 Winter Term **Graduate Teaching Assistant,** University of Western Ontario, Department of Biology
Course title: **Analysis and Interpretations of Biological Data** (Biology/Statistics 2244B)

2014 Fall Term **Graduate Teaching Assistant,** University of Western Ontario, Department of Pathology and Laboratory Medicine
Course title: **Understanding Disease** (Pathology 3240A)

2012 – 2013 **Undergraduate Research Assistant,** Department of Physiology and Pharmacology, University of Western Ontario

Honours, Awards and Recognitions

2013 - 2015 Western Graduate Research Scholarship
2013 Lawson Health Research Institute Studentship Award
2009 - 2013 Dean's Honor List
2009 Western Scholarship of Excellence

Community Involvement

2014 – 2015 **Committee Member**, Bylaws and Constitution Committee, Society of Graduate Students, University of Western Ontario

2013 – 2015 **Graduate Student Volunteer**, Let's Talk Science Outreach, University of Western Ontario

2013 – 2014 **Councillor**, Society of Graduate Students,
University of Western Ontario

Publications

Mok S, Khan ZA, Quan D, and Howlett CJ. Epithelial to mesenchymal transition in the metastatic progression of gastroenteropancreatic neuroendocrine tumours. Manuscript in preparation for submission.

Mok S, Ang L, Howlett CJ, and Khan ZA. Neovascularization in brain metastasis is through both angiogenesis and vasculogenesis. Manuscript in preparation for submission.

Conferences

2015 AACR Annual Meeting
Philadelphia PA, United States
Poster: "**Epithelial to mesenchymal transition in the metastatic progression of gastroenteropancreatic neuroendocrine tumors**"

AACR Annual Meeting
Philadelphia PA, United States
Poster: "**Neovascularization in brain metastasis is through both angiogenesis and vasculogenesis**"

2014 Till & McCulloch Meetings
Ottawa ON, Canada
Poster: "**Contribution of vasculogenesis and angiogenesis in brain metastasis**"

Annual Developmental Biology Research Day
University of Western Ontario, London ON, Canada
Poster: "**Vasculogenesis in brain metastasis**"

London Health Research Day
London ON, Canada
Poster: "**Epithelial to mesenchymal transition and cell guidance in the pathogenesis of small intestinal neuroendocrine tumours**"

Annual Pathology Research Day
University of Western Ontario, London ON, Canada
Poster: "**Epithelial to mesenchymal transition and cell guidance in**

the pathogenesis of small intestinal neuroendocrine tumours”

2013 London Health Research Day
London ON, Canada
Poster: “**Global cytogenomic changes in classical Hodgkin Lymphoma**”

Annual Pathology Research Day
University of Western Ontario, London ON, Canada
Poster: “**Global cytogenomic changes in classical Hodgkin Lymphoma**”